The Role of Voltage-Gated Sodium Channel 1.3 on Subfornical Organ Neurons

By

Shuo Huang

A thesis submitted to the Faculty of Graduate Studies of the University of Manitoba in partial fulfillment of the requirements of the degree of

MASTER OF SCIENCE

Department of Biological Sciences

University of Manitoba

Abstract

The subfornical organ (SFO) is an area in the brain characterized by lack of a blood-brain-barrier that contributes to interaction between the circulation and the central nervous system, and plays key roles in regulation of energy balance. The SFO has two subregions- the dorsolateral peripheral SFO (pSFO) and the ventromedial core of the SFO (cSFO). This study demonstrated the expression of voltage-gated Na^+ channel 1.3 (Nav1.3) in the SFO neurons, and a higher Nav1.3 expression in the pSFO. Based on the Nav1.3 expression pattern, intrinsic electrophysiological properties were compared between cSFO and non-cSFO neurons (putative pSFO neurons) identified by a SmartFlare mRNA probe. The patch clamp results revealed a bursting firing pattern in cSFO neurons and a higher spontaneous neuronal activity in non-cSFO neurons. The higher neuronal activity might be related to a more depolarized resting membrane potential and a higher trend of Na^+ current density.

Acknowledgements

I would like to thank my supervisor Dr. Mark Fry, who rendered me priceless help in the writing of my thesis and in my whole master's study. I really appreciate your high expectations, without which I wouldn't grow to be an eligible graduate student. I will carry on your critical thinking and passion in science in my future study and my entire career.

I would also like to thank my committee members Dr. Harold Aukema and Dr. Jason Treberg who gave me valuable suggestions in my project and for my thesis.

It was a great pleasure to work with my lab mates Samantha Lee, Katie Tough and Darcy Childs. Thank you for your support. I'll miss the busy but happy time in our lab.

Special thanks to Dr. Judy Anderson, who generously gave me a lot of help in both my study and life. From your eyes, I can see a better me.

I'd like to take this opportunity to thank my friends Yisha Ai, Stephanie Hans, Kai He, Weian Huang, Joana Correia, Xingyu Mao, Michelle Aljafary, Lin Li, Pan Liu, Nadine Price, Christa Szumski, Carl Szczerski, Mark Zarembo, Helia Zhang and Xiangui Zhao. You're my family in Winnipeg who kept me warm in this cold place.

I want acknowledge the Faculty of Graduate Studies of University of Manitoba and NSERC for funding.

At last, I need to say that I owe my deepest gratitude to my parents and my family, who taught me to dream big, gave me the wings and let me fly. It's your support that gives me courage to be an explorer.

Contents

List of Figures

List of Tables

List of Abbreviations

ACSF	Artificial cerebrospinal fluid
AGRP	Agouti-related peptide
α-MSH	α-melanocyte-stimulating hormone
ANG	Angiotensin
AP	Action potential
ARC	Arcuate nucleus
AVP	Arginine Vasopressin
BBB	Blood-brain barrier
BNST	Bed nucleus of stria terminalis
Calb	Calbindin
Calr	Calretinin
CART	Cocaine and amphetamine regulated transcript
CNS	Central nervous system
CRH	Corticotropin-releasing hormone
cSFO	Ventromedial core of the SFO
CVO	Circumventricular organ
DH	Dorsal horn
DRG	Dorsal root ganglion
EC_{50}	Half maximal effective concentration
GHSR	Growth hormone secretagogue receptors
I_A	Transient outward K^+ current
ICC	Immunocytochemistry

IH	Immunohistochemistry
I_h	Hyperpolarization-activated nonselective cation current
I_K	Delayed rectifier K^+ current
K_{ATP}	ATP-sensitive K^+ channel
LH	Lateral hypothalamus
MCH	Melanin-concentrating hormone
mPVN	Magnocellular paraventricular nucleus
NaCh	Voltage-gated sodium channel
Nav1.3	Voltage-gated sodium channel 1.3
NPY	Neuropeptide Y
NTS	Nucleus of solitary tract
OVLT	Organum vasculosum of lamina terminalis
PBS	Phosphate buffered saline
POMC	Pro-opiomelanocortin
pSFO	Rostrodorsal outer shell/dorsolateral peripheral SFO
pPVN	Parvocellular paraventricular nucleus
PVN	Paraventricular nucleus
qPCR	Quantitative polymerase chain reaction
RMP	Resting membrane potential
RT-PCR	Reverse transcription polymerase chain reaction
SCI	Spinal cord injury
sCVOs	Sensory circumventricular organs
SFO	Subfornical organ

TEA	Tetraethylammonium
TRH	Thyrotropin-releasing hormone

1. Introduction

1.1. Obesity

1.1.1. Obesity is a growing worldwide problem

Obesity is defined as pathologic accumulation of excess adipose tissue (Lee and Mattson, 2013). Obesity may lead to serious health crises, and obese individuals have increased risks of developing chronic health conditions such as cardiovascular diseases, type II diabetes, and musculoskeletal disorders (Must et al., 1999). Obesity is a growing worldwide problem. By the year of 2008, more than 1.4 billion adults were obese (Lehnert et al., 2013). Obesity is not only a problem limited to adults, but also a problem for children (Ball and McCargar, 2003, Wang and Lobstein, 2006). Reported by the Canadian government in 2011, in Canada, approximate 25% of the adults (Shields et al., 2010) and 8% of children and youth (Shields, 2006) were obese. The direct cost for overweight and obesity in Canada was $6 billion in 2006 (Anis et al., 2010). In the United States (U.S.), the medical cost of obesity increased from $78.5 billion in 1998 to $147 billion in 2008 (Finkelstein et al., 2009, reviewed in Lehnert et al., 2013). Without efficient control of obesity, the estimated medical cost of obesity in the U.S. will increase by $48-$66 billion per year (Wang et al., 2011). Because the increasing prevalence of obesity associated chronic health conditions and the growing economic burden, there is an urgent need for more effective approaches in the treatment and prevention of obesity.

1.1.2. The relationship between obesity and central nervous system control of energy balance

Obesity is caused by an interruption in the balance between energy intake and expenditure where excess calories are stored as fat. Obesity often results from overeating

and lack of physical activity. However, there are endogenous factors that contribute to the regulation of energy homeostasis and variations in the tendency to gain weight between individuals. The endogenous factors include but are not limited to genetic predisposition, circadian rhythms, pregnancy, and most importantly, regulation by the central nervous system (CNS) (Berthoud, 2005). The CNS is involved in the control of energy homeostasis in various aspects. For example, the reward system and the sensory system can stimulate appetite. The gut-brain interaction between the autonomic nervous system and endocrine system provides feedback of satiety to end a meal, and communication between the CNS and adipose tissue provides information regarding long term energy status of the body. An ideal strategy to treat obesity and restore the balance between calorie intake and energy expenditure is to reduce meal number and size while increasing physical activity. However this strategy is often difficult to carry out due to an failure in control of appetite which causes obese people to regain weight quickly after weight loss. The insatiable appetite may result from false signals generated by the digestive system and sent to the CNS or inaccuracy in signal processing within the CNS (Levin, 2007). Disorders in energy homeostasis can result from an inborn deficiency in the CNS and can lead to long-term or even permanent changes in the CNS, making obesity difficult to reverse (Bouret et al., 2004b, Levin, 2007). In order to develop more effective strategies to treat obesity, we must understand the mechanisms by which the CNS regulates energy balance.

1.2. CNS control of energy homeostasis

This present study focused on the subfornical organ (SFO), a CNS structure which has been demonstrated to play a key role in control of energy balance (Hindmarch et al., 2008, Smith et al., 2010). Neurons of the SFO detect key physiological parameters through the circulation and communicate this information with homeostatic control centers, including the hypothalamus. The following sections (1.2.1 and 1.2.2) will review key data describing the current mammalian paradigm (hypothalamus-centric model) for regulation of energy balance. Next (1.3.1-1.3.3) I will present crucial limitations of the hypothalamus-centric model and discuss the key data that suggests the SFO plays a crucial role in regulation of energy balance.

1.2.1. Hypothalamus is a key center for control of energy metabolism

The integration of multiple neuronal circuits involving various nuclei forms a CNS network that controls energy metabolism. The hypothalamus is a key CNS center for this network. Lesions in the hypothalamus are well-known to lead to dysregulation of body weight and feeding behaviour (Anand and Brobeck, 1951b, Elmquist et al., 1999, Schwartz et al., 1999). Hypothalamic centers including the arcuate nucleus (ARC), paraventricular nucleus (PVN) and lateral hypothalamus (LH) are crucial for the regulation of appetite.

The roles of different ARC neuronal subpopulations such as neuropeptide Y (NPY) neurons and pro-opiomelanocortin (POMC) neurons have been well-studied in energy homeostasis control. Activation of NPY neurons leads to an increase in food intake and decrease in energy expenditure while activation of POMC neurons has

opposite effects (Clark et al., 1985, Cone, 1999, reviewed in Schwartz et al., 2000, Schwartz and Porte, 2005). The activation of the NPY neurons leads to the release of NPY and up regulation of agouti-related peptide (AGRP) expression. Both NPY and AGRP are orexigenic neuropeptides that induce food intake (Stanley et al., 1986, reviewed in Schwartz et al., 2000). Conversely, activation of the POMC neurons increases the expression of anorexigenic neuropeptides α-melanocyte-stimulating hormone (α-MSH) and cocaine and amphetamine regulated transcript (CART), which results in inhibition of appetite (Fan et al., 1997, Schwartz et al., 2000, Zigman and Elmquist, 2003). NPY and POMC signaling processes are not independent from each other. (Schwartz et al., 2000, Williams et al., 2001, Schwartz and Porte, 2005, Williams and Elmquist, 2012). NPY neuronal terminals form synaptic connections with the POMC neuron (Csiffary et al., 1990, Horvath et al., 1992, for review see Zigman and Elmquist, 2003). The POMC neurons express NPY receptors (Fuxe et al., 1997) and can be inhibited by NPY. (Jegou et al., 1993). These data suggest a local circuit between the NPY and POMC neurons (Cowley et al., 1999, Williams et al., 2001). The NPY and POMC neurons also innervate second-order neurons in the PVN and the LH to influence feeding behaviours (Bai et al., 1985, Bagnol et al., 1999, Cone, 1999, Elmquist et al., 1999, Horvath et al., 1999, for review see Schwartz et al., 2000, Williams et al., 2001, Valassi et al., 2008). Hypothalamic signals from the PVN and LH can be passed onto brainstem structures including the nucleus of solitary tract (NTS), where the signals are integrated and further interact with the autonomic nervous system (Luiten et al., 1985, Rinaman, 1998, Hillebrand et al., 2002, Blevins et al., 2004). Activities of the autonomic nervous system can promote or inhibit gastrointestinal motility (Altaf and Sood, 2008).

Additionally, the autonomic nervous system can influence metabolic rate by regulating thermogenesis in brown adipose tissue (Morrison et al., 2012, 2014). Hypothalamic centers such as the LH also send projections to the cerebral cortex (Elmquist et al., 1999), which integrates conscious control of eating with the rewarding system (Berthoud, 2012). Connections between hypothalamic nuclei as well as their connections to lower or higher order CNS centers form a neuronal network for regulation of energy balance.

1.2.2. Hypothalamus regulates energy homeostasis by interacting with satiety signals

Satiety signals are the orexigenic and anorexigenic hormones carrying information of body metabolic status. The hypothalamus regulates feeding and energy balance by detecting satiety signals and processing the signals through neuronal circuits between hypothalamic nuclei. Leptin is a peptide hormone secreted from adipose tissue, providing information related to the nutritional status of the body (Friedman and Halaas, 1998). NPY and POMC neurons in the ARC express leptin receptor mRNA and the expression levels on NPY neurons can be increased by fasting (Cheung et al., 1997, Baskin et al., 1999). Increased level of leptin or insulin inhibits the NPY neurons and activate the POMC neurons both to inhibit food intake and cause weight loss. Conversely, decreased levels of leptin or insulin have opposite effects on both NPY and POMC pathways to increase body weight (Schwartz et al., 2000, Cowley et al., 2001). Ghrelin is a peptide hormone released from stomach and interacts with the CNS (Kojima et al., 1999). Growth hormone secretagogue receptors (GHSR), the ghrelin receptors, are expressed on multiple hypothalamic nuclei including ARC (Guan et al., 1997, Willesen et al., 1999). The application of ghrelin on ARC, NPY and POMC neurons influences their

electrophysiological activities (Cowley et al., 2003). Insulin is a peptide hormone secreted from pancreatic β-cells, the level of which correlates with blood glucose level and body metabolic status. Insulin receptors are expressed on neurons within the hypothalamus and involved in the glucoregulation. Insulin acts on the hypothalamic melanocortin system to regulate food intake and body weight (Benoit et al., 2002, Derakhshan and Toth, 2013).

The circulating satiety signals are processed in hypothalamus through direct synaptic connections and also through peptidergic circuitry, which involves a variety of orexigenic and anorexigenic neuropeptides. Different from satiety signals, neuropeptides are synthesized and released by neurons and act as neurotransmitters to mediate neuronal communication. The roles of NPY, AGRP, α-MSH and CART have been discussed previously. Other orexigenic neuropeptides such as orexin and melanin-concentrating hormone (MCH), and anorexigenic neuropeptide hormones including thyrotropin-releasing hormone (TRH) and corticotropin-releasing hormone (CRH) are also involved in the peptidergic pathways and serve as mediators for the action of leptin and insulin (Schwartz et al., 2000). For example, MCH is expressed in the LH and the level of expression increased in response to leptin deprivation (Qu et al., 1996, reviewed in Schwartz et al., 2000).

The levels of peptide hormones reflect energy status of the body. The information carried by these hormones interacts with and is integrated in hypothalamic nuclei, playing an important role in regulation of energy homeostasis. In next section, challenges to the model of hypothalamic regulation by circulating satiety signals will be discussed.

1.3. How CNS monitors body energy status

1.3.1. The blood-brain barrier (BBB) controversy

The BBB is a mechanism that protects the CNS by preventing polar substances and macromolecules in the circulation from passing into the interstitial fluid surrounding neurons in the brain. The BBB exists in brain blood vessels, choroid plexus and arachnoid membrane and consists of endothelial cells, astrocyte end-feet and pericytes.(Gregoire, 1989, Ballabh et al., 2004, Abbott et al., 2010). The BBB is mainly built from tight junctions between cerebral endothelial cells (Gregoire, 1989). The adjacent endothelial cells fuse to form a bimolecular layer of phospholipids enclosing capillaries to provide a relatively isolated and stable environment for the CNS. The end-feet of astrocytes surrounding endothelial cells stabilize, and also possibly induce the formation of tight junctions (Janzer and Raff, 1987, Kuchler-Bopp et al., 1999). Pericytes embedded in the basement membrane also contribute to the integrity of the BBB (Ballabh et al., 2004).

There is large volume of data supporting the idea of circulating peptide hormones act on neurons in hypothalamic centers such as ARC, which is protected by a BBB. However, there are controversies of how peptide hormones, which often have large molecular weight, can cross the BBB to access the targets at high enough concentrations.

Though the BBB prevents various hormones from efficiently interacting with neurons of the CNS, there are transport mechanisms that may facilitate the delivery of peptide hormones from the circulation into the brain. Leptin can be delivered across the BBB by transporters (Banks et al., 1996), although the identity of the transporters has yet to be discovered.

Previous studies revealed limitations in transport mechanisms for satiety signals. It has been suggested transport mechanisms might not be sufficient for energy balance control centers such as ARC to detect changes in circulating satiety signals. A previous study suggested insulin accessed the CNS through a receptor mediated transport mechanism (Baura et al., 1993, Banks et al., 1997, Banks, 2004). However, limited by saturable transport mechanisms, the cerebrospinal fluid concentration of insulin delivered by insulin transporters was much lower than the peripheral level (for review see Banks, 2008). Reported by Banks et al. (1997), brain insulin concentration = 0.0669×Serum insulin concentration/(2.50ng/ml + Serum insulin concentration). Based on a saturated concentration for transporter of 10ng/ml (Banks et al., 1997), the highest brain insulin level would be 9.50×10^{-11} M, which failed to reach the EC_{50} of insulin receptor which was 8×10^{-9} M (Kjeldsen et al., 1991). Ghrelin transporters allow transport of ghrelin from brain to blood yet whether the transport was bidirectional required further investigations (Banks et al., 2002). Moreover, reviewed by Fry and Ferguson (2010), the physiological level of circulating ghrelin ranged from 1 to 3 nM (Tschop et al., 2000, Wren et al., 2001). Through a transporter-mediated mechanism, the ghrelin concentration delivered to cerebrospinal fluid would be 1000-fold lower compared to the circulating level (Grouselle et al., 2008, for review see Fry and Ferguson, 2010), which was much lower than the EC_{50} value of ghrelin receptors which was 1-14 nM (Pulman et al., 2006, Kim et al., 2009, for review see Fry and Ferguson, 2010).

To exert accurate regulation of energy homeostasis, there may be other pathways for the brain to detect circulating hormones behind the BBB (For review see Fry and Ferguson, 2010). It has been hypothesized that peptide hormones might directly access

the hypothalamus through ARC neuron axon terminals located in median eminence, which lacks a BBB (Peruzzo et al., 2000). However it is unlikely that peptide hormones could act on ARC neuronal cell bodies through this route by retrograde transportation or through leakage and diffusion from median eminence (Krisch et al., 1978, Peruzzo et al., 2000, for review see Fry and Ferguson, 2010). Hence, the access of ARC neuron axon terminals to circulation still failed to explain how cerebral metabolic regulation centers sense circulation satiety signals.

In recent years, the sensory circumventricular organs (CVOs) have been recognized to play roles in the control of energy balance in light of the fact the neuronal cell bodies in sensory CVOs are not protected by the BBB, contain receptors for virtually all known satiety signals, are electrically responsive to these signals and project axons to homeostatic control centers (Petrov et al., 1994, McKinley et al., 2003, Hindmarch et al., 2008, for recent review, see Smith and Ferguson, 2010, Smith et al., 2010).

1.3.2. The sensory CVOs

The sensory CVOs are specialized structures located adjacent to brain ventricles. The sensory CVOs are characterized by extensive vasculature and fenestrated capillary endothelial cells, which allows the direct and rapid interaction between the CNS and the circulating system (Gross, 1992, McKinley et al., 2003). The sensory CVOs include the area postrema, the subfornical organ (SFO) and the organum vasculosum of lamina terminalis (OVLT) (McKinley et al., 2003). Sensory CVOs are abundant with neural cell bodies (McKinley et al., 2003). Neurons in sensory CVOs express a variety of peptides and hormone receptors and have connections with different autonomic control centers

(Johnson and Gross, 1993, McKinley et al., 2003, Fry and Ferguson, 2007a, Hindmarch et al., 2008). Recognized functions of the sensory CVOs include but are not limited to regulation of fluid balance, cardiovascular functions, energy homeostasis, triggering vomiting and neuroimmune responses (McKinley et al., 2003, Fry and Ferguson, 2007a). This present study focused on SFO, one of the sensory CVOs.

1.3.3. The SFO

The SFO has been well-recognized for its role in regulating hydro-mineral homeostasis and cardiovascular functions via angiotensin II and arginine vasopressin (AVP) signalings (Simpson and Routtenberg, 1973, Tanaka et al., 1985, Ferguson and Kasting, 1986, Ferguson and Bains, 1997). More recently, studies suggested that the SFO also plays an important role in regulation of energy homeostasis (Pulman et al., 2006, Fry et al., 2007, Hindmarch et al., 2008, Hoyda et al., 2009, Smith et al., 2009, Smith and Ferguson, 2010, Lakhi et al., 2013, Mimee et al., 2013).

The following sections will describe the anatomy of the SFO and the role of SFO in regulating energy balance. In addition, the heterogeneous properties in different SFO subpopulations with respect to anatomy, peptide expression and electrophysiological response to satiety signals will be discussed.

Anatomy of the SFO

The SFO is a small hemispheric structure that lies against the ventral hippocampal commissure in the anteroventral aspect of the 3rd ventricle (McKinley et al., 2003) (Figure 1-1A). There are two major functional subregions in the SFO: the rostrodorsal

outer shell/dorsolateral peripheral SFO (pSFO) and the ventromedial core of the SFO (cSFO) (Kawano and Masuko, 2010) (Figure 1-1B). The capillary density, length and surface area in the cSFO are much higher, while capillary diameter is smaller compared to the pSFO (Gross, 1991). The efferent neurons from the pSFO project to hypothalamic sites including the supraoptic, paraventricular, median preoptic and lateral hypothalamic nuclei (Miselis et al., 1979, Saper and Levisohn, 1983, Sgro et al., 1984, McKinley et al., 2003, Duan et al., 2008), Neurons from the ventromedial core have been proposed to mainly send projections to the rostral bed nucleus of stria terminalis (Swanson and Lind, 1986). While previous results (McKinley et al., 2003, Duan et al., 2008) showed SFO projections to the PVN are from the pSFO, a recent study (Kawano and Masuko, 2010) has demonstrated by injecting anterograde and retrograde tracer into rat brains that the projections to the PVN are from both the cSFO and pSFO. Interestingly, the result from the same study also showed that neurons from the cSFO and pSFO specifically projected to two PVN subregions, the parvocellular (pPVN) and the magnocellular (mPVN), respectively. In addition, neurons from the SFO also project to the ARC (Gruber et al., 1987). However whether the projections to the ARC are from cSFO or pSFO remains unclear.

The afferent projections to the SFO include median preoptic nucleus, nucleus reuniens of the thalamus, LH, NTS, and midbrain raphe (Ferguson and Bains, 1996). The NTS and the hypothalamic PVN, LH, and ARC are key energy balance regulation centers (Anand and Brobeck, 1951a, Kotz et al., 2000, Schwartz et al., 2000, Cowley et al., 2001, Williams et al., 2001, Cowley et al., 2003, Maejima et al., 2009), supporting the role of the SFO in the control of energy balance from an anatomical aspect.

A

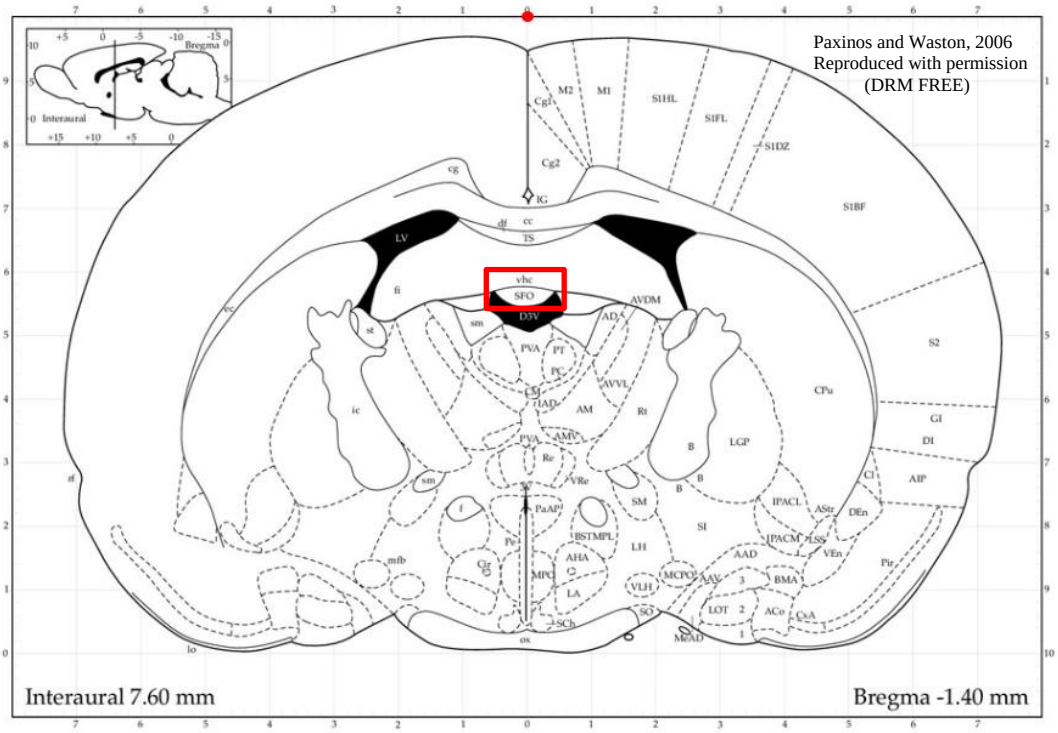

B

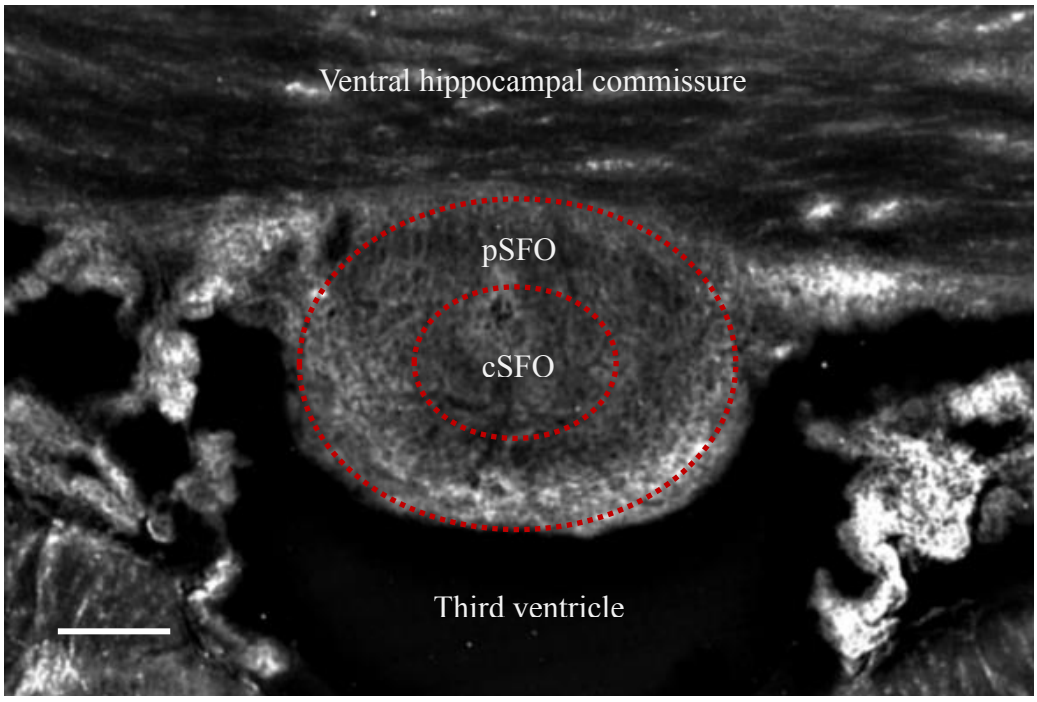

Figure 1-1. Location and subregions of the SFO. (A) Location of SFO in rat brain atlas. (B) A coronal section through rat SFO (Paxinos and Watson, 2006). *Scale bar, 100 μm*.

SFO expresses a variety of peptide hormone and hormone receptors

SFO neurons express a variety of proteins. Some of the proteins are peptide hormones, hormone receptors and ion channels which are involved in important functions of the SFO. *In situ* hybridization and immunoreactive studies demonstrated the expression of angiotensin II (ANG II), ANG-converting enzyme and ANG II receptors in SFO (Pickel et al., 1986, Matsuda et al., 1995), which play crucial roles in the ANG II signaling pathway. The expression of those proteins provided a physiological role for the SFO in regulating fluid balance. Recent studies have also examined if the SFO is involved in regulation of energy balance. A microarray analysis carried out by Hindmarch et al. (2008) demonstrated the mRNA expression of a variety of orexigenic and anorexigenic peptide hormones and hormone receptors within the SFO. Studies on SFO investigating its role in control of energy balance shows consistency with the microarray study. Smith et al. (2009) demonstrated the expression of leptin receptors in an immunohistochemistry study. Insulin receptor-like immunoreactivity was also located in the SFO (Unger et al., 1989). Pulman et al. (2006) examined the mRNA for the ghrelin receptor GHSR and showed its expression in SFO. Reported by Ahmed et al. (2014) in their RT-PCR result, the cholecystokinin receptor mRNA was also expressed in the SFO. Additionally, Kishi et al. (2005) identified the mRNA for NPY receptors in the SFO. Those results were confirmed by the Allen brain atlas (Dong, 2008). The strong expression of receptors for satiety signals in SFO indicated a possible role for the SFO in regulating energy balance.

Interestingly, the distribution of a number of proteins shows different patterns between the cSFO and pSFO. The expression of Calb in SFO is confined to the cSFO,

while Calr is expressed exclusively in the pSFO (McKinley et al., 2003). Therefore, cSFO and pSFO neurons can be identified by their expression of Calb and Calr, respectively. ANG II and ANG II receptor AT1 are both expressed at higher densities in cSFO compared to the expression level in pSFO (Lind et al., 1985, Lenkei et al., 1995, Giles et al., 1999). Immunohistochemical study by Smith *et. al.* demonstrated receptors of the satiety signal leptin are also mainly expressed in cSFO (Smith et al., 2009).

SFO plays a role in regulation of energy balance

SFO is subject to dynamic changes induced by food deprivation. A microarray analysis on SFO by Hindmarch *et. al.* demonstrated a two-fold transcriptomic change in more than 600 genes induced by fasting (Hindmarch et al., 2008). *In vivo* electrical stimulation of the SFO in satiated rats has been demonstrated to induce feeding behaviour, suggesting a role for the SFO in regulation of energy balance (Smith et al., 2010). Moreover, previous studies showed SFO neurons were sensitive to a variety of metabolic signals. It has been revealed that the application of orexigenic and anorexigenic hormones such as ghrelin, amylin (Pulman et al., 2006), leptin (Smith et al., 2009), adiponectin (Alim et al., 2010), insulin (Lakhi et al., 2013) and cholecystokinin (Ahmed et al., 2014) could cause electrophysiological changes in the SFO neurons, by altering membrane potentials and influencing spontaneous firing frequency of the neurons. These data suggested SFO neurons sense satiety signals and mediate them by encoding stimuli into changes in electrical activity, which further indicated the function of SFO in regulating metabolism and energy homeostasis.

The SFO neurons appear to be functionally heterogeneous in response to satiety signals

SFO neurons showed electrophysiological changes induced by a variety of circulating signals. Most of those studies were carried out on dissociated SFO neurons. This was mainly because recordings from SFO neurons in acutely prepared brain slices could not preclude synaptic input from other neurons. Moreover, complicated neurites would cause inaccuracies in recording. Also, from a pragmatic aspect, using dissociated neurons for patch clamp recording requires fewer animals. Interestingly, in studies using dissociated SFO neurons, not all neurons demonstrated a consistent behaviour in response to certain stimulation. In a study of the effect of AVP on the SFO, only one-half of SFO neurons showed response to AVP application, and among the AVP-sensitive subpopulation, approximately 50% neurons were excited while the remaining were inhibited (Anthes et al., 1997). This study also revealed that the AVP-sensitive subpopulation partly overlapped with the ANG II-responsive subpopulation, which indicated the existence of multiple subpopulations within the SFO involved in regulation of fluid balance. The heterogeneous behaviours did not only exist in the responses of SFO neurons to signals for hydro-mineral modulation, but also in the changes induced by satiety signals. In the study by Pulman et al. (2006), SFO neurons which were sensitive to ghrelin were not responsive to amylin administration and ghrelin also failed to activate amylin sensitive neurons, which suggested neurons that were influenced by amylin or ghrelin belonged to separate subpopulations. Further study indicated amylin-sensitive neurons might overlap with the subpopulation of leptin sensitive neurons, and while the majority demonstrated an increase in excitability, the minority behaved in an opposite way toward leptin stimulation (Smith et al., 2009). In response to insulin administration,

30% of SFO neurons were non-responsive, while 33% showed hyperpolarization, and 37% were depolarized. Further investigation in the same study demonstrated the heterogeneous responses were caused by different ionic mechanisms. The hyperpolarization was induced by opening of K_{ATP} channels, and the depolarization was mediated by I_h channels (Lakhi et al., 2013). The application of glucose either excited or inhibited the SFO neurons, and those effects were induced by an inward nonspecific cation current and an outward K_{ATP} current respectively (Medeiros et al., 2012). Under adiponectin application, 21% of the SFO neurons demonstrated a more depolarized membrane potential and 35% behaved in the opposite way (Alim et al., 2010). In the study of cholecystokinin's effect on SFO (Ahmed et al., 2014), while the majority of cholecystokinin responsive neurons demonstrated a depolarized membrane potential, the minority were hyperpolarized. The mechanisms that led to heterogeneous behaviours in response to adiponectin or cholecystokinin have not yet been investigated.

It is of great interest to understand if the SFO subpopulations which demonstrated a depolarization/hyperpolarization response to different hormones actually belong anatomically distinct regions (i.e. cSFO and pSFO) or were distributed throughout the SFO. With the dissociation procedure it was not possible to determine the original locations of neurons within the SFO. Therefore, the pattern of distribution of SFO neurons with heterogeneous electrophysiological responses to circulating hormones remains unclear.

The cSFO and pSFO neurons demonstrated heterogeneous reactions towards stimulations, as determined by non-electrophysiological methods

Previous studies showed evidence that subregions of SFO neurons from cSFO and pSFO behaved differently under particular stimuli. McKinley et al. (1998) demonstrated higher levels of activity in response to relaxin were seen particularly in the pSFO. A c-fos experiment demonstrated that osmotic stimulation by hypertonic saline only activated neurons in pSFO, while the response to hypovolaemic shock by polyethylene glycol injection was mainly in cSFO (Smith and Day, 1995). Together those studies provided further evidence that cSFO and pSFO subpopulations were functionally different. There has yet to be an electrophysiological study that demonstrated heterogeneous behaviour of cSFO and pSFO neurons. Moreover, while previous studies demonstrate the existence of different SFO subpopulations based on their electrophysiological behaviour, there is no study that can further categorize those subpolulations, or determine whether they overlap cSFO or pSFO subpopulations.

Heterogeneous intrinsic electrical properties in different SFO neuron subpopulations

Studies also demonstrated biophysical differences in intrinsic electrical properties (the properties exhibited by neurons without chemical stimulation) between SFO neuronal subpopulations. In the study of Lakhi et al. (2013) on insulin's effect on SFO neurons, the mean baseline input resistance of the neurons which showed hyperpolarizing response to insulin was 1.5 ± 0.3 GΩ, compared to 2.0 ± 0.2 GΩ in neurons which had depolarizing response. In another example of heterogeneous properties, Ferguson and Bains (1996) reported SFO neurons showed either a single spike or a burst of action

potentials in response to depolarizing pulses. In the study by Okuya *et. al.* (Okuya et al., 1987), the majority of spontaneously active SFO neurons had continuous or irregular firing pattern, while 16% of them demonstrated a short burst firing pattern (less than 2s). However in the study by Ferguson and Li (1996), SFO neurons only exhibited bursting spontaneous firing pattern. Another electrophysiological study on dissociated SFO neurons showed difference in K^+ channel properties between SFO subpopulations: the SFO neurons which project to PVN had a significantly higher degree of inactivating type of K^+ current (Anderson et al., 2001). This result was consistent with Washburn *et. al.*'s observation, which described two types of K^+ current I_K (the delayed rectifier K^+ current) and I_A (transient outward K^+ current) in different SFO subpopulations (Washburn et al., 1999). Since dissociated neurons can not normally provide information for their original location or projections, it is difficult to assess how subpopulations with heterogeneous intrinsic electrical properties map onto cSFO and pSFO subregions. Thus further studies need to be carried out to contribute to a better categorization of SFO neurons by their electrophysiological correlation with anatomical locations, which is the goal of the hypothesis II in present study.

1.4. Voltage-gated sodium channel 1.3 (Nav1.3)

Voltage-gated sodium channels (NaCh) are critical for generating action potentials in excitable cells. They are the main contributors for the rising phase of an action potential, generating persistent current and subthreshold oscillations (Fry and Ferguson, 2007b, Kiss, 2008). The density, localization and biophysical behaviour of NaCh largely determine the electrophysiological properties of neurons such as action

potential frequency, cell input resistance, action potential threshold, and action potential shape. Changes in electrophysiological properties often cause a shift in cell excitability. A number of isoforms of NaCh have been identified including Nav1.1-Nav1.9 and each exhibits specific properties and patterns of expression. Like all NaCh, Nav1.3 protein consists of four repeating motifs in α-subunit, and each motif contains six transmembrane segments (S1-S6), with a voltage sensor S4. The loop connecting the S5 and S6 is known as P-region that forms the selective filter for sodium ions. Specific details of NaCh structure and function are reviewed in (Yu and Catterall, 2003, Catterall, 2012)

1.4.1. Nav1.3 is strongly regulated

Nav1.3 is a unique Nav isoform because its expression is strongly regulated. Previous studies have demonstrated changes in Nav1.3 expression during development (Beckh et al., 1989), neural trauma (Hains et al., 2003) and food restriction (Hindmarch et al., 2008).

In the embryonic development of vertebrates, Nav1.3 is expressed at a high level throughout the brain and spinal cord. However, Nav1.3 expression decreases after the first or second postnatal weeks (Beckh et al., 1989). In adults, weak expression of Nav1.3 has been detected in the cerebral cortex, hippocampus, midbrain, colliculi and, medulla-pons, retina, cerebellum and spinal cord, but at very low level (Beckh et al., 1989, Lindia and Abbadie, 2003).

Other studies on Nav1.3 focused on its role in neuropathic pain after neural trauma. Hains *et. al.* demonstrated the up regulation of Nav1.3 in dorsal horn (DH) neurons after spinal cord injury (SCI). The increase in expression of Nav1.3 induced

hyperexcitability of DH neurons, which was associated with neuropathic pain (Hains et al., 2003). Further studies revealed the number of dorsal root ganglion (DRG) neurons that expressed Nav1.3 was in proportion to the degree of neural trauma, and that the increase in Nav1.3 expression was primarily on sensory neurons that were not damaged from injury (Lindia et al., 2005). Furthermore, Hains et al. (2005) demonstrated an increase in Nav1.3 expression on the ventrobasal complex of the thalamus, the third-order neurons of the primary sensory neurons, four weeks after SCI. The change in Nav1.3 expression altered the electrophysiological properties including an increase in spontaneous discharging rate and hyperresponsiveness to peripheral stimuli. In addition to neuropathic pain, studies also demonstrated seizure led to an increase in Nav1.3 expression in the hippocampus (Bartolomei *et al.*, 1997, Guo et al., 2008).

A recent microarray study by Hindmarch *et al.* (2008) on adult rats revealed that Nav1.3 is expressed within the SFO. More interestingly, it was noted that Nav1.3 within the SFO was down regulated twofold after a 48h fast, indicating a link between Nav1.3 and regulation of energy homeostasis. The change in Nav1.3 expression has been confirmed by qPCR (unpublished data from Dr. M. Fry's lab). Following a 48h fast, Nav1.3 levels in rat SFO were reduced by 54%, compared to sated group. However the correlation of Nav1.3 expression level within SFO subregions or whether the expression was within neurons (as opposed to glia cells) still remain to be investigated. In addition, further experiments using patch clamp electrophysiology demonstrated that after a 48h fast, action potential threshold, height and duration showed a significant change, while a concomitant decrease in Na^+ current density and a depolarizing shift in voltage dependence of Na^+ current activation and voltage-dependent inactivation were observed

(unpublished data). Together those studies reflected the notion that SFO is a dynamic sensor for energy balance.

1.4.2. Electrophysiology of Nav1.3

The electrophysiology of Nav1.3 has been studied but not fully revealed. Cummins *et al.* (2001) suggested the properties of Nav1.3 could increase overall cell excitability. Their results showed Nav1.3 contributed to a slower development of voltage-dependent inactivation but a faster recovery, and a more hyperpolarized kinetics of persistent Na^+ current. Those data indicated the expression of Nav1.3 is prone to hyperpolarize action potential threshold and increase action potential frequency of a neuron. Lampert et al. (2006) drew consistent conclusion with the Cummins study. They showed up regulation of Nav1.3 expression in DRG neurons after SCI resulted in a larger persistent Na^+ current and a depolarized shift in both Na^+ current voltage-dependent inactivation, which together enhanced overall neuronal activity. This study was not able to preclude the interference from other ion channels, yet Nav1.3 was the main contributor to the electrophysiological changes.

Based on the strong regulation of Nav1.3 and its potential role in regulating energy balance, investigating the distribution of Nav1.3 is the focus of hypothesis I in the present study.

1.5. Hypotheses

Previous studies suggested the SFO plays an important role in regulating energy balance. SFO neurons express a wide variety of receptors for satiety signals, some of

which are localized to cSFO or pSFO. Hindmarch et al. (2008) showed food restriction down regulated the expression of Nav1.3 in the SFO. Dr. M. Fry's unpublished data confirmed this change and showed the down regulation could lead to changes in electrophysiological properties of SFO neurons, specifically inhibition of neuron excitability. Electrophysiological studies revealed the responses of SFO neurons to many satiety signals are heterogeneous, with subpopulations being excited, inhibited or non-responsive. Some endogenous variability in SFO neurons was also observed, including spontaneous action potential frequency, cell input resistance and K^+ current inactivation.

Therefore, the first goal of this project was to use immunohistochemistry to investigate spatial distribution of Nav1.3 in SFO to determine if observed heterogeneity maybe related to differential expression in cSFO versus pSFO.

Hypothesis 1: Nav1.3 is expressed in SFO neurons and the levels of expression are more exclusively in one subregion.

In this present study, immunofluorescent staining was carried out by using an antibody against the Nav1.3 α-subunit to examine Nav1.3 expression on the SFO. Immunofluorescent staining for Calb and Calr was also performed to outline cSFO and pSFO subregions. Immunofluorescent staining for Nav1.3 and Calr on adjacent sections were quantified and compared to investigate the overlap of Nav1.3 expression on pSFO subregion.

Interestingly, the immunohistochemistry results demonstrated a higher expression level of Nav1.3 in pSFO. Previous studies have shown different excitability of cSFO and pSFO neurons in response to certain stimuli such as ANG II or relaxin application and

osmotic change. Studies have also indicated the existence of separate subpopulations of SFO neurons based on differences in their intrinsic electrical properties. Cummins *et al.* (2001) suggested that Nav1.3 played a unique role in determining cell electrophysiological properties. Because Nav1.3 immunohistochemistry showed colocalization with Calr in pSFO, we hypothesized that the observed heterogeneity in SFO electrophysiology might be related to the distribution of Nav1.3. Therefore, a study aimed to investigate and compare the electrical properties of the neurons from cSFO and pSFO would provide necessary and important information regarding potential roles of Nav1.3 in the SFO neurons.

Hypothesis 2: There are differences in the intrinsic electrophysiological properties of neurons from different SFO subregions.

To examine this hypothesis, a Calb mRNA-specific fluorescent probe (SmartFlare, Millipore) was applied to dissociated rat SFO neurons to identify putative cSFO neurons from other SFO neurons. The Calb probe was chosen (as opposed to Calr which colocalized with Nav1.3) because microarray analysis showed Calb was more strongly expressed and would thus make a better target for the probe (Hindmarch et al., 2008). Immunocytochemistry was applied to investigate the relationship between Calb/Calr immuno-positive and Calb SmartFlare-positive neurons to validate the SmartFlare RNA probe. Patch clamp recordings were then carried out on SmartFlare-Calb positive and negative neurons. Intrinsic electrical properties such as spontaneous activity, resting membrane potential, action potential properties and Na^+ channel properties were quantified and compared between putative cSFO and non-cSFO neurons.

2. Material and methods

2.1. Investigation of Nav1.3 distribution in SFO

2.1.1. Immunocytochemistry (ICC) study

ICC for Nav1.3 was carried out to demonstrate Nav1.3 expression in dissociated SFO neurons.

Animal care

Male Sprague-Dawley rats (150-250g) were used for this study. Animals were maintained under a 12h:12h light-dark cycle with free access to food and water. All experiments involved animals were carried out in accordance with the Canadian Council on Animal Care Committee Guidelines, and were approved by the University of Manitoba Animal Care Committee.

Cell culture of SFO neurons

SFO neurons were cultured essentially as described (Brewer, 1997, Fry and Ferguson, 2007b). Briefly rats were decapitated, the brain was removed from the skull and immediately placed into ice-cold, oxygenated artificial cerebrospinal fluid (ACSF) (87mM NaCl, 2.5mM KCl, 1.25mM NaH_2PO_4, 7mM $MgCl_2$, 25mM D-glucose, 75mM sucrose, 25mM $NaHCO_3$, 0.5mM $CaCl_2$, prepared in MilliQ H_2O, pH=7.4) for 2min. The tissue block containing the SFO was cut using a brain matrix. The first cut was rostral, at the beginning of the optic chiasm, followed by a second cut 3mm caudal to the first cut (Figure 2-1).

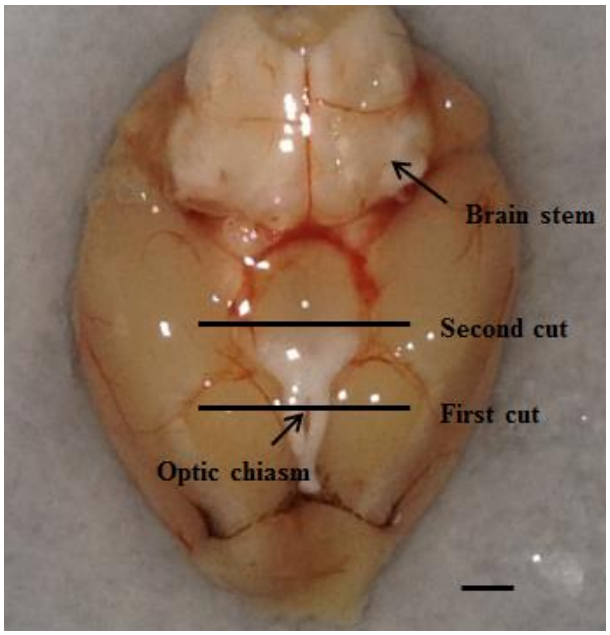

Figure 2-1. A rat brain labeled with the two cutting sites. The tissue block between two cuttings contained SFO. *Scale bar*, 2 mm.

The tissue block was then immediately transferred into a petri dish containing sterile Hibernate A media (Brain Bits, Springfield, IL, USA) and B27 supplement (Gibco, Burlington, ON). Microdissection of the SFO was performed using a dissecting microscope (Olympus). The SFO was digested in a sterile papain (Worthington Biochemical Corp., Freehold, NJ, USA) solution (2mg/ml in Hibernate A without B27) at 30˚C for 30min. The SFO was then washed twice and triturated with 1ml pipette tips in sterile Hibernate A-B27. The undispersed pieces were allowed to settle for 1-2 minute. The supernatant, containing dispersed cells, was removed and placed in a fresh tube. Sediment containing undispersed neurons was re-suspended in 2ml Hibernate A-B27 and triturated again. This process was repeated once more for a total of three sets of trituration. Cell suspensions collected from each set of trituration were combined and centrifuged at 240g for 6min. Supernatant was gently removed and cells were re-suspended in 500-1000µl Neurobasal media (Gibco) supplemented with B27 and 1×Glutamax (Gibco). 100µl of cell suspension containing approximately 30 SFO neurons was plated onto each glass bottom culture dish (MatTek, Ashland, MA, USA). Neurons were allowed to settle for 3h in a CO_2 incubator (5% CO_2 at 37 ˚C) before 2ml Neurobasal media-B27-Glutamax was added to each dish. Half of the media was changed every day. All the sterile procedures were carried out in biosafety cabinet.

Immunocytochemistry on dissociate SFO neurons

Immunocytochemistry for Nav1.3 was carried out on isolated SFO neurons. Cells used for ICC experiments were plated on Poly-L-Lysine (Sigma-Aldrich, Oakville, ON, Canada) coated dishes. Culture media was slowly replaced by warm (37 ˚C) phosphate

buffered saline (PBS) (137mM NaCl, 2.7mM KCl, 10mM Na2HPO4 • 2 H2O, 2mM KH2PO4, pH = 7.4) (MP Biomedicals, Irvine, CA, USA), and cells were gently washed three times with PBS. PBS was then slowly replaced with 4% paraformaldehyde in PBS (Alfa Aesar, Ward Hill, MA, USA) (room temperature). Cells were fixed for 30min at room temperature. After fixation, cells were washed three times with PBS, followed by a 10min permeablization with 0.25% TritonX-100 in PBS. Cells were washed three times and then treated with blocking vehicle (0.5% BSA+5% donkey serum in PBS) for 45min at room temperature. Cells were incubated at room temperature in primary antibody for Nav1.3 (1:20, sc-22202, Santa Cruz, CA, USA) for 1h and fluorescent secondary antibody (1:500, Jackson ImmunoResearch, PA, USA) for 45min before being visualized under an epifluorescence microscope.

2.1.2. Immunohistochemistry (IH) studies on SFO from brain sections

Immunohistochemistry for Nav1.3 was carried out on 20µm brain sections to demonstrate spatial localization of Nav1.3 within SFO. IH for Calb and Calr was also carried out to outline the pSFO and cSFO subregions (McKinley et al., 2003), providing landmarks for studying Nav1.3 distribution. Rats were decapitated, brain removed from the skull and immediately placed into ice-cold, oxygenated ACSF for 2min. A 3mm-thick tissue block containing the SFO was cut using a brain matrix and quickly transferred into ice-cold fixation solution of 4% paraformaldehyde in PBS. After 3.5h of fixation at 4˚C, coronal sections of 20-30µm through the SFO were made using a vibratome (Leica VT 1000S, Leica Microsystems, Germany). Sections were washed in ice-cold 1X PBS four times, for 5min each, with gentle shaking at 4˚C. For Calr and Nav1.3 staining, sections

were incubated with blocking vehicle containing 10% donkey serum (Jackson ImmunoResearch) and 0.3% TritonX-100. Sections were incubated with primary antibodies at 4˚C overnight, washed with ice-cold vehicle four times and then incubated with secondary antibodies for 1h at 4 ˚C, protected from light (please see Table 2-1 for primary and secondary antibody information). Sections were washed with ice-cold vehicle, 1×PBS, and 0.5×PBS sequentially, for 5min each. Sections were mounted on clean slides and air-dried for 20min before mounting media (Polysciences) was added. Coverslips were applied to each section and sealed with nail polish.

For Calb IH, antigen retrieval was carried out to obtain optimal staining signal (McNicol and Richmond, 1998, Snow et al., 2013). After fixation, brain sections containing SFO were made and washed with 1×PBS. Citrate buffer (10mM citric acid, pH=6.0) was preheated to 80˚C in a water bath. Citrate buffer was added to sections and heated at 80˚C for 25min. Sections were cooled at room temperature for 20min. The following steps of IH with antigen retrieval are the same as regular IH (p28). Sections were then washed in ice-cold PBS three times before incubation in blocking vehicle containing 10% goat serum (Cedarlane, ON, Canada). Sections were incubated in primary antibody for Calb (1:1000, cat. No. CB300, Swant, Switzerland) overnight at 4˚C. Sections were washed with ice-cold vehicle four times and then incubated with secondary antibody (1:500, Alexa Fluor 488, cat. No. A11001, Invitrogen) for 1h at 4˚C. Sections were washed with ice-cold vehicle, 1×PBS, and 0.5×PBS sequentially, for 5min each. Sections were mounted on clean slides and air dried for 20min. Afterwards, mounting media (Polysciences) was added. Coverslips were applied to each section and sealed with nail polish.

Table 2-1. Primary and secondary antibody combinations for IH

Primary Antibodies	Dilution	Secondary Antibodies	Dilution
Mouse anti-Calb Swant CB300	1:1000	Goat anti-Mouse F488 Invitrogen A11001	1:500
Rabbit anti-Calr Swant 7699/4	1:1000	Goat anti-Rabbit F555 Invitrogen A21428	1:500
Rabbit anti-Calr Swant 7699/4	1:1000	Goat anti-Rabbit F546 Invitrogen A11010	1:500
Goat anti-Calr Santa Cruz LV1486604	1:1000	Donkey anti-Goat Cy3 Jackson ImmunoResearch	1:500
Goat anti-Nav1.3 Santa Cruz sc-22202	1:20	Donkey anti-Goat Cy3 Jackson ImmunoResearch	1:500
Rabbit anti-Nav1.3 Chemicon AB5208-50UL	1:20	Goat anti-Rabbit F555 Invitrogen A21428	1:500
Rabbit anti-Nav1.3 Abcam ab65164	1:100	Goat anti-Rabbit F555 Invitrogen A21428	1:500

Antigen retrieval was also carried out for Calr and Nav1.3 staining but the process made the IH signal worse for these two (data not shown).

Double IH

Double IH was carried out to investigate the colocalization of Nav1.3 and Calb or Nav1.3 and Calr. Compared to regular IH on adjacent sections, double IH provides a more precise colocalization. For double IH, sections were washed in ice-cold 1×PBS four times, for 5min each, with gentle shaking at 4˚C before incubation in an blocking vehicle containing 10% serum from host species of secondary antibodies and 0.3% TritonX-100. If host animals of the secondary antibodies were not the same, the blocking vehicle contained 1% BSA and 0.3% TritonX-100. The primary antibodies were mixed together and applied simultaneously. Sections were incubated in primary antibodies at 4˚C overnight. Sections were washed with ice-cold vehicle four times and then incubated with secondary antibodies for 1h at 4˚C, protected from light. Secondary antibodies could not be added at the same time if two antibodies could react with each other (please see Table 2-2 and Table 2-3 for antibody information). Sections were washed with ice-cold vehicle, 1×PBS, and 0.5×PBS sequentially, for 5min each. Sections were then mounted on clean slides and air dried for 20min. Mounting media was added, sections were coverslipped and sealed with nail polish. In double IH results, immunofluorescent signals for all combinations were much weaker compared to single IH. Thus only single IH images are presented in the Results section.

Preadsorption of Nav1.3 primary antibody

Preadsorption tests the specificity a primary antibody incubating it with target antigen that ought to weaken or abolish staining in tissue which stained positive previously. The anti-Calb and Calr antibodies are well characterized and exhibit specificity (Gracia-Llanes et al., 2010, Meier et al., 2014). In contrast the anti-Nav1.3 antibody is not as well characterized. Therefore we carried out a preadsorption study to confirm its specificity for the Nav1.3 antigen.

Nav1.3 antibody (sc-22202, Santa Cruz) was preadsorbed with corresponding Nav1.3 blocking peptide (sc-22202 P, Santa Cruz) overnight at 4˚C. Blocking peptide was added at the ratio of 5:1 to antibody by molecular weight. After overnight incubation, the antigen-antibody mix was centrifuged at 20,000 g for 30 min. The supernatant was then carefully collected and applied to sections in the same manner as was the primary antibody. Reduction of staining, as compared to parallel processing without preadsorption, and negative control without primary antibody was measured and analysed using one-way ANOVA (please see Image acquisition and analysis).

Table 2-2. Primary and secondary antibody combinations for double IH

(Secondary antibodies added separately)

Primary antibodies	First added secondary antibody	Second added secondary antibody
Mouse anti-Calb (Swant)	Cy3 Donkey anti-Goat	F488 Goat anti-Mouse
Goat anti-Nav1.3 (Santa Cruz)	(Jackson ImmunoResearch)	(Invitrogen)

Table 2-3. Primary and secondary antibody combinations for double IH

(Secondary antibodies added together)

Primary antibodies	Secondary antibodies (added together)
Rabbit anti-Calr (Swant)	F488 Donkey anti-Rabbit (Invitrogen)
Goat anti-Nav1.3 (Santa Cruz)	Cy3 Donkey anti-Goat (Jackson)

Image acquisition and analysis

IH and ICC results were initially visualized using an upright epifluorescence microscope (Olympus BX51WI, Olympus, Tokyo, Japan) equipped with a LMPlanFLN (Olympus) 5X regular, and UMPlanFl (Olympus) 20X and 40X water-immersion objectives. The UV light was sourced from an EXFO X-Cite Series 120 illuminator (EXFO, Mississauga, ON, Canada), filtered by appropriate filter sets for Alexa 488 and Cy3 (Semrock, NY, USA). Pictures were captured using a CCD digital camera (QImaging Exi Aqua, QImaging, Surrey, BC, Canada). To increase resolution, some IH results were also visualized using an ApoTome microscope (Axio Imager Z1, Carl Zeiss, Oberkochen, Germany). The ApoTome microscope provided better resolution through use of an optical grid, which reduces the amount of scattered light and allows the focus to be optimized for fine layers of tissue.

To analyze pixel intensity of Calb, Calr and Nav1.3 IH and preadsorption images, ImageJ software (US National Institutes of Health, Bethesda, MD, USA) was used to measure pixel value and OriginPro software (OriginPro 9.0 Student Version, Originlab, Northampton, MA, USA) was used to process data. For comparing the staining pattern of Calb, Calr and Nav1.3 on SFO, straight line tool was used to select lines through the center of the SFO to measure pixel intensity. For each image, the average pixel intensity from three lines was normalized and plotted as normalized pixel intensity curve using OriginPro software. For evaluating preadsorption results, a rectangular area with same size and location was selected on each image. The pixel intensity in Calb, Calr and Nav1.3 IH was obtained with ImageJ and compared using one-way ANOVA and post-hoc Tukey test with OriginPro software.

2.2. Investigation of electrophysiological differences between cSFO and non-cSFO neurons

2.2.1. Validation of SmartFlare reagent

A Calb mRNA probe SmartFlare reagent was applied to identify putative cSFO neurons in culture for patch clamp recording. The identification is based on Calb is thought to be expressed only in cSFO neurons (McKinley et al., 2003). Thus it is important to evaluate if SmartFlare reagent can effectively identify neurons that express Calb. To validate the SmartFlare reagent for Calb, the Calb and Calr ICC on SmartFlare-treated dissociated SFO neurons was carried out respectively to investigate the correlation between Calb/Calr ICC signal and SmartFlare signal. Double ICC for Calb and Calr was also carried out on dissociated neurons to investigate the proportion of Calb and Calr immuno positive neurons among all SFO neurons. The double ICC result served as a positive control for ICC experiments on SmartFlare-treated neurons.

.

SmartFlare treatment

SmartFlare is an RNA probe developed by EMD Millipore that enables the detection of specific mRNA transcripts within live cells. The RNA probe enters cells by endocytosis. The RNA probe contains a gold nanoparticle core conjugated with multiple single-stranded RNAs (capture RNA) which are complementary to the target mRNA. Each capture RNA is attached to a short reporter RNA strand that is conjugated to a fluorophore. When the target mRNA (i.e. Calb mRNA) is absent, the fluorophore is quenched by the gold nanoparticle (Figure 2-2A). When target mRNA approaches an RNA probe, the target mRNA binds to the capture RNA strand and causes release of the

reporter RNA strand, allowing the fluorophore to fluoresce under UV light (Figure 2-2B). The fluorescent signal can be visualized using an epifluorescence microscope, allowing the detection of live cells expressing specific mRNA.

SmartFlare reagent for Calb mRNA (cat. No. SFC-297, Millipore Inc., Bedford, MA, USA) was reconstituted from lyophilized powder with sterile nuclease free water and stored at room temperature, as described in the manufacturer's instructions. Before use, a working solution of SmartFlare reagent was prepared by diluting SmartFlare reagent 1:20 in sterile, room temperate PBS. The working solution was added into each dish at the ratio of 1:50 to culture media. Cells treated with SmartFlare were incubated overnight (12-18h) before use.

Double ICC for Calb and Calr

Double ICC experiments were carried out on dissociated SFO neurons to investigate the proportions of SFO neurons that express Calb and Calr. Culture media was slowly replaced by warm PBS (37 ˚C), and cells were gently washed three times with PBS. PBS was then slowly replaced with 4% paraformaldehyde in PBS (Alfa Aesar, Ward Hill, MA, USA) (room temperature). Cells were fixed for 30min at room temperature. After fixation, cells were washed three times with PBS, followed by a 10min permeablization with 0.25% TritonX-100 in PBS. Cells were washed three times and then treated with blocking vehicle (0.5% BSA+5% donkey serum in PBS) for 45min at room temperature. Cells were incubated at room temperature in primary antibody for Calb (Swant CB300) and Calr (Swant 7699/4) for 1h. Two primary antibodies were mixed and added together. Cells were the incubated with

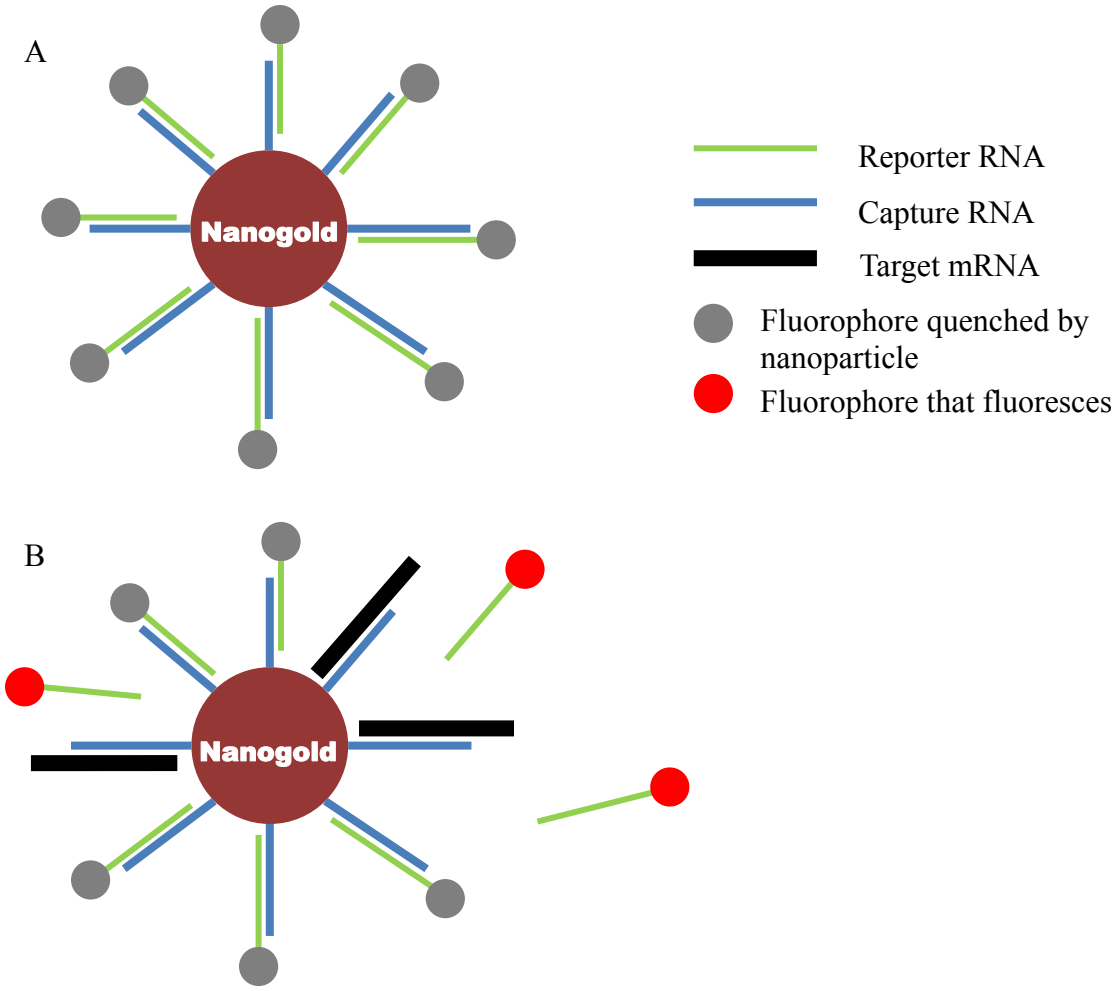

Figure 2-2. Principle of SmartFlare RNA probe. (A) The SmartFlare probe consists of a gold nanoparticle conjugated to multiple capture RNA strands which are complimentary to the target mRNA. Each capture RNA is hybridized with a reporter RNA strand which is attached to a fluorophore. The fluorophores are quenched by the gold nanoparticle in the absence of a target mRNA. (B) When the target mRNA is present, it displaces the reporter RNA, which releases the quenching by gold nanoparticle and enables the fluorophores to fluoresce.

fluorescent secondary antibodies Alexa F488 (Invitrogen) and F555 (Invitrogen) for 45min before visualized under an epifluorescence microscope. Two secondary antibodies share the same host species thus were also mixed and added together (For antibodies applied in double ICC, please see Table 2-4).

Validation of SmartFlare reagent: Calb/Calr ICC on SmartFlare-treated SFO neurons

ICC for Calb and Calr was carried out on SmartFlare-treated SFO neurons respectively to investigate the correlation of Calb SmartFlare signal and Calb/Calr ICC signal, which examined the effectiveness of the SmartFlare reagent. Because SmartFlare signal can be quenched by fixation procedure, a photo of every same cell was taken before fixation for SmartFlare signal and after fixation for Calb ICC signal. Culture dishes with labeled grid (cat. No. P35G-2-14-CGRD, MatTek) were used to locate the same cell before and after fixation.

Pixel intensity of SmartFlare signal and Calb/Calr ICC signal from each cell was measured using ImageJ software. Cells were delineated using elliptical selection and the mean value of the histogram of the selected area was used as signal intensity. The mean pixel intensity of SmartFlare, Calb and Calr of each cell was plotted and analyzed with Origin software to investigate the correlation.

Table 2-4. Primary and secondary antibody combinations for double ICC

Primary antibodies	Secondary antibodies (added together)
Mouse anti-Calb (Swant)	F488 Goat anti-Mouse (Invitrogen)
Rabbit anti-Calr (Swant)	F555 Goat anti-Rabbit (Invitrogen)

2.2.2. Patch clamp recording

Electrophysiological procedures

Patch clamp electrophysiology aims to detect electrical signals from cells in order to study their electrophysiological properties. In this study, patch clamp recordings were made using cell-attached and whole-cell configurations. In patch clamp recording, a micropipette approached a neuron controlled by a manipulator under an inverted microscope with phase contrast and epifluorescence optics (Zeiss IM35). To achieve cell-attached configuration, light suction was applied to facilitate the micropipette forming tight seal (> 1GΩ) with the cell membrane. In cell-attached configuration, electrical signals from a small patch of cell membrane enclosed within the micropipette can be studied without perturbation to the cell. In cell-attached configuration, spontaneous activity of SFO neurons was recorded.

After cell-attached configuration was established, a quick but more powerful suction was applied to rupture the small patch of cell membrane. At this stage whole-cell configuration was established, allowing the study of electrical activities throughout the entire cell membrane. In whole-cell configuration, either current clamp or voltage clamp recording was carried out, depending on whether membrane potential or current is under the control by the amplifier. Current clamp recording injects current generated from the amplifier and records membrane potential and action potentials. Conversely, voltage clamp recording holds the membrane potential at a given level and records current passing through ion channels on cell membrane.

Patch clamp recordings were carried out on both Calb SmartFlare positive and negative cells to investigate the intrinsic electrical properties of putative cSFO and non-

cSFO neurons. Cell-attached voltage clamp recordings were first applied to study spontaneous action potential activity (Figure 2-3A). For further investigation of mechanisms that lead to the change in spontaneous activity, whole-cell current clamp and voltage clamp were carried out. Basic biophysical properties such as resting membrane potential, action potential threshold and cell input resistance were analysed by using whole-cell current clamp recording (Figure 2-3B). Na^+ current properties such as voltage dependence of activation, voltage-dependent inactivation, transient current density, persistent current and time-dependent recovery from inactivation were examined by using voltage clamp recording with Na^+ reduced extracellular recording solution (Figure 2-3B). K^+ currents were also analysed from whole-cell voltage clamp recording but using physiological extracellular recording solution (Figure 2-3B).

Patch-clamp recordings were carried out on isolated SFO neurons after overnight treatment with SmartFlare reagent. Neurons were identified with Zeiss IM35 inverted microscope (Carl Zeiss) equipped with an illuminator (Nikon Instruments, Melville, NY, USA) and filter set for epifluorescence. Neurons were bathed in the extracellular recording solution (Table 2-5 and Table 2-7) during experiments. Glass micropipette (Sutter, USA) used for recordings had resistance from 2-7 MΩ (2-4 MΩ for Na^+ current recordings, 4-7 MΩ for cell attached and K^+ current recordings) when filled with intracellular recording solution (Table 2-6 and Table 2-8). All recordings used a micro-agar salt bridge electrode for stabilization of electrode potentials as described (Fry and Ferguson, 2007b, Shao and Feldman, 2007).

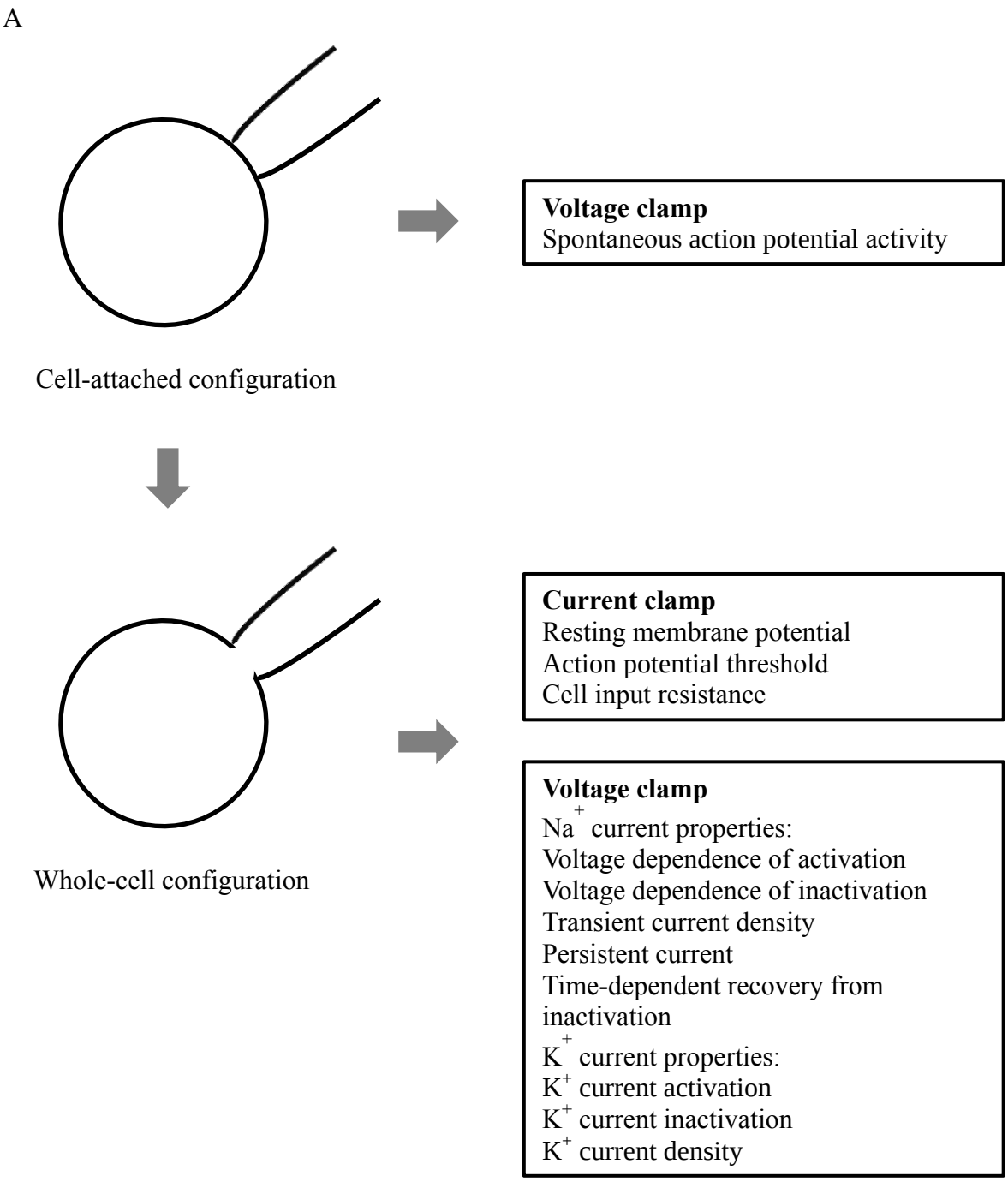

Figure 2-3. Intrinsic electrical properties investigated by patch clamp recording. (A) Spontaneous action potential activity was recorded with cell-attached configuration. (B) Whole-cell configuration was established to study basic biophysical properties and K^+ and Na^+ channel properties.

Chemicals were supplied by Sigma, Fisher Scientific, OmniPur (EMD chemicals, Gibbstown, NJ, USA) and MP Biomedicals. Electrical signals were amplified with a HEKA EPC 10 patch clamp amplifier (HEKA Elektronik, Chester, NS) under the control of PatchMaster software (Version V2x69, HEKA Elektronik). Data were acquired at 10 to 50 kHz and filtered at 1 kHz. Series resistances were controlled below 15 MΩ in both whole-cell voltage and current clamp recordings, and series resistance compensation was set from 65% to 80% for all voltage clamp recordings. Neurons that were able to fire an action potential with a peak over +20 mV were considered suitable.

The rationale for using Na^+ reduced solution in recording Na^+ currents was to reduce the driving force for Na^+ ions. As a result, peak Na^+ current amplitude was reduced, which enabled the amplifier to better control membrane potential. Na^+ reduced solution was able to provide better resolution for Na^+ conductance curves. In addition, the Na^+ reduced extracellular recording solution contained K^+ and Ca^{2+} channel blockers in order only to analyse Na^+ currents (Table 2-7).

Table 2-5. Physiological extracellular recording solution

Compound	Molecular weight	concentration (mM)
NaCl	58.44	140
KCl	74.55	4
$MgCl_2$	203.3	1
HEPES	260.29	10
Glucose	180.16	10
$CaCl_2$	147.02	1

pH = 7.4 at 22°C Osm was adjusted to 280±5mOsm/Kg

Table 2-6. Physiological intracellular recording solution

Compound	Molecular weight	concentration (mM)
NaCl	58.44	10
Potassium Gluconate	234.25	120
$MgCl_2$	203.3	1
HEPES	260.29	10
EGTA	380.4	10
Na_2ATP	605.24	4
GTP	523.18	0.1

pH = 7.2 at 22°C Osm was adjusted to 280±5mOsm/Kg

Table 2-7. Extracellular recording solution for Na^+ current recording

(Na^+ reduced extracellular recording solution)

Compound	Molecular weight	concentration (mM)	Function
NaCl	58.44	50	
TEA-Cl	165.70	100	Block K^+ current
$MgCl_2$	203.3	1	
HEPES	260.29	10	
Glucose	180.16	10	
CsCl	168.36	1	Block K^+ current
$CdCl_2$	183.35	0.3	Block Ca^{2+} current
$BaCl_2$	244.26	1	Block K^+ current
$CaCl_2$	147.02	2	

pH = 7.4 at 22°C Osm was adjusted to 295±5mOsm/Kg

Table 2-8. Intracellular recording solution for Na^+ current recording

Compound	Molecular weight	concentration (mM)	Function
CsCl	168.36	10	Block K^+ current
$CsMeSO_4$	228	130	Block K^+ current
$MgCl_2$	203.3	1	
HEPES	260.29	10	
EGTA	380.4	1	
Na_2ATP	605.24	2	
GTP	523.18	0.1	

pH = 7.2 at 22°C Osm was adjusted to 295±5mOsm/Kg

Patch clamp stimulation protocols and data analysis

Spontaneous activity

In cell attached configuration, a 5min recording of current of spontaneous action potential activity was recorded from each cell. The number of action potential and interspike intervals of action potential was determined using Spike2 software (Version 6.12, Cambridge Electronic Design, Cambridge, UK). Interspike interval represents the time difference between two consecutive action potentials. Action potential frequency was calculated as the reciprocal of the mean of interspike intervals. The coefficient of variation (standard deviation divided by the mean) of interspike intervals was analysed with Origin software to evaluate the regularity of firing.

Biophysical properties of SFO neurons measured in current clamp configuration

Resting membrane potential, input resistance and threshold of action potential generation for SFO neurons were measured using current clamp. Resting membrane potential was directly read from the PatchMaster software (HEKA Elektronik) when there was no current injection. Input resistance, a reflection of cell excitability, was determined using a series of 1500mS 5pA current steps starting from -20pA. According to Ohm's law R = V/I, input resistance was calculated from dividing membrane potential of each voltage trace by the corresponding injecting current. Threshold of generation of action potential, also a reflection of excitability, was determined using a 100mS depolarizing current ramp of 20pA from a hyperpolarizing pre-step of -10pA. The first derivative curves, which represent the rate of depolarization, were generated from voltage traces and smoothed with Savitzky-Golay Smooth (25 points) using Origin software.

Threshold was determined at the point where first derivative of the voltage trace was 10mV/ms (Fry, 2006).

Na^+ and K^+ channel properties

Voltage clamp was used to analyse Na^+ current properties including voltage dependence of activation and inactivation, transient current density, persistent current and time-dependent recovery from inactivation, and K^+ current properties including voltage dependence of activation, inactivation, and current density. In order to determine the voltage dependence of activation and transient current density of voltage-gated Na^+ current, cells were subjected to a series of 10ms depolarizing voltage steps in 10mV increments from -85mV to +35mV from a holding potential at -105mV. I-V curve was plotted from the measurement of peak current I from each current trace. Reversal potential E_{Na} was determined from I-V curve. Peak conductance (g) for each voltage step was calculated from the equation $g = I/(V_m - E_{Na})$ where V_m was membrane potential. The normalized conductance curve was fitted with Boltzmann function $G/Gmax = 1/(1 + \exp[(V-V_{1/2})/k])$ using Origin software, to determine voltage of half activation $V_{1/2}$ and slope factor k. Current density was calculated from dividing peak current by cell capacitance, which represents cell surface area. To examine the voltage dependence of inactivation of voltage-gated Na^+ current, a two-pulse stimulation protocol was applied to cells from a holding potential at -115mV. The first pulse contained a series of 200ms depolarizing steps in 10mV increments, followed by a 10ms -15mV test pulse. The normalized conductance curves were fitted with Boltzmann function where $V_{1/2}$ and k were determined. To investigate persistent Na^+ current, a 1200ms 110mV voltage ramp from a holding potential of -105mV was applied to cell. Liner leakage current was

subtracted from current traces using Origin Software. Persistent Na^+ density was calculated from dividing peak persistent Na^+ current by peak transient Na^+ current. To examine the time-dependent recovery of Na^+ channel from inactivation, cells were depolarized by two 5mV pulses from a holding potential at -105mV, separated by a variable interpulse interval of 2ms to 1400ms. The fraction of recovery was calculated by dividing the peak current elicited from the second voltage step by the peak current from the first voltage step, plotted and fitted with a double exponential function: $I(t) = A0 + A1 \times e^{-t/\tau 1} + A2 \times e^{-t/\tau 2}$. A0, A1 and A2 were constants, t was time, and $\tau 1$ and $\tau 2$ were time constants for fast and slow components, respectively.

K^+ current properties were analysed from current traces elicited from a series of 100ms depolarizing voltage steps in 10mV increments from -95mV to +35mV from a holding potential at -105mV. To investigate K^+ current activation, peak K^+ current elicited from different membrane potentials from -95 to 35mV was measured, normalized and plotted as conductance curves. To study K^+ current density, the peak K^+ current at 35mV was measured and divided by cell capacitance. The proportion of K^+ current inactivation was calculated from dividing the difference between peak K^+ current and K^+ current at 100ms by the peak K^+ current at 35mV. The time points at the peak K^+ current indicating K^+ channel types were also measured and compared.

Statistics

Patch clamp data were compared between SmartFlare positive and SmartFlare negative neurons. Shapiro-Wilk test was applied to determine the normality of data. Student's t-test was used to test for significance if data were normally distributed. If data were rejected from normal distribution by the normality test, or normality could not be

assumed, non-parametric Mann-Whitney test was used to test for statistically significant differences. Difference was considered significant at the level of 0.05. All statistics were carried out in Origin software (OriginPro 9.1). Data were plotted as mean ± standard error of the mean.

The outliers were calculated using an online outlier calculator (http://www.miniwebtool.com/outlier-calculator/). The calculator considered a number as an outlier when the number was below Q1 - 1.5×IQR or exceeded Q3 + 1.5×IQR, where Q represented the quartile and the IQR was the value of Q3 - Q1 (Q1 was the value at 25% of the data, Q3 was the value at 75% of the data) (Moore and McCabe, 1993).

3. Results

3.1. Investigation of Nav1.3 distribution in the SFO

3.1.1. Expression of Nav1.3 on dissociated SFO neurons

A previous study demonstrated Nav1.3 mRNA expression within the SFO (Hindmarch et al., 2008). In the present study, ICC for Nav1.3 on dissociated SFO neurons was carried out to investigate whether Nav1.3 expression was in neuronal cell bodies, neurites, or glia cells. ICC result was visualized using ApoTome microscope, showing the expression of Nav1.3 was on the cell membrane and in cytoplasm of neuronal cell bodies (Figure 3-1).

IH for Nav1.3 on SFO sections were also carried out to investigate if the Nav1.3 expression was in a consistent pattern in dissociated SFO neurons and SFO sections. The Nav1.3 IH image taken using ApoTome microscope demonstrated a low level of Nav1.3 staining in nuclei and a ring-like pattern of Nav1.3 expression in SFO neurons (Figure 3-2), indicating the expression was on SFO neuronal cell membrane and in cytoplasm, which was consistent with the expression pattern on isolated SFO neurons and consistent with expected ion channel staining (Berret et al., 2013).

3.1.2. Nav1.3 expression is higher in the pSFO

IH for Nav1.3, Calb and Calr were carried out on SFO sections to investigate the distribution of Nav1.3 in the pSFO versus the cSFO. Consistent with previous study (McKinley et al., 2003), Calb and Calr were expressed in the cSFO and pSFO subregions, respectively (Figure 3-3 A,B). The IH for Nav1.3 showed Nav1.3 expression was mainly in pSFO subregion, consistent with the pattern of Calr expression (Figure 3-3 C).

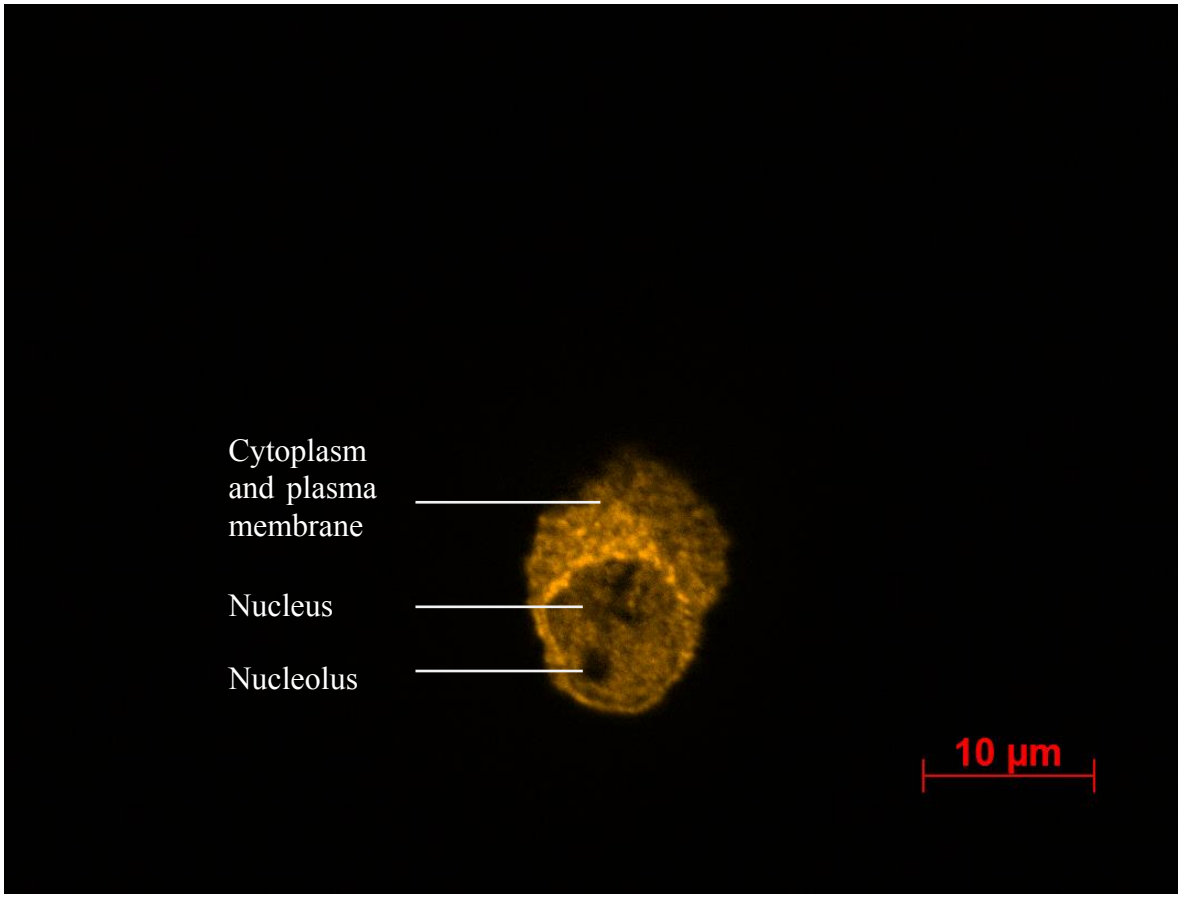

Figure 3-1. ICC for Nav1.3 in dissociated culture of SFO neuron revealed Nav1.3 localized on plasma membrane or/and in cytoplasm of SFO neuronal cell body. *Scale bar = 10µm.*

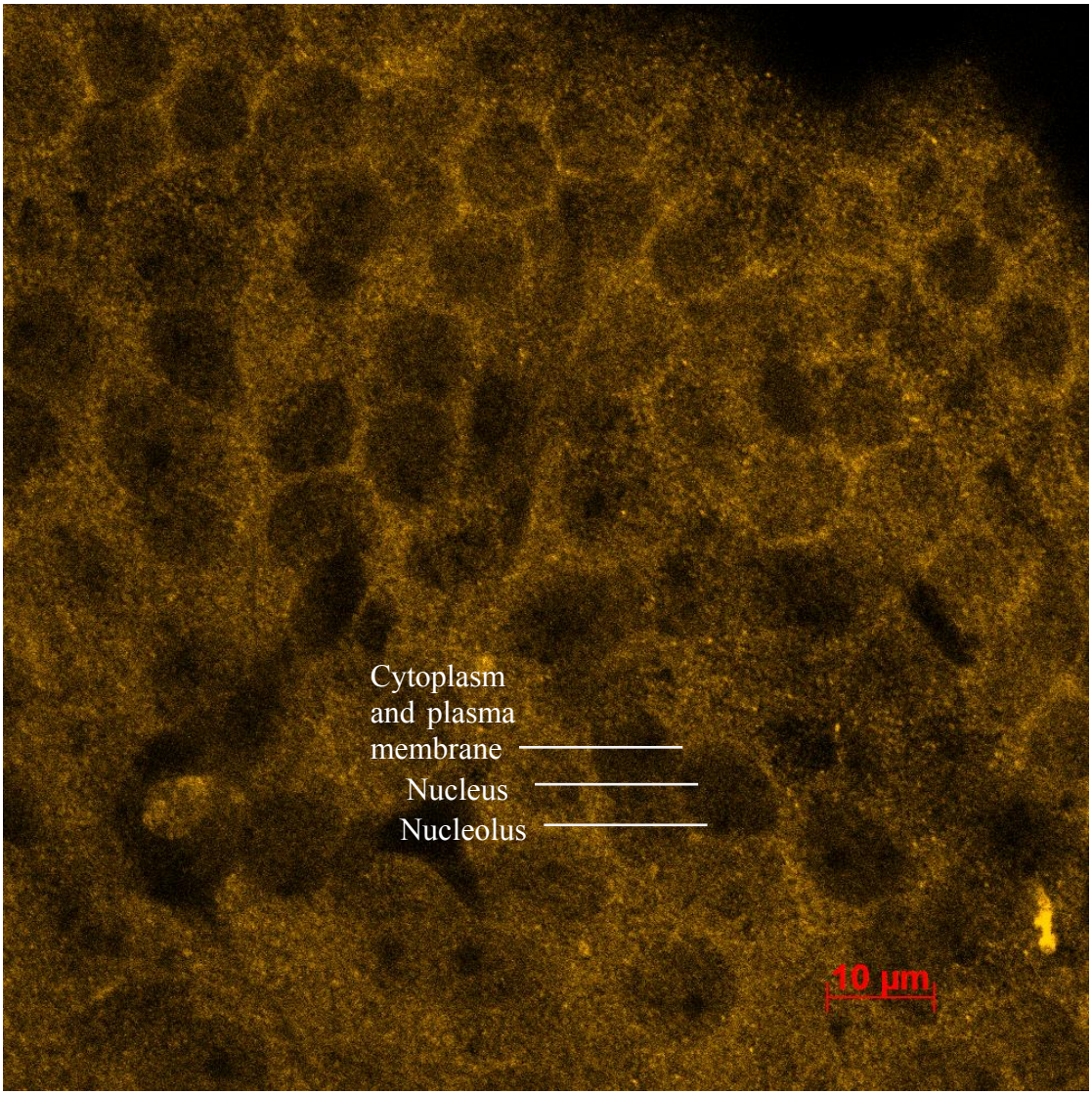

Figure 3-2. IH for Nav1.3 showed a ring-like pattern of expression. The IH signals from nuclei of SFO neurons were very low, compared to the stronger signals surrounding nuclei, indicating Nav1.3 expression was localized on neuronal cell membrane or/and in cytoplasm. Image was taken from the pSFO subregion. *Scale bar = 10µm.*

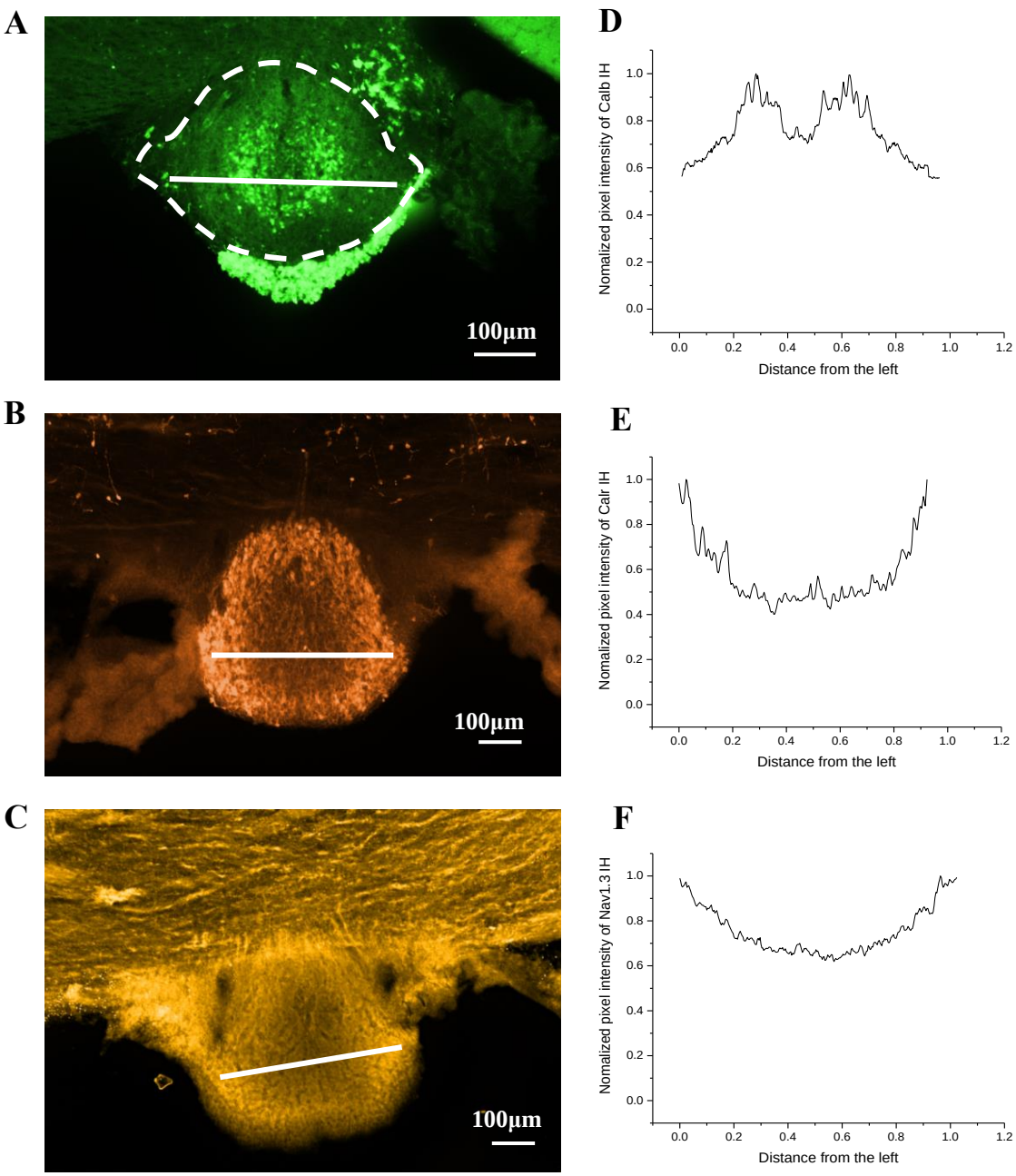

Figure 3-3. IH of Calb, Calr and Nav1.3 demonstrated Nav1.3 expression was mainly in the pSFO subregion. (A,B,C) IH for Calb, Calr and Nav1.3 on SFO sections. B and C were carried out on adjacent sections. The white dashed line in A delineates the SFO. The solid white lines in A, B, and C indicate where the pixel intensities were measured. (D,E,F) Nomalized pixel intensity of Calb, Calr and Nav1.3 signals, together with A,B, and C, showed Calb expression was in the cSFO; Nav1.3 expressions was in consistent pattern with Calr expression and was mainly in the pSFO. *Scale bar = 100µm*.

The pixel intensities through the core region of SFO for Calb, Calr and Nav1.3 staining were measured and plotted. The pixel intensity curve was normalized to a range between 0 to 1. Normalized pixel intensity curve of Calb signals indicated Calb expression is higher in the cSFO and lower (background level) in the pSFO (Figure 3-3). The normalized pixel intensity curves showed the signal intensities for both Nav1.3 and Calr staining was low in the middle which was the cSFO subregion, and much higher at each end which represents the pSFO subregion (Figure 3-3). The distribution of the pixel value curve for Nav1.3 signals was in a consistent pattern with that of Calr staining, which further demonstrated Nav1.3 expression followed Calr expression and was at a higher level in the pSFO subregion.

3.1.3. Nav1.3 antibody is specific

Preadsorption was carried out to evaluate the specificity of Nav1.3 antibody (sc-22202, Santa Cruz). The average pixel intensity in preadsorption group was higher than the negative control without primary antibody (Tukey test, $p<0.001$). However compared to Nav1.3 IH result, the preadsorption significantly decreased (Tukey test, $p<0.001$) the brightness of Nav1.3 signal and abolished the ring-like pattern of Nav1.3 staining which indicated the staining on plasma membrane (Figure 3-4 and Figure 3-5). This suggested Nav1.3 antibody effectively bound to Nav1.3 protein which showed the specificity of the antibody and suggested the Nav1.3 staining was specific.

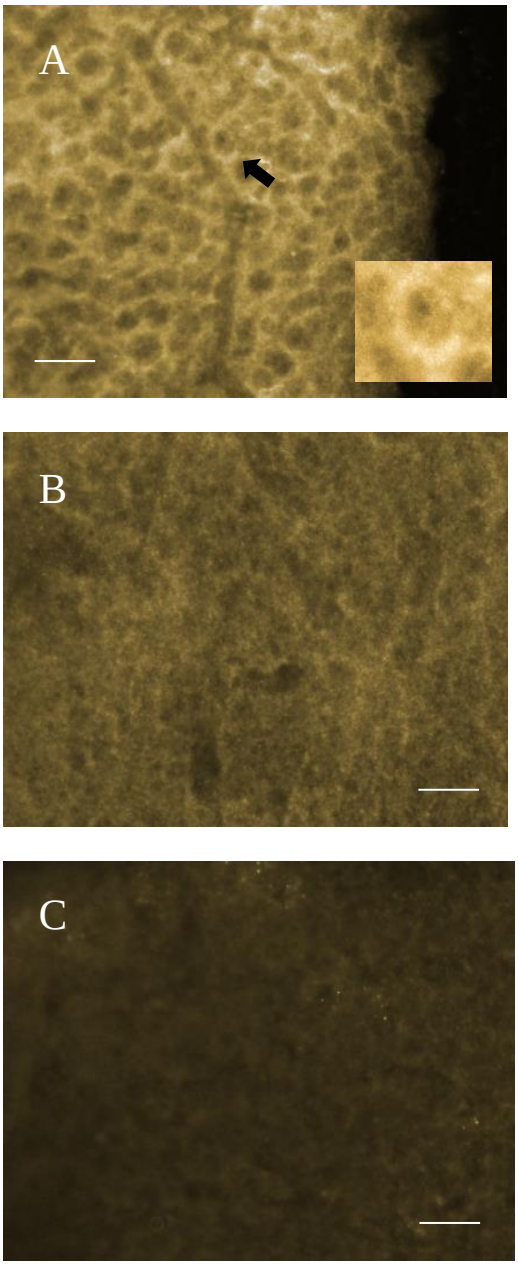

Figure 3-4. Preadsorption results demonstrated specificity of the Nav1.3 antibody. (A) IH staining for Nav1.3 on an SFO section. Inset was the same neuron indicated by the arrow, showing a ring-like pattern. (B) IH on SFO with Nav1.3 antibody preadsorbed with Nav1.3 peptide. The staining was drastically attenuated compared to A and the ring-like staining pattern was abolished. (C) Negative control without primary antibody. *Scale bar = 10µm*. Image A, B and C were taken at the same camera setting. IH of the three sections were carried out in parallel.

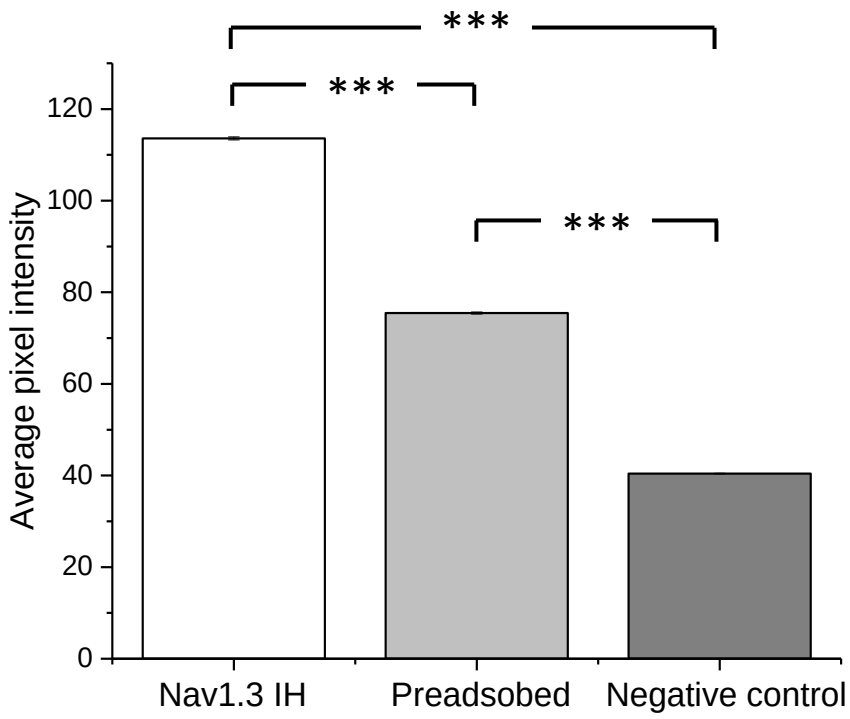

Figure 3-5. Bar graph showing preadsorption of antibody reduced staining, demonstrating specificity of the Nav1.3 antibody. The average pixel intensities of the Nav1.3 signal were measured in the preadsorption group and the control groups. The difference between the three groups was significant (One-way ANOVA, $p<0.001$). Tukey's post-hoc test showed significant difference of pixel intensity between the preadsorption group and Nav1.3 IH without preadsorption treatment and also between the preadsorbed and negative control groups ($p<0.001$), suggesting preadsorption of Nav1.3 antibody could efficiently attenuate (but not completely abolish) the staining.

3.2. Investigation of electrophysiological differences between cSFO and non-cSFO neurons

Our IH results demonstrated the higher expression of Nav1.3 in pSFO neurons. Given Nav1.3 is one of the main contributors to the Na^+ current in SFO neurons, we aimed to carry out patch clamp recording to further investigate whether this differential expression was associated with different intrinsic electrical properties of neurons from cSFO and pSFO subregions.

In order to do this, a strategy to identify Calb from Calr neurons had to be developed. Thus the novel SmartFlare RNA probe from Millipore was used in the present study. SmartFlare reagent enables the identification because Calb mainly expressed in the cSFO. Theoretically, the probe is uptaken by all neurons and only those with Calb mRNA fluoresce. In a preliminary set of experiments the sensitivity and specificity of the SmartFlare probe was evaluated. First double ICC for Calb and Calr was carried out to investigate the proportion of Calb and Calr neurons in the SFO culture, and the proportion of overlap which were neurons that express both Calb and Calr (Section 3.2.1). In the double ICC, Calb antibody was used to label Calb neurons. Second, cells were treated with uptake control (positive control) of SmartFlare reagent, which was structurally similar with Calb SmartFlare probe but always fluoresce. The uptake control demonstrated the SmartFlare probe could be absorbed well into the SFO neurons and also gave a referential positive level of the SmartFlare signal (Figure 3-6).

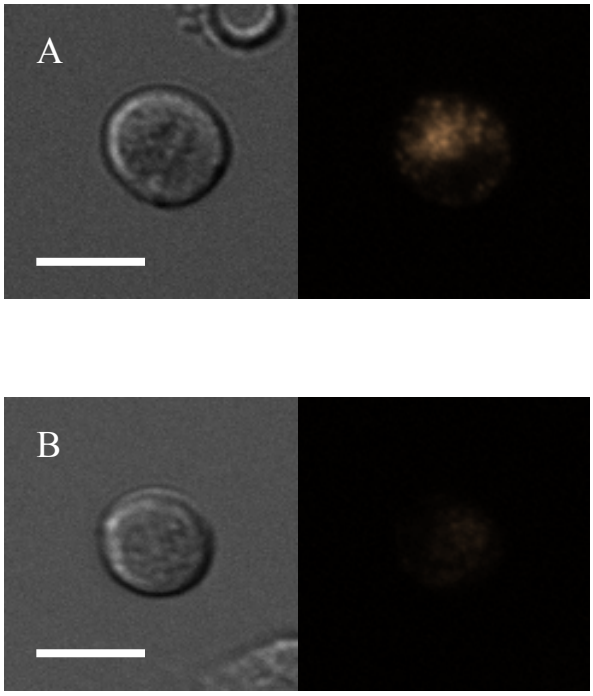

Figure 3-6. Positive and negative controls demonstrated referential positive and negative levels of SmartFlare signals. (A) SmartFlare Cy3 signal from an SFO neuron treated with uptake positive control. On the left is bright field, and the right is the Cy3 fluorescent signal from the same cell. (B) SmartFlare Cy3 signal from an SFO neuron treated with scrambled negative control. A and B were taken using the same camera setting. *Scale bar = 10µm.*

Next, cells were treated with scrambled control (negative control) for SmartFlare reagent, which contained capture strands that match any mRNA in a cell thus demonstrated the background level of the SmartFlare probe (Figure 3-6). Afterwards, the proportion of Calb and Calr neurons in SFO culture was examined again but using SmartFlare reagent for Calb to label the Calb neurons (Section 3.2.1). Additionally, the correlation between Calb ICC signal and Calb SmartFlare signal was examined.

3.2.1. Calb SmartFlare RNA probe is consistent with Calb ICC

Double ICC experiments for Calb and Calr were carried out on dissociated SFO neurons to investigate the proportions of Calb and Calr neurons and the overlap of Calb and Calr signals (Figure 3-7). According to the expression pattern of Calb and Calr showed in the IH results, Calb and Calr do not usually express in the same SFO neurons. Therefore few neuron showing overlap of Calb and Calr signal would be expected in the double ICC result.

For the Calb and Calr double ICC, 90 cells from three sets of SFO cultures were examined. Of the 90 cells, 21 (23%) cells were only Calb positive and 41 (46%) cells were only Calr positive. There were 25 (28%) cells that were neither Calb nor Calr positive, while only 3 (3%) cells showed positive in both Calb and Calr signals (Figure 3-8).

The 3 cells had overlap of Calb and Calr signal in double ICC result indicated that 3 of 24 (12.5%) neurons chance to be Calr positive if Calb positive, and 3 of 44 (7%) neurons chance to be Calb positive if Calr possible.

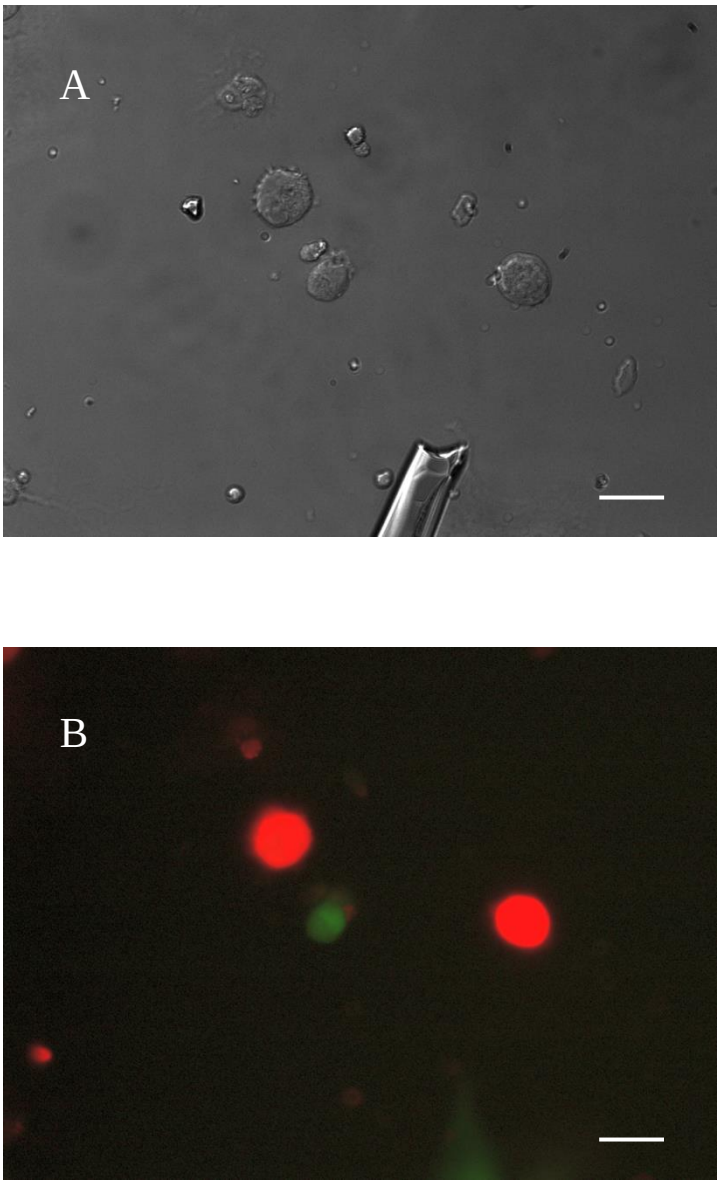

Figure 3-7. Double ICC images of dissociated SFO neurons express Calb (green) and Calr (red). (A) Brightfield channel. (B) Overlap of Calb (Alex Fluor 488) and Calr (Cy3) fluorescent signal. *Scale bar = 10μm.*

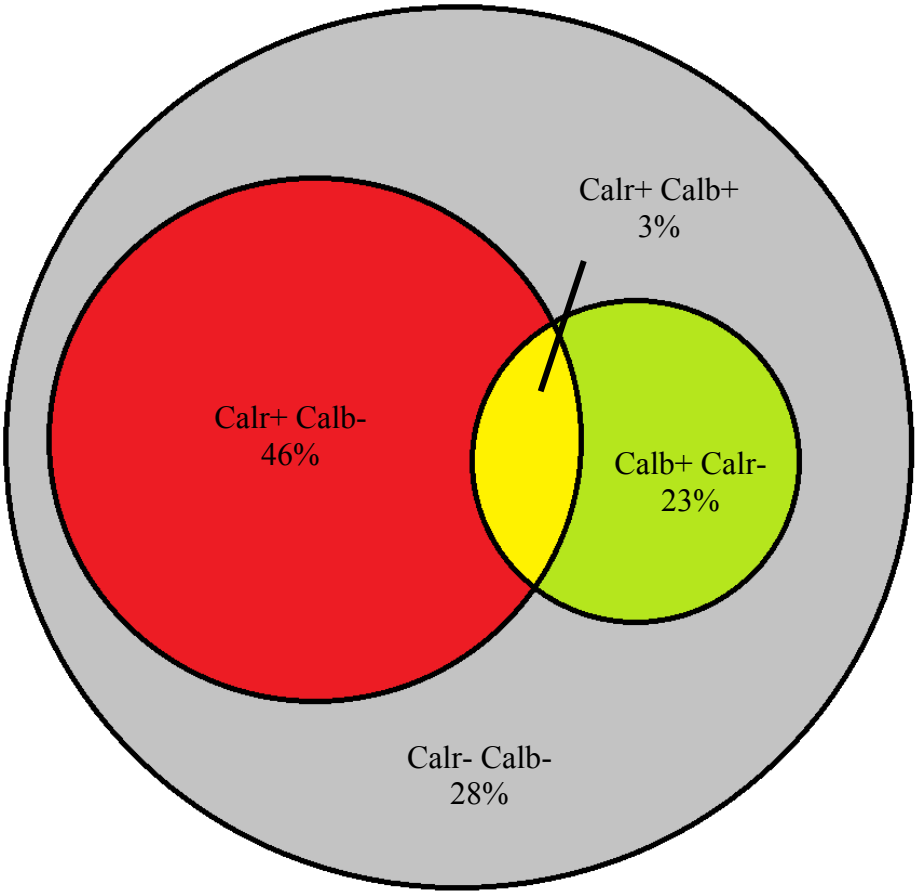

Figure 3-8. The proportion of Calb and Calr SFO neurons according to double ICC results. Among 90 cells from three replications, 46% cells were only Calr positive (red), 23% were only Calb positive (green), 28% were neither Calb nor Calr positive (grey), and 3% were positive in both (yellow). (Positive: +; Negative: -)

Calr ICC on Calb SmartFlare treated neurons

In order to investigate the sensitivity and specificity of Calb SmartFlare reagent, after the double ICC, Calr ICC was carried out on Calb SmartFlare treated cells. This experiment was fundamentally the same as the double ICC but using SmartFlare for Calb instead of Calb antibody to label the Calb SFO neurons.

The pixel intensity of both Calr ICC signal and Calb SmartFlare signal was measured from each cell and plotted as scatter plot (Figure 3-9). The pixel density of Calr ICC at 10000 was the threshold of Calr signal. Cells above the Calr threshold are considered as Calr positive cells. The pixel intensity of Calb SmartFlare at 1069 was the threshold for Calb SmartFlare signal, determined by the positive uptake control and negative scrambled control for SmartFlare reagent. Cells to the right of the threshold are considered as Calb positive cells. The result showed among 43 neurons from three replications, 20 (47%) were Calr positive, 5 (12%) were Calb positive, 2 (5%) had signal for both Calb and Calr and 16 (37%) had signal for neither.

Fisher's exact test showed the proportions of Calb positive neurons labeled by Calb antibody (26%) and SmartFlare (16%) were not significantly different ($p=0.273$), suggesting though the sensitivity of SmartFlare shows a lower trend compared to Calb antibody, the sensitivity of the SmartFlare probe is still satisfying. The proportion of SFO neurons showing both Calb and Calr signals in double ICC (3%) and Calr ICC on SmartFlare treated neurons (5%) was also compared using fisher's exact test, which shows no significant difference between the two groups ($p=0.658$), suggesting good specificity of the SmartFlare probe. We further used fisher's exact test to compare the proportions of neurons showing Calb signal, Calr signal, both signals and no signal

between double ICC and Calr staining on SmartFlare treated neurons, and there is no significant different between the two groups (p=0.357). This data suggests that SmartFlare Calb signal is consistent with ICC Calb signal, demonstrating SmartFlare probe is an efficient reagent for identification of Calb neurons in SFO cultures.

Calb ICC on Calb SmartFlare treated neurons

To further determine the correlation between Calb SmartFlare signal and Calb ICC signal, ICC of Calb on SmartFlare treated cells (n=83, three replications in total) were carried out.

The pixel intensity of both Calb ICC signal and Calb SmartFlare signal was measured from each cell and plotted as scatter plot (Figure 3-10). Cells with Calb ICC pixel intensity above 2000 were considered as Calb ICC positive cells. Cells with Calb SmartFlare pixel intensity above 1250 were considered as SmartFlare positive cells.

The scatter plot did not show a linear correlation between the Calb ICC and Calb SmartFlare signal.

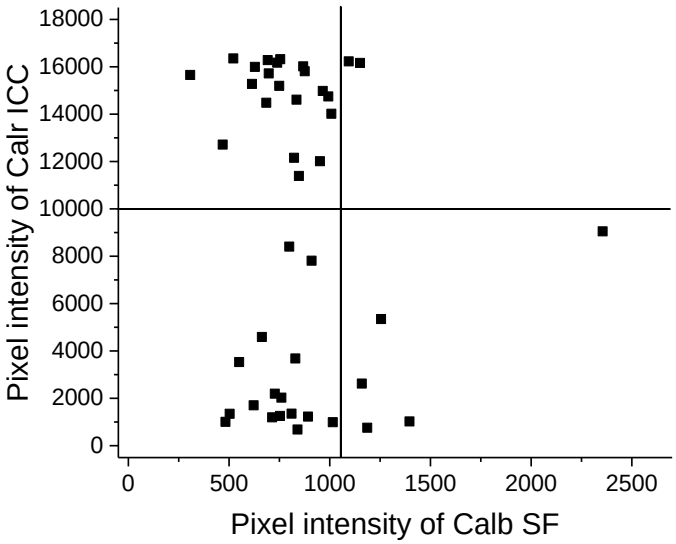

Figure 3-9. Scatter plot of pixel intensity of Calr ICC signal and Calb SmartFlare (SF) signal. Cells with Calr signal exceeding 10000 are considered as Calr positive cells. Cells with SmartFlare signal exceeding 1069 are considered as Calb positive cells. Among 43 neurons from three replications, 20 (47%) were Calr positive, 5 (12%) were Calb positive, 2 (5%) had signal for both Calb and Calr and 16 (37%) had signal for neither.

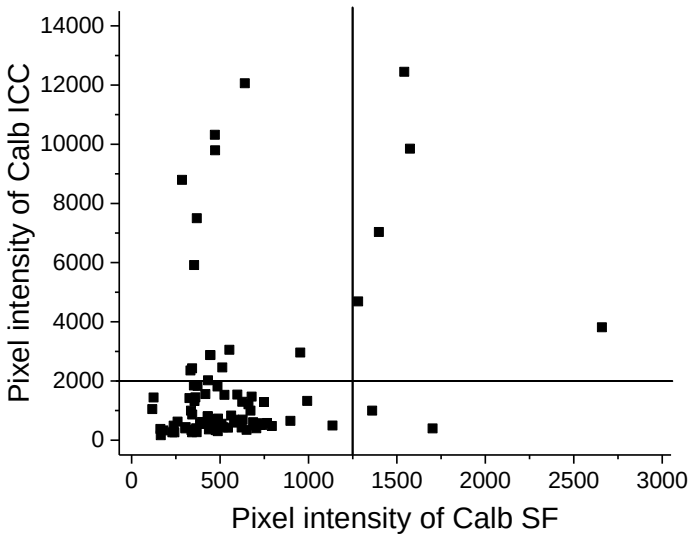

Figure 3-10. Scatter plot of pixel intensity of Calb ICC signal and Calb SmartFlare (SF) signal. Cells with Calb signal exceeding 2000 are considered as Calb positive cells. Cells with SmartFlare signal exceeding 1250 are considered as Calb positive cells. The scatter plot did not show a linear correlation between the Calb ICC and Calb SmartFlare signal.

3.2.2. Patch clamp recording results

Non-cSFO and cSFO neurons demonstrated different spontaneous activity which related to hyperpolarized resting membrane potential

Given that the SmartFlare reagent was shown to be adequate for identification of putative cSFO neurons in dissociated culture, patch clamp recordings were carried out on both SmartFlare positive and negative neurons (Figure 3-11) to analyse and compare the intrinsic electrophysiological properties between *putative* cSFO and *putative* non-cSFO neurons respectively. We measured spontaneous action potential activity, biophysical properties and Na^+ and K^+ current properties. The results are discussed in turn.

Cell-attached voltage clamp recording was carried out to study spontaneous action potential activity. In cell-attached recording, 52% (22 of 42) of non-cSFO neurons demonstrated spontaneous action potential activity, which was much lower compared to 78% (21 of 27) of cSFO neurons ($p<0.05$, Chi-square test). Spontaneous action potential frequency was compared between the non-cSFO and cSFO neurons which demonstrated spontaneous activity. Normality could not be assumed in the distribution of action potential firing frequency in both non-cSFO and cSFO neurons. Mann-Whitney test was applied and showed the mean spontaneous action potential firing frequency in non-cSFO neurons was significantly higher compared to that in cSFO neurons ($p=0.012$), suggesting an elevated activity in non-cSFO neurons (Figure 3-12). The median of the mean action potential frequency was 3.77 and 1.95times/s in the non-cSFO and cSFO neurons, respectively.

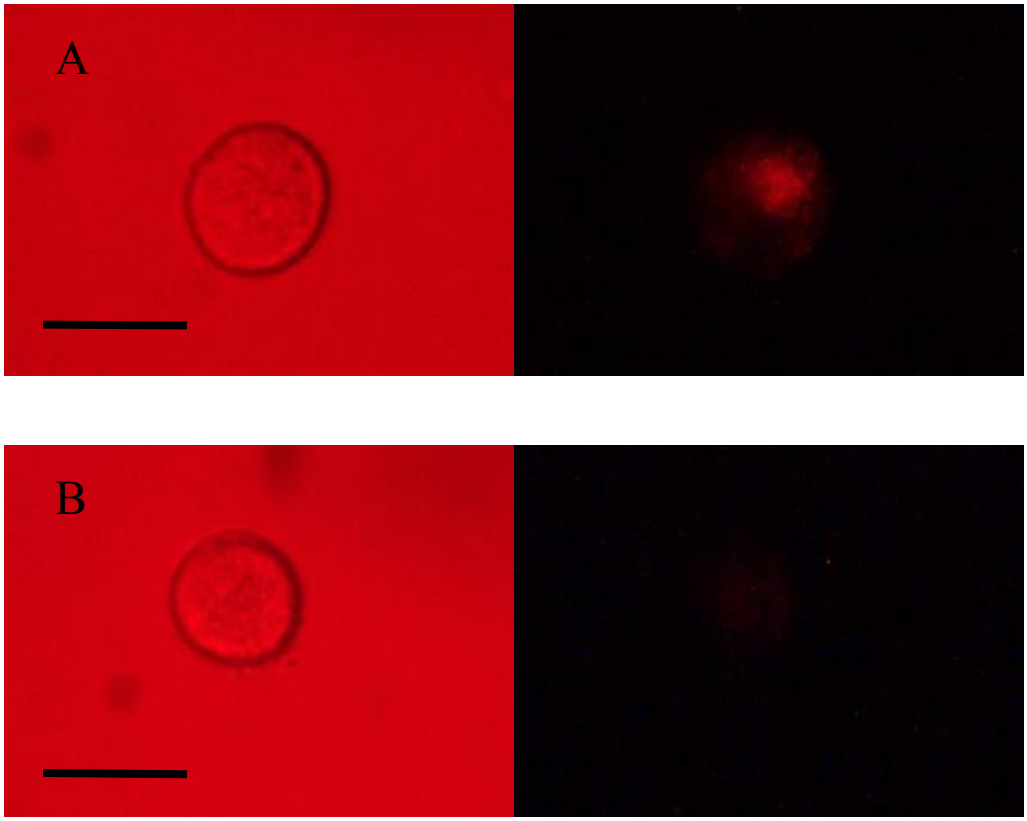

Figure 3-11. SmartFlare positive and negative neurons in patch clamp recording. (A) A representative putative cSFO neuron showed strong SmartFlare Cy3 signal under an epi-fluorescence microscope for patch clamp recording (Zeiss IM35). On the left is bright field, and the right is the Cy3 fluorescent signal from the same cell. (B) A representative non-cSFO neuron showed no SmartFlare signal. *Scale bar = 10μm.*

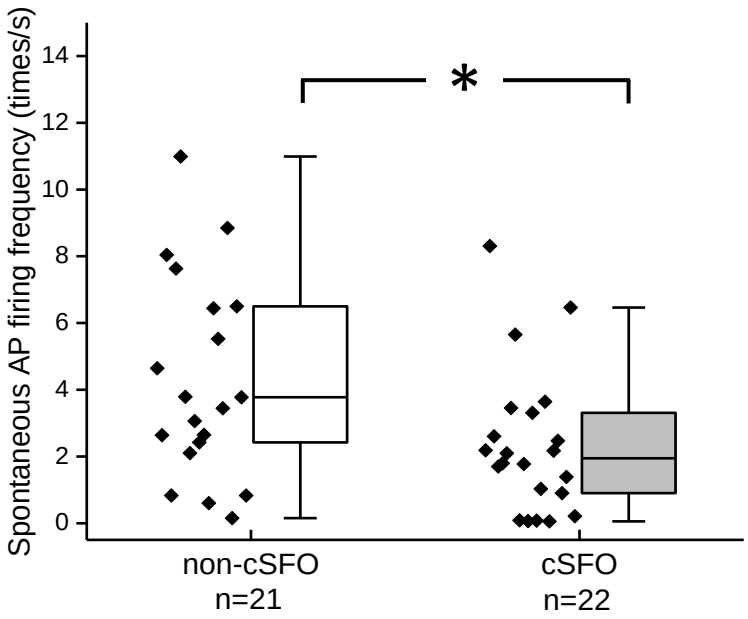

Figure 3-12. Box plot demonstrating that among the spontaneously active neurons, non-cSFO neurons showed a significantly higher spontaneous action potential (AP) frequency compared to cSFO neurons (Mann-Whitney test, $p<0.05$). The median of the interspike intervals was 3.77s in non-cSFO neurons and 1.95times/s in cSFO neurons.

Among neurons with spontaneous activity, non-cSFO neurons mainly showed a regular action potential firing behaviour (Figure 3-13, A), while cSFO neurons tended to fire in a bursting pattern (Figure 3-13, B). The coefficient of variation of interspike intervals was compared between the non-cSFO and cSFO neurons to determine if the observed difference in spontaneous action potential firing patterns was statistically significant. Normality could not be assumed in the distribution of the coefficient of variation of interspike intervals. Thus a Mann-Whitney test was applied for the statistical test for coefficient of variation. The coefficient of variation of interspike intervals was significantly lower ($p=0.025$) in non-cSFO neurons (Figure 3-14), which was consistent with an observed more regular action potential firing behaviour in non-cSFO neurons and a more bursting action potential firing pattern in cSFO neurons.

In order to investigate mechanisms that may lead to the differences in spontaneous activates, biophysical properties including resting membrane potential (RMP), cell capacitance, cell input resistance and action potential threshold were examined.

RMP was measured in current clamp recording when there was no injected current. RMP in non-cSFO neurons was -41 ± 1.5 mV, which was significantly more depolarized compared to -47 ± 2.2 mV in cSFO neurons (t-test, $p=0.017$) (Figure 3-15). The more depolarized RMP in non-cSFO neurons was consistent with the higher spontaneous action potential firing frequency, suggesting higher cell excitability.

Cell capacitance indicated cell surface area. Student's t-test showed no difference in cell capacitance between non-cSFO and cSFO neurons ($p=0.277$) (Figure 3-16), which suggested cSFO and non-cSFO neurons had similar cell body size.

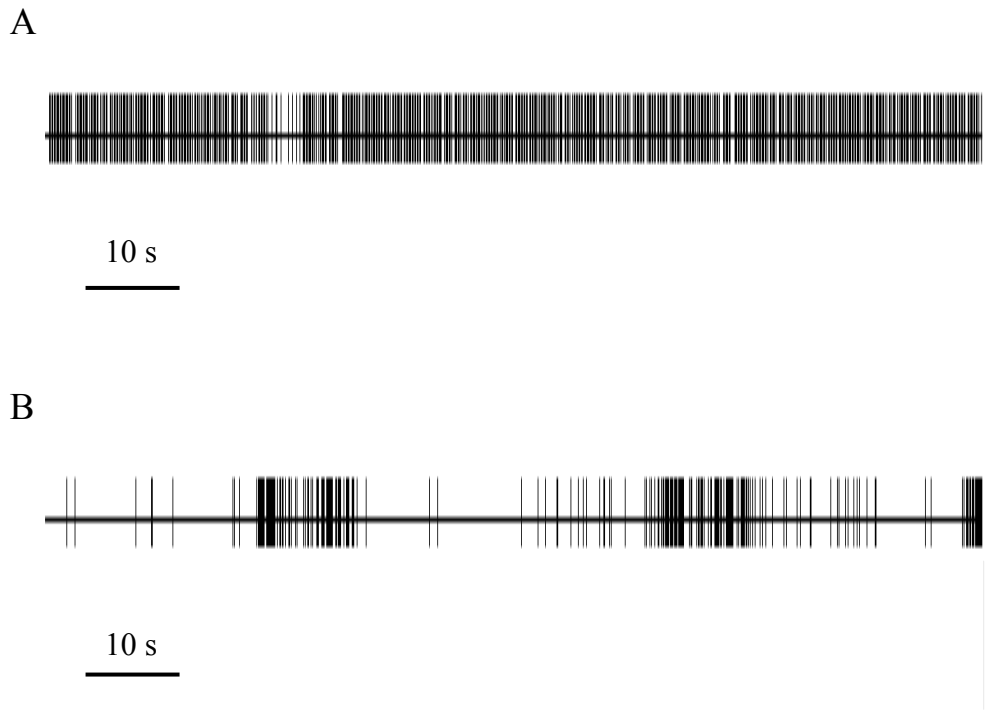

Figure 3-13. Typical action potential firing patterns in non-cSFO and cSFO neurons. (A) Non-cSFO neurons mainly demonstrated a regular action potential firing pattern. (B) Most cSFO neurons showed bursting action potential firing pattern. Each spike represents an action potential.

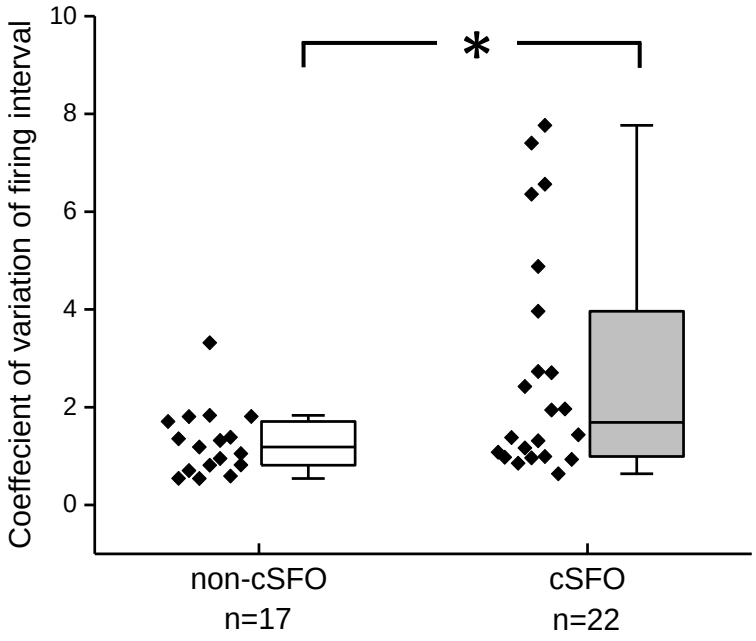

Figure 3-14. Box plot of the coefficient of variation of action potential interspike intervals. The coefficient of variation was significantly lower in non-cSFO neurons compared to cSFO neurons (Mann-Whitney test, $p<0.05$).

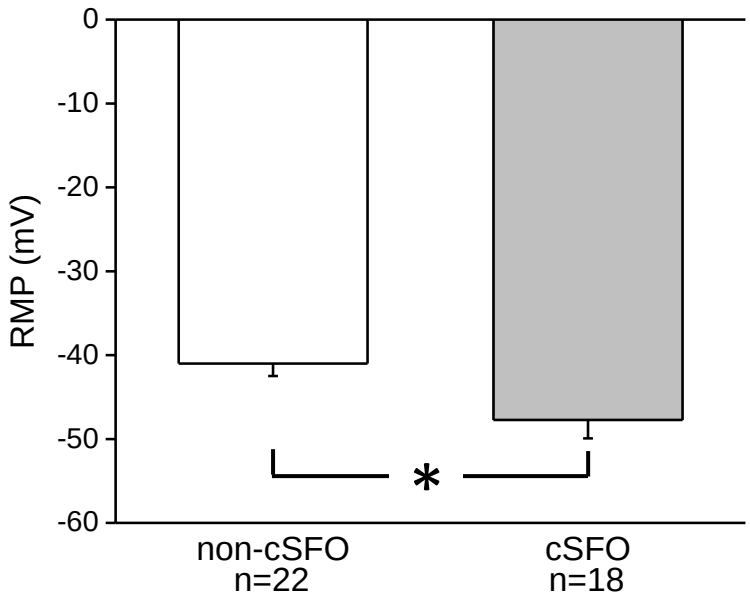

Figure 3-15. Bar graph showing RMP of non-cSFO neurons was significantly more depolarized compared to that in cSFO neurons (t-test, $p<0.05$).

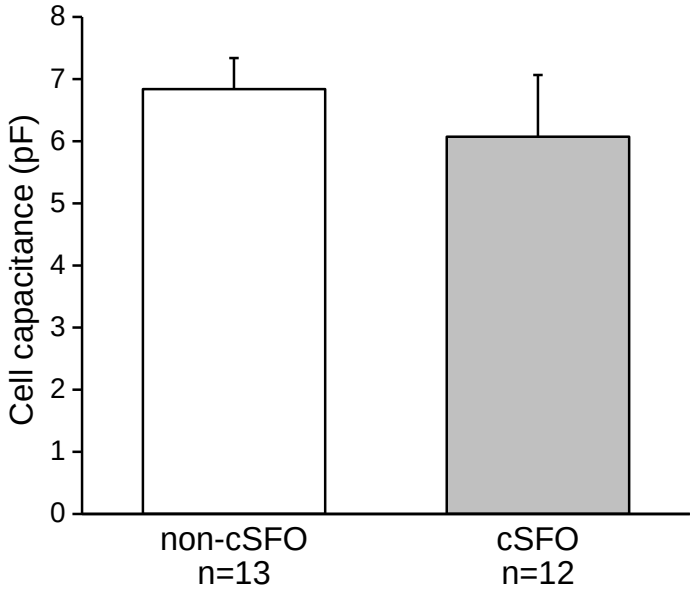

Figure 3-16. Bar graph showing no difference was observed in cell capacitance between non-cSFO and cSFO neurons (t-test, p=0.277).

Cell input resistance was calculated from dividing membrane potential by injected current (Figure 3-17). Higher input resistance can suggest higher cell excitability. The input resistance was 2.3±0.46 and 2.3±0.43 GΩ in the non-cSFO and cSFO neurons respectively. The input resistance did not show a significant difference between the non-cSFO and cSFO neurons (t-test, p=0.996) (Figure 3-18). This indicated the difference in spontaneous activity between cSFO and non-cSFO neurons was not caused by a difference in cell excitability induced by different cell input resistance.

Action potential threshold was calculated from the voltage trace stimulated by a current ramp. (Figure 3-19). The membrane potential where instantaneous slope reached 10mv/ms was determined as action potential threshold (Fry, 2006). Action potential threshold is a parameter that also reflects cell excitability. A more hyperpolarized action potential threshold would suggest higher cell excitability. The action potential threshold in the non-cSFO and cSFO neurons was -49±1.1 and -50±1.3 mV, respectively. Student's t-test showed no difference in action potential threshold between the non-cSFO and cSFO neurons (p=0.773) (Figure 3-20), suggesting the cSFO and non-cSFO neurons would start firing from a similar membrane potential. This eliminated the possibility that the elevated spontaneous activity in non-cSFO neurons was caused by a hyperpolarization in action potential threshold.

Investigation of Na^+ and K^+ current properties of the non-cSFO and cSFO neurons

To further investigate the potential mechanism for a higher spontaneous action potential frequency and more depolarized RMP in non-cSFO neurons, Na^+ and K^+ current properties were examined.

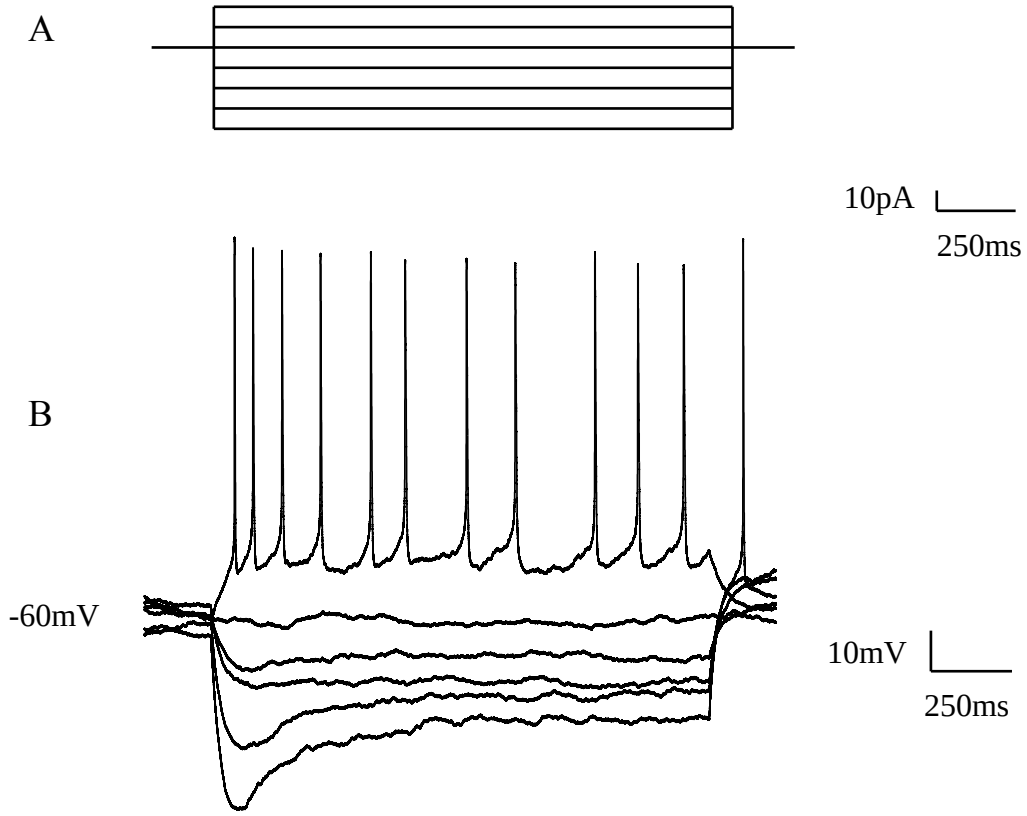

Figure 3-17. Input resistance was calculated using a series of current steps. (A) Cells were stimulated with a series of 1500ms 5pA current steps starting from -20pA. (B) Representative voltage traces showing changes in membrane potential in response to injected currents.

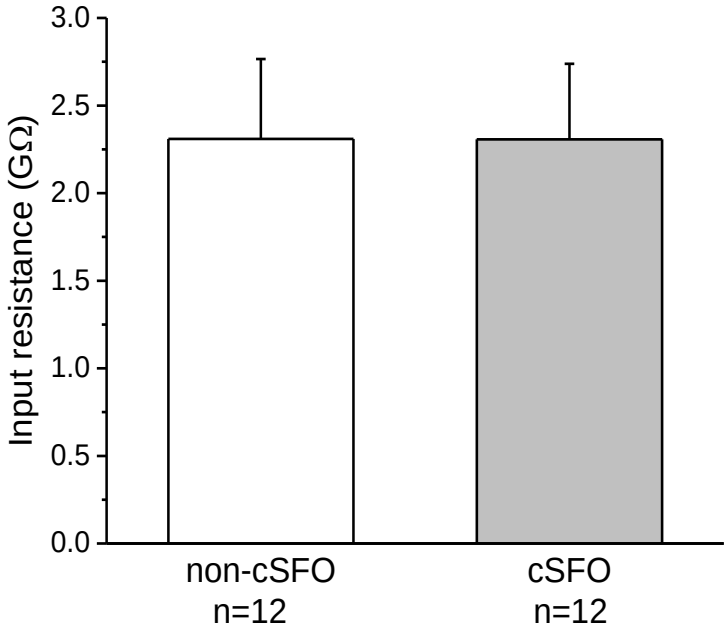

Figure 3-18. Bar graph showing no difference in the input resistance was found between non-cSFO and cSFO neurons (t-test, p=0.996).

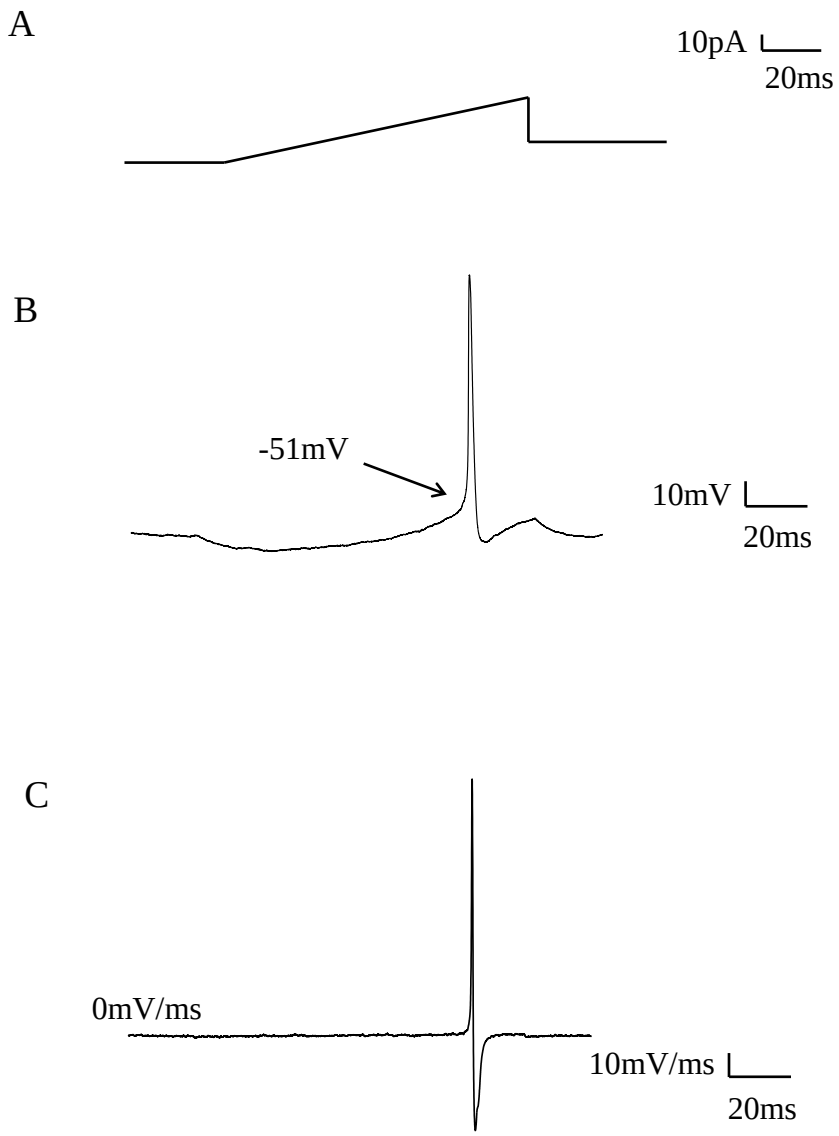

Figure 3-19. Action potential threshold was determined using a depolarizing current ramp. (A) The injected current ramp stimulation protocol for determining action potential threshold. (B) A representative voltage trace stimulated by the current ramp. (C) First derivative of the voltage trace (representing instantaneous slope).

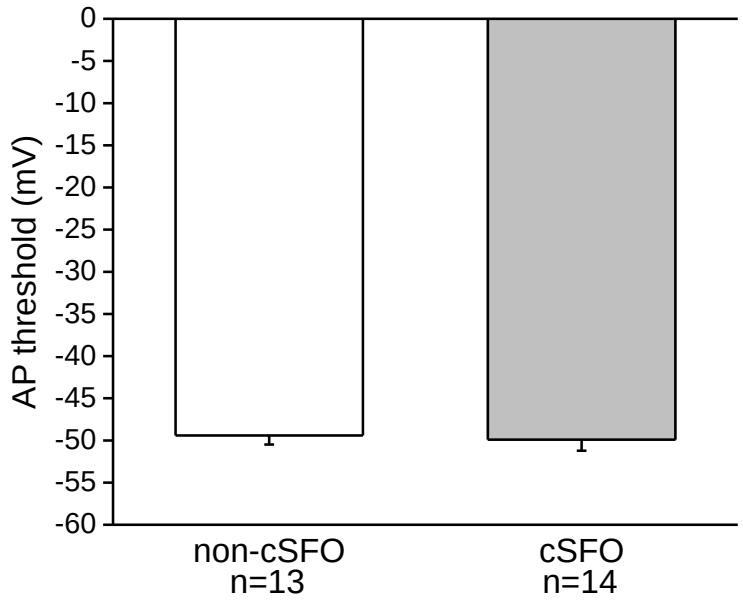

Figure 3-20. Bar graph showing no difference in the action potential threshold was found between non-cSFO and cSFO neurons (t-test, p=0.773).

Na^+, K^+ current are important to study because they are responsible for different phases of an action potential. An action potential consists of a depolarizing phase, a repolarizing phase and a hyperpolarizing phase (refractory period). When the membrane potential exceeds the threshold for action potential, NaCh are activated, leading to the depolarizing phase. The depolarized membrane potential then start inactivating Na^+ channels and activates voltage-dependent K^+ channels, leading to the repolarizing phase. The voltage-gated K^+ channels remain open after the membrane potential is restored, which leads to the hyperpolarizing phase. The hyperpolarizing phase is important for cell excitability and the time phase of action potentials, which can be influenced by K^+ current density and K^+ channel inactivation. Thus in this present study, Na^+ current properties including the voltage-dependent activation and inactivation, peak current density, persistent current, time-dependent recovery from inactivation, and K^+ current properties including the current density, activation and inactivation were investigated.

The normalized conductance curve for voltage-dependent activation of Na^+ current reflects the proportion of Na^+ channels that open at different membrane potentials. The voltage-dependent activation was determined by a series of depolarizing voltage steps (Figure 3-21). The peak current from each sweep was measured and plotted as an I-V curve (Figure 3-21). The conductance curve was calculated from the I-V curve, normalized and fitted with Boltzmann function. The $V_{1/2}$ of activation curves of the non-cSFO (n=10) and cSFO (n=16) neurons were -26.4±1.2 and -27.7±1.0mV respectively. The slope factor of activation curve in non-cSFO was 6.92±0.25 compared to 6.89±0.29 in cSFO neurons. The normalized conductance curve for voltage-dependent inactivation of Na^+ current shows the proportion of Na^+ channel that become unavailable at different

membrane potentials. The inactivation curve was determined by a two-pulse stimulation protocol (Figure 3-21). The peak current from each recorded sweep was measured (Figure 3-21), and the fraction of inactivation at different membrane potentials was calculated, plotted and fitted with Boltzmann function. The $V_{1/2}$ of inactivation curves was

-64.9±2.0mV in non-cSFO neurons (n=12) and -63.9±2.2mV in cSFO neurons (n=10). The slope factors of inactivation curve were 6.88±0.38 and 6.70±0.41 in non-cSFO and cSFO neurons, respectively. In both voltage-dependent Na^+ current activation and inactivation curves, there was no significant difference in $V_{1/2}$ or slope factor between the non-cSFO and cSFO neurons (t-test, $p>0.05$) (Figure 3-21). This excluded the possibility that the difference in spontaneous activity between the non-cSFO and cSFO neurons resulted from different kinetics in Na^+ current activation or inactivation.

The Na^+ current density in non-cSFO neurons was -0.64±0.14nA/pF, which was much greater compared to -0.39±0.06nA/pF in cSFO neurons. Though the difference did not reach statistical significance (t-test, $p=0.051$) (Figure 3-22), it is still worth noting because a higher Na^+ current density suggested a higher NaCh density, which would increase the chance that NaCh being activated thus resulting in a higher spontaneous action potential firing frequency.

The recovery of Na^+ channel from inactivation gate is a rate limiting factor for generation of a second action potential. The time-dependent recovery from inactivation of Na^+ current was studied using a two-pulse stimulating protocol (Figure 3-23). The fractional recovery was fitted to a double exponential function (Figure 3-23).

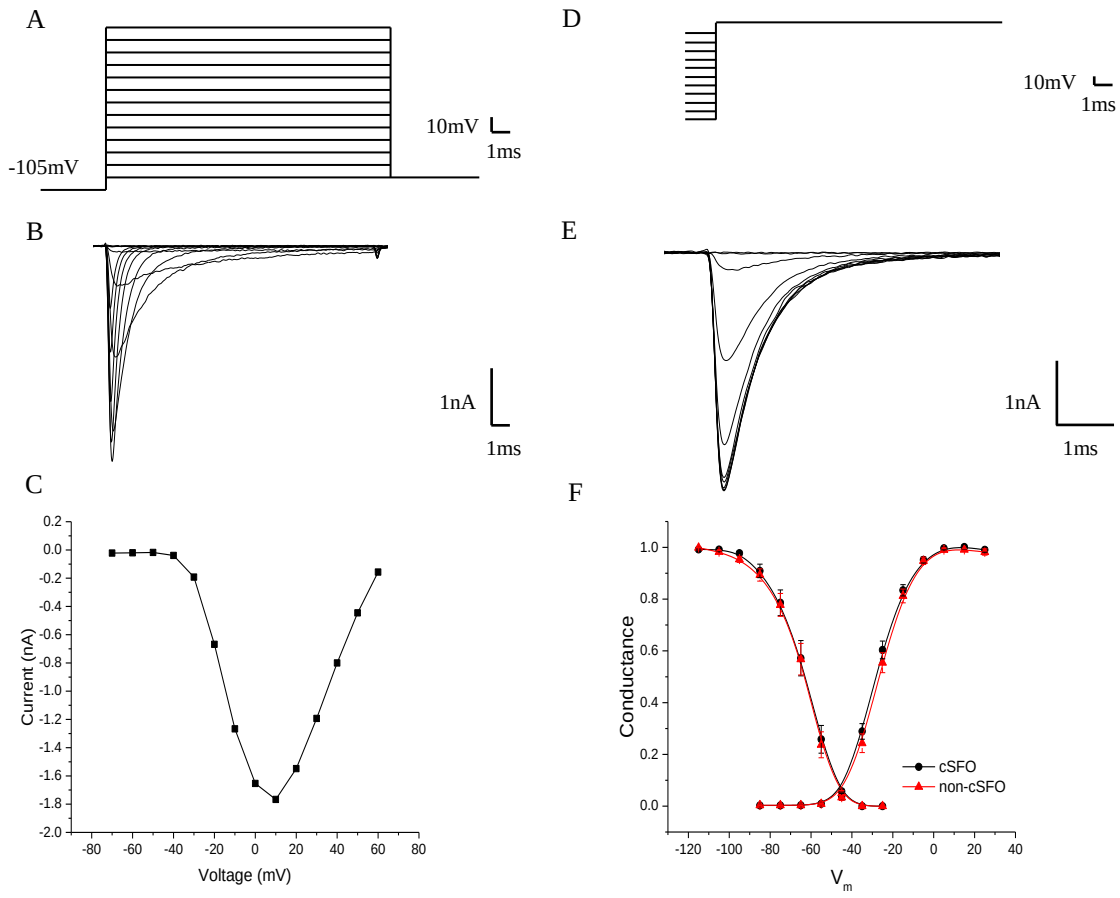

Figure 3-21. (A) A series of 10mS depolarizing voltage steps in 10mV increments was used for studying voltage dependent activation of Na^+ current. (B) Representative current traces elicited by A. Peak current from each trace was measured and plotted as (C) an I-V curve. (D) A pre-pulse stimulation contains a series of 10mV depolarizing pre-potentials followed by a test pulse was used for studying voltage-dependent inactivation of Na^+ current. (E) Representative current traces elicited by D. (F) Normalized conductance curves of voltage-dependent activation and inactivation of Na^+ current (red triangle: cSFO neurons; black square: non-cSFO neurons. n=10 to 16). In both voltage-dependent Na^+ current activation and inactivation curves, there was no significant difference in $V_{1/2}$ or slope factor between the non-cSFO and cSFO neurons (t-test, $p>0.05$).

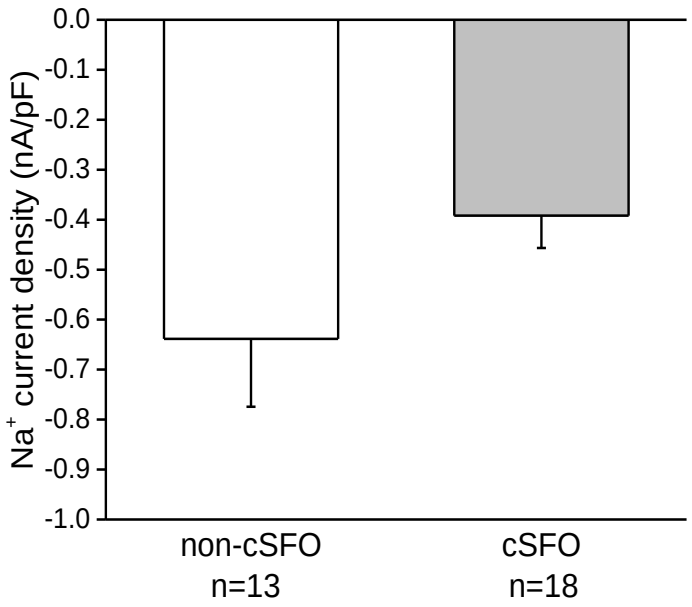

Figure 3-22. Na^+ current density in non-cSFO neurons was -0.64±0.14nA/pF, which was 39% higher compared to -0.39±0.06nA/pF in cSFO neurons. However the difference did not reach statistical significance (t-test, p=0.051).

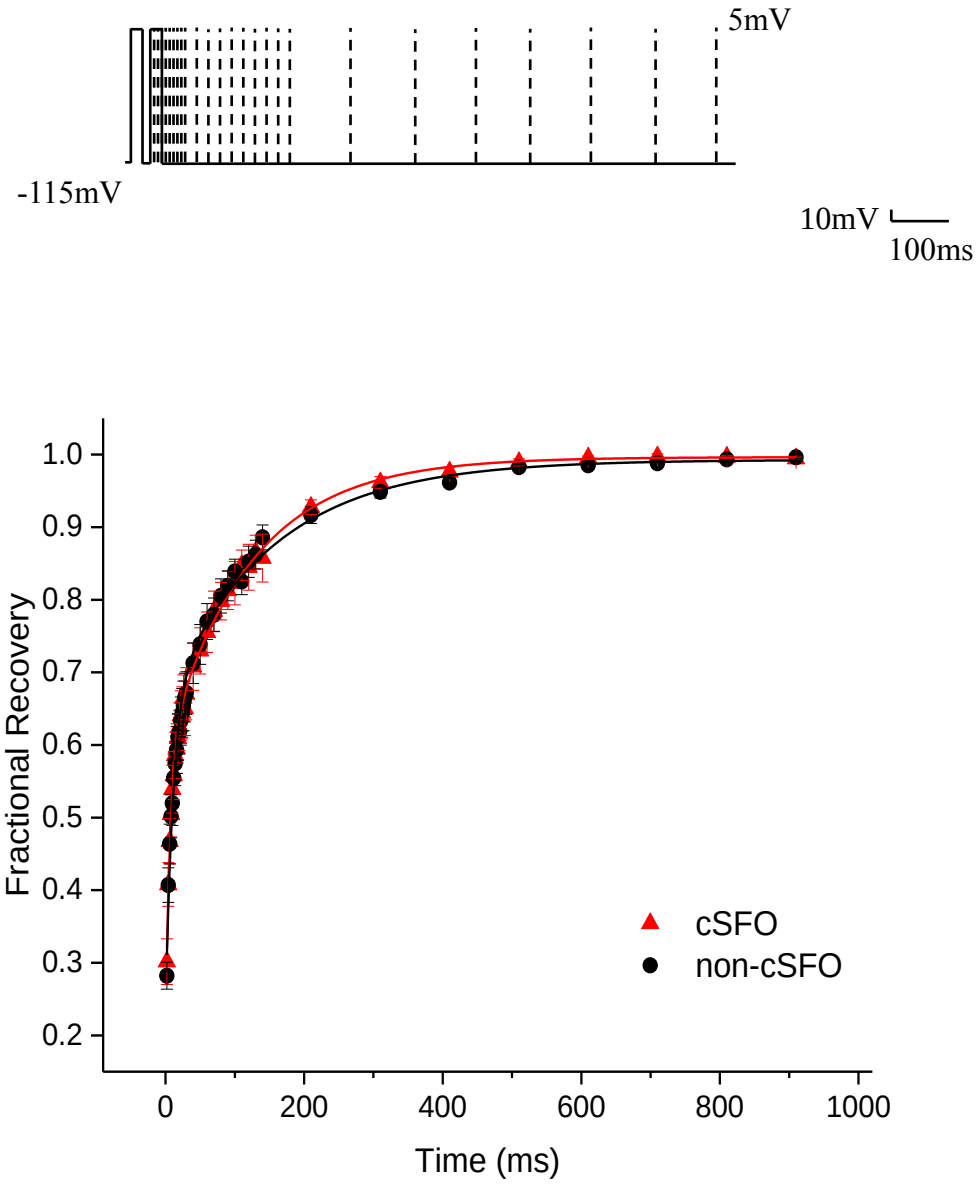

Figure 3-23. (A) A two-pulse protocol with inter-pulse intervals varied from 2 to 1400ms was applied to investigate time-dependent recovery of NaCh from inactivation. The dashed lines represent the starting point of the second pulse in each sweep after the first sweep. (B) The fractional recovery was plotted and fitted with a double exponential function: $I(t) = A0 + A1 \times e^{-t/\tau 1} + A2 \times e^{-t/\tau 2}$. The fast and slow components A1, A2, and the fast and slow time constants $\tau 1$, $\tau 2$ did not show a difference between the non-cSFO and cSFO neurons (t-test, $p>0.05$).

The fast and slow components A1, A2 and the fast and slow time constants $\tau 1$, $\tau 2$ determine the shape of the recovery curves and were compared between the non-cSFO (n=9) and cSFO (n=10) neurons. There was no significant difference (t-test) in any of the four variables A1 (-0.38±0.03 in non-cSFO neurons, and -0.39±0.05 in cSFO neurons, p=0.827), A2 (-0.42±0.04 in non-cSFO neurons, and -0.41±0.03 in cSFO neurons, p=0.858), $\tau 1$ (6.29±0.56 in non-cSFO neurons, and 6.82±0.60 in cSFO neurons, p=0.527), and $\tau 2$ (102.2±7.3 in non-cSFO neurons, and 107.3±8.2 in cSFO neurons, p=0.653). This suggested a similar rate of Na^+ channel recovery from inactivation between non-cSFO and cSFO neurons and the higher firing frequency in non-cSFO neurons did not result from a more rapid recovery of the Na^+ channels.

Persistent Na^+ current is the non-inactivating portion of the voltage-gated Na^+ current. Persistent Na^+ current plays a role in setting a subthreshold membrane potential and influences repetitive firing (Kiss, 2008). To determine persistent Na^+ current, neurons were subjected to a voltage ramp (Figure 3-24). Peak persistent current was measured and divided by the peak transient Na^+ current to calculate the percentage of persistent Na^+ current to the transient Na^+ current. No significant difference in persistent Na^+ current density was observed between the non-cSFO (0.61±0.04%, n=13) and cSFO (0.619±0.04%, n=16) neurons (t-test, p=0.912, Figure 3-24), which indicated the higher neuronal activity and more depolarized RMP was not a result from a larger persistent Na^+ current.

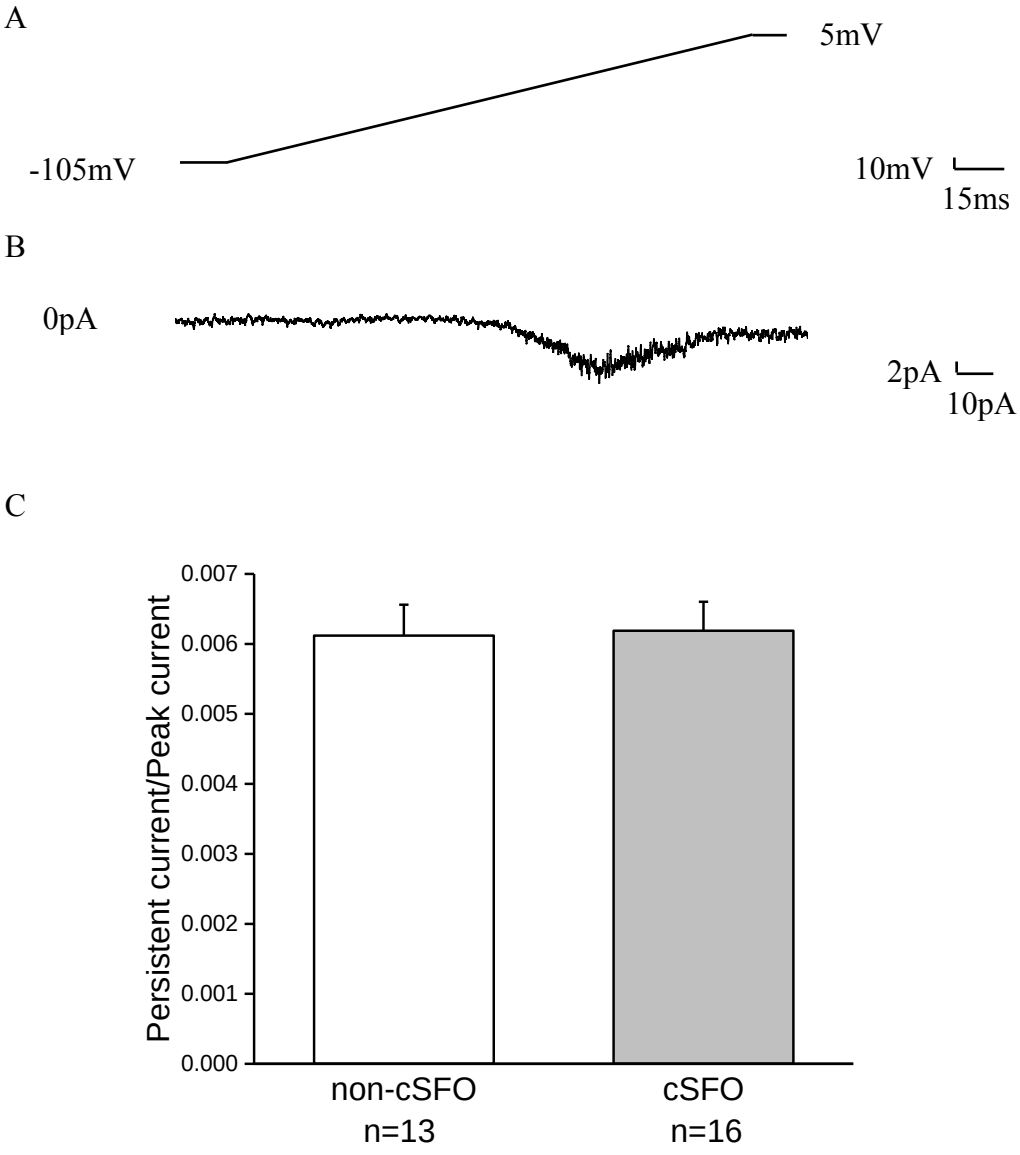

Figure 3-24. (A) To investigate persistent Na^+ current, cells were subjected to a 1200-ms voltage ramp from -105 to 5mV. (B) Representative current elicited by A.
(C) Peak persistent Na^+ current was measured from B and current density was calculated from dividing the peak current by transient Na^+ current. The persistent Na^+ current density did not show a difference between the non-cSFO and cSFO neurons (t-test, $p>0.05$).

The voltage-dependent activation of K^+ current was investigated by giving cells a series of 100-ms depolarizing voltage steps. The peak current was measured at each membrane potential and conductance was calculated and normalized. The normalized conductance curves of K^+ current activation were very similar between the non-cSFO and cSFO neurons (Figure 3-25).

K^+ current density which indicated K^+ channel density was compared between the non-cSFO and cSFO neurons (Figure 3-26). The K^+ current density was 0.25±0.02 and 0.26±0.02nA/pF in non-cSFO neurons and cSFO neurons respectively, which showed no significant difference (t-test, p=0.708).

The inactivation of K^+ current was also investigated by a series of 100ms depolarizing voltage steps in 10mV increments from a holding potential at -105mV. The fraction of K^+ current inactivation and the time at the peak current were investigated because they indicate types of K^+ current inactivation and reflect the types of K^+ channels. The peak K^+ current and K^+ current at 100ms was measured from the last sweep (at 35mV) and the fraction of inactivation was calculated and compared between the non-cSFO (32.0±3.4%, n=15) and cSFO (34.0±4.7%, n=11) neurons. The time to peak K^+ current was also measured and was 7.3±0.8ms in the non-cSFO (n=14) and 9.6±2.1ms in cSFO neurons (n=11). There was no difference in fraction of K^+ current inactivation (t-test, p=0.733) or time at the peak K^+ current (t-test, p=0.260) between the non-cSFO and cSFO neurons (Figure 3-27).

This data suggested the higher neuronal activity and more depolarized RMP in non-cSFO neurons was not a result of the difference in K^+ current properties.

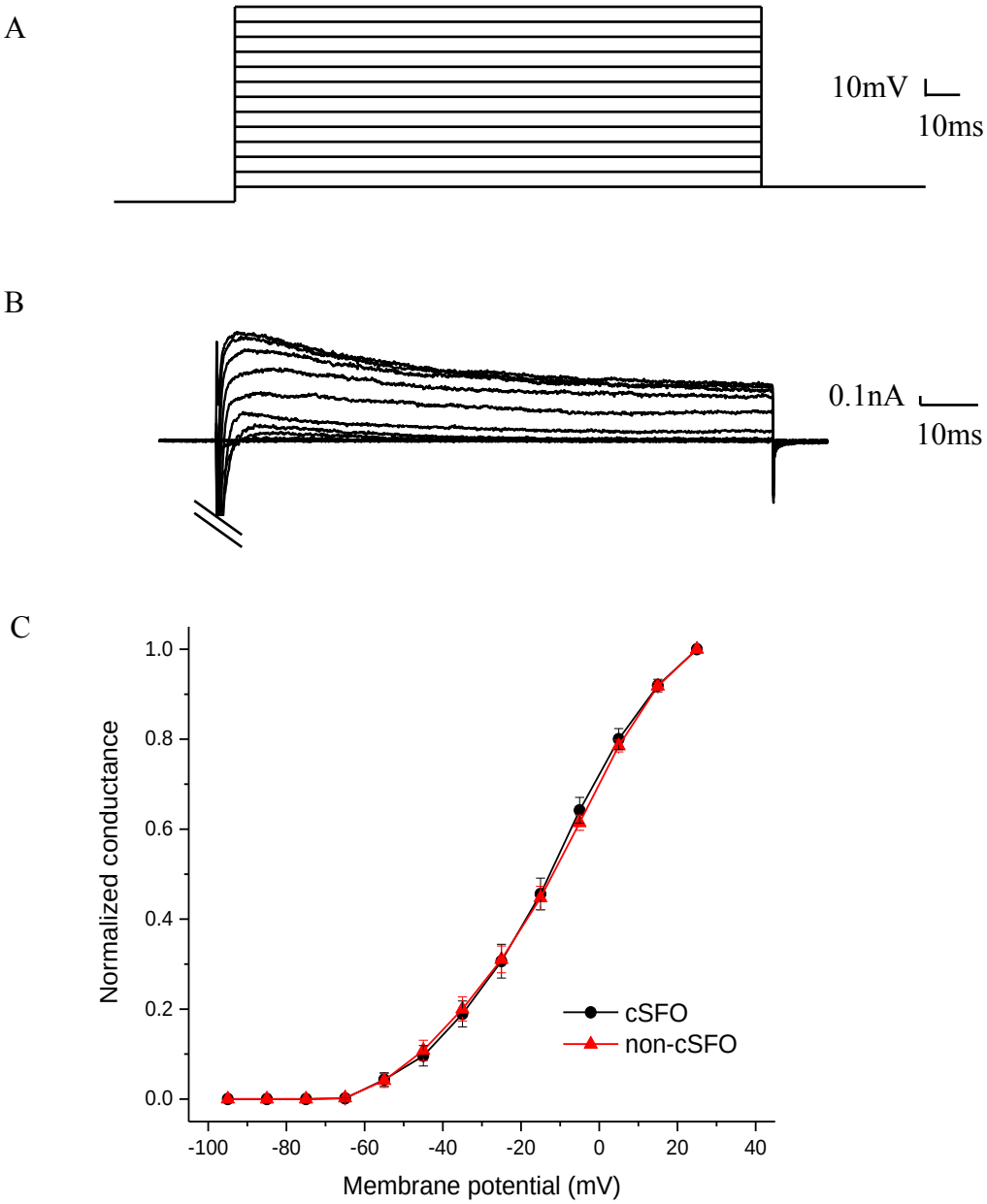

Figure 3-25. Voltage-dependent activation of K^+ current. (A) Voltage-dependent activation of K^+ current was determined using a series of 100-ms depolarizing voltage steps in 10mV increments from -95mV to +35mV from a holding potential at -105mV. (B) Representative K^+ current traces elicited by the stimulation protocol showed in A. (C) The peak current elicited by different membrane potentials were measured from B. Conductance at each membrane potential was normalized and plotted as activation curves. The activation curves of K^+ current were very similar between cSFO and non-cSFO neurons.

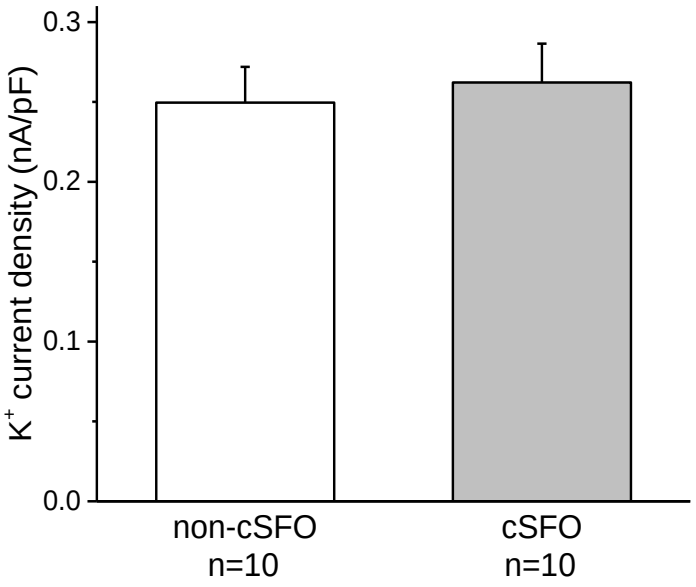

Figure 3-26. K^+ current density was calculated by dividing the peak current at 35mV by cell capacitance. No significant difference was observed between non-cSFO and cSFO neurons (t-test, p=0.708).

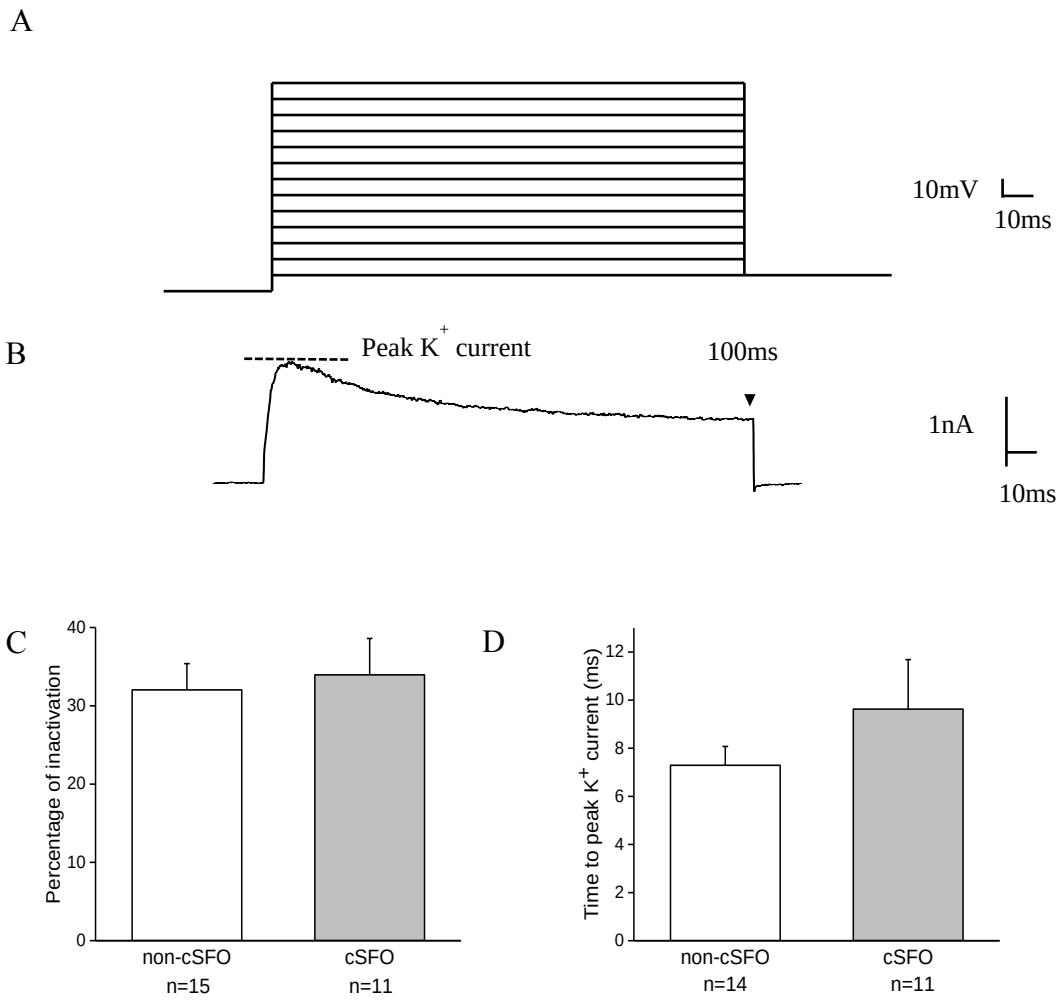

Figure 3-27. (A) In order to study K^+ current inactivation, a series of 100-mS depolarizing voltage steps in 10mV increments was used. (B) Representative K^+ current elicited by the last sweep from A. (C) The peak K^+ current and K^+ current at 100ms were measured and the fraction of inactivation was calculated and compared. There was no difference in fraction of K^+ current inactivation between non-cSFO and cSFO neurons (t-test, p=0.733). (D) Time to peak K^+ current was also measured and did not show a difference between the non-cSFO and cSFO neurons (t-test, p=0.260).

4. Discussion

This study demonstrated higher expression of Nav1.3 in pSFO subregion and differences in electrophysiology between neurons in the cSFO and pSFO subregions. This study was the first to show that Nav1.3 protein is expressed on neuronal cell bodies within the SFO. Additionally, Nav1.3 distribution followed Calr expression, which was mainly in pSFO subregion. Because Nav1.3 is one of the key contributors for Na^+ current in SFO neurons, this study also investigated if electrical properties were different between neurons from the cSFO and pSFO subregions. This study was the first to use SmartFlare reagent, an mRNA probe for live cells, to identify dissociated cSFO and non-cSFO neurons and compare the electrophysiological properties between them. Patch clamp recording demonstrated a higher spontaneous action potential firing frequency in non-cSFO neurons and a bursting pattern of action potential firing in cSFO neurons. Further investigation suggested the elevated spontaneous activity in non-cSFO neurons was related to a more depolarized resting membrane potential and a trend towards higher Na^+ current density.

4.1. Nav1.3 expression on the SFO

This present study was the first to use immunostaining to investigate Nav1.3 expression in SFO. The ICC and IH results not only demonstrated expression of Nav1.3 on SFO neuronal cell bodies but also revealed a higher expression level in the pSFO subregion compared to the cSFO. The immunostaining results were consistent with previous studies showing expression of Nav1.3 mRNA on the SFO (Hindmarch et al.,

2008, unpublished data by Wong), but were more in detail by providing the distribution patterns in isolated SFO neurons and also in different SFO subregions.

Immunostaining for NaCh is very challenging. According to microarray analysis results (Hindmarch et al., 2008), among the ten isoforms of the NaCh, Nav1.1, Nav1.2, Nav1.3, Nav1.7 and Na_X are expressed in the SFO. Before this present study, only the distribution of the voltage sensor Na_X has been revealed by immunostaining (Nehme et al., 2012, Berret et al., 2013). One challenge of the NaCh immunostaining comes from the low expression level of NaCh, which gives very weak staining signal. The other challenge is due to that fixation procedure can weaken or abolish the immunostaining signal of NaCh, and light fixation (2-4h) makes it very difficult to obtain thin tissue sections using vibratome. However, in order to have good resolution of the immunostaining signal, thin section (less than the diameter of cells) is required because overlap of cells can increase background noise. Thus, a balance between the signal brightness (determined by fixation time) and resolution (determined by section thickness) can be crucial to the success in NaCh immunostaining. In this present study, brain tissue was fixed for 3.5h and optimally 20μm tissue sections through the SFO were made. The diameter of SFO neurons was 10 to 15μm in this study and the 20μm thickness would still result in overlap of neurons. To optimize the signal resolution, Apotome microscope was used for the IH and ICC image because it allows focus for fine layers of tissue and reduction of scattered light. Antigen retrieval was tested in Nav1.3 IH, aiming to improving signal brightness but failed because it introduced background noise and resulted in false staining (data not shown).

The present data showed that Nav1.3 was mainly expressed in pSFO subregion, consistent with Calr expression. This expression pattern of Nav1.3 is unique and important. Compared to present study, Na_X which is one of the NaCh did not show differential expression between the cSFO and pSFO subregion (Nehme et al., 2012). Calr is a Ca^{2+} binding protein, which involved in Ca^{2+} signaling (Edmonds et al., 2000, Schwaller et al., 2002). Interestingly, though Calb and Calr proteins have similar structure and functions, they are often complementary in the central nervous system and show low degree of overlap (Dong, 2008). This distribution is poorly understood. The consistent expression pattern of Nav1.3 and Calr in the SFO suggested a possibility that Nav1.3 related to Calr signaling in the SFO and the co-expression of Nav1.3 might contribute to a different physiological role of Calr in SFO compared to that of Calb, which would be interesting future directions to investigate. In addition, relaxin activates the pSFO instead of cSFO neurons, and the role of Nav1.3 in relaxin singnaling pathway in SFO is also worth investigating.

In this study, the ICC and IH results revealed there was Nav1.3 expression in cytoplasm or plasma membrane of the SFO neurons. Berret et al. (2013) used 4',6-diamidino-2-phenylindole (DAPI) to label the neuronal nucleus to locate the Na_X staining on SFO neurons and demonstrated Na_X expression in cytoplasm and plasma membrane, which was in a consistent pattern with the Nav1.3 expression in present study. The expression pattern of Nav1.3 observed in present ICC and IH results was consistent with the NaCh expression pattern not only in SFO neurons, but also in other neurons or different cell types (Weiss et al., 2011, Black et al., 2012, Ednie et al., 2013, Cheng et al., 2014).

4.2. Intrinsic electrical properties of SFO neurons reported by present and previous studies were consistent

Several previous studies have characterized the intrinsic electrophysiological properties of SFO neurons. Among those electrical properties reported by previous studies, most of them were consistent with the present data, qualifying the cell condition and patch clamp recording skill in this study. From the double ICC, the proportion of non-cSFO and cSFO neurons was 46% and 23% respectively, so the value of some electrical properties such as action potential frequency, resting membrane potential reported in previous studies were closer to the values of non-cSFO neurons in the present study.

In the present study, in spontaneously active non-cSFO neurons the median action potential frequency was found to be 3.77spikes/s and in spontaneously active cSFO neurons the median action potential frequency was 1.95spikes/s. As reported by Okuya et al. (1987), in a cell-attached configuration, the mean action potential frequency of spontaneously active SFO neurons was 4.63spikes/s. The median as opposed the mean was reported in the present study because normality could not be assumed for the distribution of the data and the non-parametric Mann-Whitney test was used for statistics. The portion of spontaneously active SFO neurons was 52% in non-cSFO neurons and 78% in cSFO neurons in this present study, compared to 53% reported by Washburn et al. (2000).

For the biophysical properties in this present study, the resting membrane potential in the non-cSFO and cSFO neurons was -47±2.2 and -41±1.5mV respectively.

The input resistance was high and was 2.3±0.46GΩ, which showed no difference between the non-cSFO and cSFO neurons. A whole-cell study on forebrain slices by Ferguson and Li (1996) also characterized the basic electrical properties of SFO neurons including the mean resting membrane potential at -57±2.5mV, and a high cell input resistance of 0.9±0.1GΩ. Pulman et al. (2006) and Smith et al. (2009) separately reported that the mean resting membrane potential of dissociated SFO neurons was -48±1.2mV and -49±2.1mV respectively, which were more depolarized compared to Ferguson and Li's result though dissociation procedure should not cause change in electrophysiological properties (Ferguson and Bains, 1996). Besides resting membrane potential, Pulman et al. (2006) and Alim et al. (2010) also revealed a high mean input resistance of 1.5-2.2GΩ. Because patch clamp in this study was carried out on dissociated neurons, the resting membrane potential and input resistance in present study were more consistent with previous data on dissociated SFO neurons compared to that on tissue sections.

In the present study, for Na^+ current properties, the peak transient current amplitude was found to be -2.89±0.3nA in non-cSFO neurons and -2.91±0.4 in cSFO neurons. NaCh began to activate at approximately -55mV. The $V_{1/2}$ and slope factor of activation was -26.4 to -27.7mV and 6.89 to 6.92 respectively. Those data were consistent with the Na^+ current properties reported by Fry and Ferguson (2007b). For the voltage-dependent inactivation, Na^+ current started inactivating at approximately -100mV and the $V_{1/2}$ and slope factor was -63.9 to -64.9 and 6.70 to 6.88 respectively, which was more hyperpolarized compared to previous study (Fry and Ferguson, 2007b). The time constants τ_1 and τ_2 in the double exponential curve for time-dependent recovery from inactivation was 6.29 to 6.82 and 102.2 to 107.3 respectively, which varied from the

published values (Fry and Ferguson, 2007b) and the variation might be caused by a difference in holding potential. In addition, the mean persistent current amplitude was 21.9±2.8pA in this study which was much smaller compared to 68.5±15.4pA reported by Fry and Ferguson (2007b).

4.3. Different spontaneous activity in the cSFO and non-cSFO neurons and possible mechanisms

This present study suggested cSFO neurons could be characterized by a bursting firing behaviour in spontaneous action potential firing. Bursting pattern in action potential firing behaviour in SFO neurons has been previously described by Washburn et al. (2000). They reported 9 out of 15 SFO neurons exhibited bursting behaviour in their *in vivo* single unit recording, and indicated the proportion of the SFO neurons showing a bursting spontaneous activity was comparable to the proportion of ANG-immunoreactive neurons in SFO. Interestingly, both the ANG II receptor AT1 and ANG II is mainly expressed in cSFO subregion (Lind et al., 1985, Lenkei et al., 1995, Giles et al., 1999), suggesting that neurons which exhibit a bursting pattern in action potential firing are cSFO neurons, which is consistent with the findings in the present study.

Further studies demonstrated that the bursting firing behaviour could be caused by subthreshold oscillation of membrane potential mediated by persistent Na^+ current (Washburn et al., 2000, Fry and Ferguson, 2007b). The bursting firing behaviour induced by persistent Na^+ current was observed not only in SFO neurons, but also in other neuron groups (Mantegazza et al., 1998). In this present study, persistent Na^+ current was compared between non-cSFO and cSFO neurons, however no significant difference was

observed. This does not mean that the results in the present and previous studies conflict. The present data showed most of the spontaneously active non-cSFO neurons had irregular firing pattern. Washburn et al. (2000) did not exclude the possibility that the irregular firing behaviour was also facilitated by the persistent Na^+ current. In fact the facilitation of persistent Na^+ current by anemone toxin increased neuron firing frequency and turned the bursting firing pattern into a high-rate irregular firing pattern (Washburn et al., 2000). In addition to Na^+ current, Ca^{2+} and K^+ current may also play a role in generating bursting behaviour (McCormick and Huguenard, 1992, Ghamari-Langroudi and Bourque, 1998, Krahe and Gabbiani, 2004, Teruyama and Armstrong, 2007), which suggested bursting behaviour might be caused by more than one mechanisms. The present data did not show a difference in K^+ current density or K^+ channel inactivation. Ca^{2+} current properties were not examined by this present study, and it could be a direction for further investigation.

The present data suggested the higher firing frequency in non-cSFO neurons might be caused by a more depolarized resting membrane potential. The action potential threshold between non-cSFO and cSFO neurons did not show a significant difference and the value varied from -47.9 to -51.3mV. The resting membrane potential in cSFO neurons was -47±2.2mV, which varied around the action potential threshold. Thus the oscillation of membrane potential would lead to a bursting firing behaviour in cSFO neurons, which resulted in an average lower firing frequency because of the quiet periods between bursts of action potentials. The resting membrane potential in non-cSFO neurons was -41±1.5mV, which was more depolarized compared to the action potential threshold thus led to constant firing in a high frequency. A higher action potential firing frequency was

also predicted at a more depolarized membrane potential in a computational model (Hopfield, 1982). Nevertheless, the more depolarized resting membrane potential in non-cSFO neurons might also be a result of a higher spontaneous action potential frequency. The resting membrane potential in this present study was measured in current clamp when there was no injecting current. So it was the membrane potential at spontaneous status instead of absolutely resting status (no action potential at all) of the cell. The repetitive firing of action potentials might prevent the completion of repolarizing phase thus made the resting membrane potential more depolarized.

In order to further investigate the mechanisms that may lead to higher neuronal activity in non-cSFO neurons, Na^+ current properties including voltage dependence of activation and inactivation, peak current density, persistent current and time-dependent from inactivation and K^+ current properties including current density, activation and inactivation were examined. In this present study, there was no significant difference in Na^+ or K^+ current properties between non-cSFO and cSFO neurons. However, it was noted that the Na^+ current density in non-cSFO neurons was -0.64±0.14nA/pF, which was much higher compared to -0.39±0.06nA/pF in cSFO neurons. Though the difference failed to reach statistical significance (t-test, p=0.051), a higher Na^+ current density which likely reflects a higher Na^+ channel density, increases the likelihood that a neuron will fire spontaneous action potentials. The higher Na^+ current density in non-cSFO neurons was consistent with the IH result showing a higher level of Nav1.3 expression in the pSFO subregion. However, whether the higher Na^+ current density is related to the expression of other isoforms of NaCh still remains to be investigated.

4.4. Heterogeneous electrophysiological behaviours in the SFO neurons

Previous studies have demonstrated heterogeneous electrophysiological behaviours in different SFO neuronal subpopulations in response to specific peptide hormones. Smith et al. (2009) revealed in their IH result that the leptin receptors mainly expressed in the cSFO subregion and the leptin sensitive SFO neurons might be the same subpopulation with the amylin sensitive SFO neurons. In their study, SFO neurons showed either a depolarization or hyperpolarization response to leptin demonstrated a bursting firing pattern which was also observed in the amylin sensitive SFO neurons. Those observations were consistent with the present data showing a bursting behaviour in cSFO neurons.

Washburn et al. (1999) reported that SFO neurons projecting to the PVN had a significantly higher degree of K^+ current inactivation. The percentage of inactivation of K^+ current was examined in this present study and no difference was observed between the non-cSFO and cSFO neurons, indicating neurons that project to the PVN may not be exclusively the non-cSFO or cSFO neurons. Although a previous study has indicated that SFO projections to PVN originated from the pSFO subregion (McKinley et al., 2003, Duan et al., 2008), a more recent study showed both cSFO and pSFO neurons projected to the PVN (Kawano and Masuko, 2010), which supported the present data.

4.5. The role of Nav1.3 in electrophysiology of the SFO neurons

The immunofluorescence results in the present study demonstrated Nav1.3 was more strongly expressed in the pSFO subregion and relatively weak in the cSFO subregion. In this present study, neurons from the pSFO showed a higher spontaneous

action potential firing frequency and a more depolarized resting membrane potential, which is consistent with previous reports suggesting Nav1.3 expression is positively correlated to overall neuronal activity (Cummins et al., 2001, Lampert et al., 2006). This did not preclude the possibility that higher overall activity might also relate to expression patterns of other NaCh isoforms.

The exact mechanisms by which Nav1.3 contributes to an increase in neuronal activity remain controversial. Cummins et al. (2001) demonstrated that a slower development, but faster recovery of the voltage-dependent inactivation of Na^+ current resulted in hyperpolarization of action potential threshold and a concomitant increase in action potential frequency. On the other hand, Lampert et al. (2006) suggested a larger persistent Na^+ current and a depolarized shift in voltage-dependent Na^+ current activation and inactivation was responsible for increase in neuronal activity. In the present study, no significant difference in the voltage-dependent activation or inactivation of Na^+ current, action potential threshold, or persistent Na^+ current was observed. However the Na^+ current density in non-cSFO neurons was approximately 40% higher than that in cSFO neurons ($p=0.051$), which would tend to increase the probability that spontaneous action potential was triggered thus leading to an increase in the overall neuronal activity.

4.6. Physiological relevance

This present study demonstrated the Nav1.3 was most strongly expressed in the pSFO subregion. During food deprivation, Nav1.3 was down regulated (Hindmarch et al., 2008 and unpublished data by Wong). According to the role of Nav1.3 of increasing overall neuronal activity (Cummins et al., 2001, Lampert et al., 2006), down regulation of

Nav1.3 would lead to a decrease in the overall neuronal activities in pSFO neurons, which has been suggested by a previous study (unpublished data by Lakhi et al.). The decrease in neuronal activities may present as decrease in spontaneous action potential firing frequency or reduction in Na^+ current density (unpublished data by Lakhi et al.).

It has been demonstrated that neurons from pSFO project to mPVN, LH and probably ARC (Gruber et al., 1987, McKinley et al., 2003). A decrease in pSFO neuronal activity will probably result in inhibition effects or release of inhibition in their second-order neurons. Because ARC, mPVN and LH are crucial hypothalamic nuclei for regulating energy balance, the pSFO may transmit information reflecting energy status by innervating certain neuronal populations within those hypothalamic nuclei. Neurons in the mPVN mediated NPY expression (Kalra et al., 1991, Yokosuka et al., 2001) and formed a neuronal network with ARC NPY neurons that regulated feeding behaviour (Bouret et al., 2004a). NPY level could be elevated during fasting (Sahu et al., 1988, Brady et al., 1990, White and Kershaw, 1990), indicating an elevated neuronal activity. Thus the high-rate spontaneous activity in pSFO neurons might give constant inhibitory inputs onto neurons in ARC or PVN which are involved in NPY neuronal network and the inhibition is released during fasting. In contrast, the synaptic inputs from the pSFO might be excitatory if they project to neurons that are involved in POMC neuronal circuit. Thus whether the inputs from the pSFO neurons to their second-order neurons are excitatory or inhibitory depends on whether the subpopulation in higher-order nuclei is involved in orexigenic or anorexigenic neuronal circuit. Which subpopulation of ARC, mPVN and LH is innervated by pSFO and whether neurons in those hypothalamic nuclei

are inhibited or excited by down regulation of Nav1.3 in pSFO still needs to be further investigated.

The cSFO neurons mainly project to rostral bed nucleus of stria terminalis (BNST), which plays a role in stress and anxiety responses (Walker et al., 2003) and may be also involved in AVP pathway (van Leeuwen and Caffe, 1983). Kawano and Masuko (2010) reported neurons from cSFO also project to pPVN. It has been reported that the deletion of the ANG II receptor AT1 abolished the response to the ANG II in the pPVN neurons (de Kloet et al., 2013), which indicated the pPVN neurons were involved in the ANG II neuronal circuit. Neurons in cSFO express ANG II and ANG II receptors and play an important role in ANG II signaling pathway. The role of the ANG II was not only limited in regulation of fluid balance but also related to diet-induce obesity (de Kloet et al., 2013). Thus the connections between the cSFO and pPVN neurons might serve as an important part of the ANG II neuronal network participating in regulation of energy balance. The bursting firing in cSFO neurons may carry the information of energy balance or osmolality information and influence the firing behaviour of the second-order neurons. However the information coded into the bursting firing pattern still remains to be investigated.

4.7. SmartFlare RNA probe

SmartFlare RNA probe for Calb was applied in this present study to distinguish live neurons that express Calb mRNA, which were the putative cSFO neurons, from the putative non-cSFO neurons. This is the first study using a RNA probe to identify dissociated cells for patch clamp recording. Before choosing SmartFlare RNA probe, ICC

for Calb and Calr on live SFO neurons (without fixation and permeablization) was carried out to try to identify putative cSFO and pSFO neurons based on the Calb/Calr expression. ICC on live cells was described by Volgin et al. (2004) to identify biochemically defined neuronal subpopulations. However, ICC on live cells failed on SFO neurons in present study because no immunofluorescent signal was detected. Before the present study, single-cell RT-PCR (reverse transcription polymerase chain reaction) has been used for identification of dissociated cells collected in patch clamp recording (Eberwine et al., 1992, Sucher et al., 2000, Koizumi et al., 2004, Hoyda et al., 2007). However, the single-cell RT-PCR is a difficult technique to perform. RNase-free condition needs to be provided during recording to prevent contamination (Sucher et al., 2000), and small amount of cytoplasm makes it difficult to harvest RNA in good quality and successfully carry out the needed enzyme reaction. In contrast, only overnight incubation before recording is required by the SmartFlare reagent and cells with target mRNA can be easily identified using an epifluorescence microscope. In addition to single-cell RT-PCR, ICC labeling on grid culture dish after patch clamp recording has been used to identify cells. However, neither single-cell RT-PCR nor ICC after recording provides expression information before or during recording, which could introduce inaccuracy in measurement of expression level. Transgenic mice have also been used for biochemically identifying of certain group of neurons (Lalchandani et al., 2013, Liu et al., 2014). However, rats instead of mice were used in this study and transgenic rat technology is not well developed. Thus the SmartFlare reagent is the most suitable approach to differentiate cSFO neurons from non-cSFO neurons in this present study.

Validation of the SmartFlare reagent was carried out in this present study. Calb antibody and Calb SmartFlare reagent were used to label Calb neurons in SFO culture in two sets of experiment respectively, which enables the statistical comparison of the proportion of Calb positive, Calr positive, double positive and double negative neurons. Fisher's exact test demonstrated no significant difference in any of the proportion between the double ICC and Calr ICC on SmartFlare treated neurons, suggesting a good sensitivity and specificity of the SmartFlare reagent.

However, the sensitivity of SmartFlare reagent shows a lower trend (16%) compared that of Calb antibody (26%). Also, the result of Calb ICC on SmartFlare treated neurons revealed there was no linear correlation between Calb ICC signal and Calb SmartFlare signal. Those inaccuracies could be possibly caused by two reasons:

1. The mRNA and protein expression might not be perfectly correlated. A neuron might express high levels of Calb protein but have lower levels of mRNA. Expression of proteins could vary over time in response to stimulations (Lowenstein et al., 1991, Fiumelli et al., 2000) and during dissociation procedure. Though Ferguson et al. (1997) argued dissociated neurons maintained their membrane properties, Ono et al. (2012) reported changes in expression levels of proteins brought by dissociation and the first day of cell culture.

2. The fluorescence of the Calb SmartFlare probe may not have a linear correlation with Calb mRNA. The SmartFlare RNA probe is a new technology came onto the market in 2013. There has been several publications that successfully used SmartFlare reagent to identify cells with target mRNA (Seftor et al., 2014, Vaidyanathan et al., 2014), however this new reagent still needs to be further evaluated by more future

studies. The manufacture validated SmartFlare reagent by showing both flow cytometry detecting of SmartFlare signal and RT-PCR result demonstrated a higher expression of APRIL protein in SW-480 cells than A549 cells. However this result was based on signals from a massive quantity of cells instead of signals from individual cells. This present study tested the possibility to broaden the way that the SmartFlare reagent can be applied and the possibility to use it on primary neuron culture than only on established cell lines. In addition, the uptake rate of SmartFlare reagent could vary from neuron to neuron, depending on the cell activity (http://www.researchgate.net/post/Does_SmartFlare_live-cell_RNA_labeling_work_well). This might lead to a possibility that a neuron with low expression level of Calb absorbed high amount of SmartFlare reagent and showed a strong SmartFlare signal. Thus a negative scrambled control is always suggested to be used with the SmartFlare probe. We currently have no mechanism to test whether the fluorescence of the Calb SmartFlare probe correlates with mRNA in a single cell.

The lower trend of sensitivity of the SmartFlare reagent would inevitably introduce false negatives into the non-cSFO group, which may increase the standard error in the data analysis. This means the difference between the non-cSFO and cSFO neurons needs to be robust to reach the significant level. This might explain why there was a trend of higher Na^+ current density in the pSFO neurons, but the difference was close to but failed to reach significant level.

Though there were several factors that could influence the correlation between SmartFlare and ICC signals, the result of validation still demonstrated the effectiveness of the SmartFlare reagent. Though there are more than one approach (i.e. ICC, RT-PCR) to identify cell expressing specific proteins, none of them are perfect. For example,

though single-cell RT-PCR is widely used in biochemically identification of cells, the effectiveness is only 70-80% (Fink et al., 2000, Stahlberg et al., 2014). Therefore compared to other possible techniques, currently the SmartFlare reagent is still the most efficient and convenient approach for identification of dissociated cSFO neurons for patch clamp recording.

4.8. Conclusion

This present study demonstrated the expression pattern Nav1.3 in the SFO and differences in electrical properties between neurons from different SFO subregions. It was revealed non-cSFO neurons expressed higher level Nav1.3, and had higher action potential firing frequency with fairly regular firing pattern in their spontaneous activity. Nav1.3 expression was much lower in cSFO neurons, and cSFO neurons could be characterized by firing in a bursting pattern. The higher firing frequency in non-cSFO neurons may be related to a more depolarized resting membrane potential and a trend of higher Na^+ current density. This data suggested a potential role of Nav1.3 in enhancing SFO neuronal activity, though the contribution of Nav1.3 versus other NaCh remained unclear. Nav1.3 expression level may signal information of body energy status, the changing of which will influence neuronal activity mainly in pSFO neurons and further influence their second-order neurons to regulate energy balance. This study also demonstrated an efficient and simple method of using SmartFlare mRNA probe to identify different SFO neuron subpopulations in culture for patch clamp recording, which could be applied to biochemically define neurons in future electrophysiological studies.

4.9. Future directions

The present study demonstrated a higher spontaneous firing frequency in non-cSFO neurons, which may be related to the higher expression of Nav1.3 in the pSFO subregion. However, whether the higher neuronal activity is related to expression pattern of other NaCh still remains unclear. Thus it would be interesting to investigate the expression pattern of Nav1.1, Nav1.2 and Nav1.7 in the SFO, using IH and ICC described in this study.

Previous studies showed down regulation of Nav1.3 mRNA induced by food restriction (Hindmarch et al., 2008). Because Nav1.3 IH has been successfully carried out, a potential future direction could be investigation of Nav1.3 expression level in rat SFO before and after fasting using immunostaining.

The present study that SmartFlare mRNA probe can be used to distinguish cSFO neurons from non-cSFO neurons. A potential future direction includes using current clamp recording to investigate the response of SmartFlare labelled putative cSFO neurons to peptide hormones such as ANG II or leptin. ANG II and leptin receptors were reported to be expressed mainly in the cSFO (Lenkei et al., 1995, Giles et al., 1999, Smith et al., 2009). It would be interesting if only the putative cSFO neurons show certain response to ANG II or leptin and this future study could further validate the SmartFlare reagent. In the future, SmartFlare for Calr (with a different fluorescent color) could be applied together with SmartFlare for Calb, allowing better identification of the pSFO neurons in patch clamp recording and also further validating the SmartFlare reagent using double ICC on SmartFlare treated SFO neurons.

Non-cSFO neurons demonstrated a more depolarized resting membrane potential compared to cSFO neurons. Na^+, K^+ current properties were examined but more studies might be required to fully explain the difference in resting membrane potential. Previous studies suggested Ca^{2+} current may also play a role in determining resting membrane potential (McCormick and Huguenard, 1992, Ghamari-Langroudi and Bourque, 1998, Krahe and Gabbiani, 2004, Teruyama and Armstrong, 2007). Thus investigation of Ca^{2+} current in cSFO and no-cSFO neurons will be an interesting direction for future study.

The present study emphasized the difference between cSFO and pSFO neurons. The IH result showed Nav1.3 was mainly expressed in pSFO, and previous study demonstrated a down regulation of Nav1.3 in response to food deprivation (unpublished result by Hindmarch et al., 2008). Thus, it would be interesting to further investigate the respective changes in cSFO and non-cSFO neurons respectively in response to food deprivation. This would provide more specificity than studying the response to fasting on the SFO as a whole.

In addition, the role of Nav1.3 in pSFO neurons could be further studied using siRNA for Nav1.3 mRNA to attenuate Nav1.3 expression, and using patch clamp recording to investigate the electrophysiological changes in the siRNA treated neurons. This will contribute to the knowledge how food deprivation influences the pSFO neurons by down regulating Nav1.3 expression.

5. References

Abbott NJ, Patabendige AA, Dolman DE, Yusof SR, Begley DJ (2010) Structure and function of the blood-brain barrier. Neurobiology of disease 37:13-25.

Ahmed AS, Dai L, Ho W, Ferguson AV, Sharkey KA (2014) The subfornical organ: a novel site of action of cholecystokinin. American journal of physiology Regulatory, integrative and comparative physiology.

Alim I, Fry WM, Walsh MH, Ferguson AV (2010) Actions of adiponectin on the excitability of subfornical organ neurons are altered by food deprivation. Brain research 1330:72-82.

Altaf MA, Sood MR (2008) The nervous system and gastrointestinal function. Developmental disabilities research reviews 14:87-95.

Anand BK, Brobeck JR (1951a) Hypothalamic control of food intake in rats and cats. The Yale journal of biology and medicine 24:123-140.

Anand BK, Brobeck JR (1951b) Localization of a "feeding center" in the hypothalamus of the rat. Proc Soc Exp Biol Med 77:323-324.

Anderson JW, Smith PM, Ferguson AV (2001) Subfornical organ neurons projecting to paraventricular nucleus: whole-cell properties. Brain Res 921:78-85.

Anis AH, Zhang W, Bansback N, Guh DP, Amarsi Z, Birmingham CL (2010) Obesity and overweight in Canada: an updated cost-of-illness study. Obesity reviews : an official journal of the International Association for the Study of Obesity 11:31-40.

Anthes N, Schmid HA, Hashimoto M, Riediger T, Simon E (1997) Heterogeneous actions of vasopressin on ANG II-sensitive neurons in the subfornical organ of rats. The American journal of physiology 273:R2105-2111.

Bagnol D, Lu XY, Kaelin CB, Day HE, Ollmann M, Gantz I, Akil H, Barsh GS, Watson SJ (1999) Anatomy of an endogenous antagonist: relationship between Agouti-related protein and proopiomelanocortin in brain. The Journal of neuroscience : the official journal of the Society for Neuroscience 19:RC26.

Bai FL, Yamano M, Shiotani Y, Emson PC, Smith AD, Powell JF, Tohyama M (1985) An arcuato-paraventricular and -dorsomedial hypothalamic neuropeptide Y-containing system which lacks noradrenaline in the rat. Brain research 331:172-175.

Ball GD, McCargar LJ (2003) Childhood obesity in Canada: a review of prevalence estimates and risk factors for cardiovascular diseases and type 2 diabetes. Canadian journal of applied physiology = Revue canadienne de physiologie appliquee 28:117-140.

Ballabh P, Braun A, Nedergaard M (2004) The blood-brain barrier: an overview: structure, regulation, and clinical implications. Neurobiology of disease 16:1-13.

Banks WA (2004) The source of cerebral insulin. European journal of pharmacology 490:5-12.

Banks WA (2008) The blood-brain barrier: connecting the gut and the brain. Regulatory peptides 149:11-14.

Banks WA, Jaspan JB, Kastin AJ (1997) Selective, physiological transport of insulin across the blood-brain barrier: novel demonstration by species-specific radioimmunoassays. Peptides 18:1257-1262.

Banks WA, Kastin AJ, Huang W, Jaspan JB, Maness LM (1996) Leptin enters the brain by a saturable system independent of insulin. Peptides 17:305-311.

Bartolomei F, Gastaldi M, Massacrier A, Planells R, Nicolas S, Cau P (1997) Changes in the mRNAs encoding subtypes I, II and III sodium channel alpha subunits following kainate-induced seizures in rat brain. Journal of neurocytology 26:667-678.

Baskin DG, Breininger JF, Schwartz MW (1999) Leptin receptor mRNA identifies a subpopulation of neuropeptide Y neurons activated by fasting in rat hypothalamus. Diabetes 48:828-833.

Baura GD, Foster DM, Porte D, Jr., Kahn SE, Bergman RN, Cobelli C, Schwartz MW (1993) Saturable transport of insulin from plasma into the central nervous system of dogs in vivo. A mechanism for regulated insulin delivery to the brain. The Journal of clinical investigation 92:1824-1830.

Beckh S, Noda M, Lubbert H, Numa S (1989) Differential regulation of three sodium channel messenger RNAs in the rat central nervous system during development. EMBO J 8:3611-3616.

Benoit SC, Air EL, Coolen LM, Strauss R, Jackman A, Clegg DJ, Seeley RJ, Woods SC (2002) The catabolic action of insulin in the brain is mediated by melanocortins. The Journal of neuroscience : the official journal of the Society for Neuroscience 22:9048-9052.

Berret E, Nehmé B, Henry M, Toth K, Drolet G, Mouginot D (2013) Regulation of Central Na+ Detection Requires the Cooperative Action of the NaX Channel and α1 Isoform of Na+/K+-ATPase in the Na+-Sensor Neuronal Population. The Journal of Neuroscience 33:3067-3078.

Berthoud HR (2005) Brain, appetite and obesity. Physiology & behavior 85:1-2.

Berthoud HR (2012) The neurobiology of food intake in an obesogenic environment. The Proceedings of the Nutrition Society 71:478-487.

Black JA, Frezel N, Dib-Hajj SD, Waxman SG (2012) Expression of Nav1.7 in DRG neurons extends from peripheral terminals in the skin to central preterminal branches and terminals in the dorsal horn. Molecular pain 8:82.

Blevins JE, Schwartz MW, Baskin DG (2004) Evidence that paraventricular nucleus oxytocin neurons link hypothalamic leptin action to caudal brain stem nuclei controlling meal size. American journal of physiology Regulatory, integrative and comparative physiology 287:R87-96.

Bouret SG, Draper SJ, Simerly RB (2004a) Formation of projection pathways from the arcuate nucleus of the hypothalamus to hypothalamic regions implicated in the neural control of feeding behavior in mice. The Journal of neuroscience : the official journal of the Society for Neuroscience 24:2797-2805.

Bouret SG, Draper SJ, Simerly RB (2004b) Trophic action of leptin on hypothalamic neurons that regulate feeding. Science 304:108-110.

Brady LS, Smith MA, Gold PW, Herkenham M (1990) Altered expression of hypothalamic neuropeptide mRNAs in food-restricted and food-deprived rats. Neuroendocrinology 52:441-447.

Brewer GJ (1997) Isolation and culture of adult rat hippocampal neurons. Journal of neuroscience methods 71:143-155.

Catterall WA (2012) Voltage-gated sodium channels at 60: structure, function and pathophysiology. The Journal of physiology 590:2577-2589.

Cheng KI, Wang HC, Chuang YT, Chou CW, Tu HP, Yu YC, Chang LL, Lai CS (2014) Persistent mechanical allodynia positively correlates with an increase in activated microglia and increased P-p38 mitogen-activated protein kinase activation in streptozotocin-induced diabetic rats. Eur J Pain 18:162-173.

Cheung CC, Clifton DK, Steiner RA (1997) Proopiomelanocortin neurons are direct targets for leptin in the hypothalamus. Endocrinology 138:4489-4492.

Clark JT, Kalra PS, Kalra SP (1985) Neuropeptide Y stimulates feeding but inhibits sexual behavior in rats. Endocrinology 117:2435-2442.

Cone RD (1999) The Central Melanocortin System and Energy Homeostasis. Trends in endocrinology and metabolism: TEM 10:211-216.

Cowley MA, Pronchuk N, Fan W, Dinulescu DM, Colmers WF, Cone RD (1999) Integration of NPY, AGRP, and melanocortin signals in the hypothalamic paraventricular nucleus: evidence of a cellular basis for the adipostat. Neuron 24:155-163.

Cowley MA, Smart JL, Rubinstein M, Cerdán MG, Diano S, Horvath TL, Cone RD, Low MJ (2001) Leptin activates anorexigenic POMC neurons through a neural network in the arcuate nucleus. Nature 411:480-484.

Cowley MA, Smith RG, Diano S, Tschöp M, Pronchuk N, Grove KL, Strasburger CJ, Bidlingmaier M, Esterman M, Heiman ML (2003) The distribution and mechanism of action of ghrelin in the CNS demonstrates a novel hypothalamic circuit regulating energy homeostasis. Neuron 37:649-661.

Csiffary A, Gorcs TJ, Palkovits M (1990) Neuropeptide Y innervation of ACTH-immunoreactive neurons in the arcuate nucleus of rats: a correlated light and electron microscopic double immunolabeling study. Brain research 506:215-222.

Cummins TR, Aglieco F, Renganathan M, Herzog RI, Dib-Hajj SD, Waxman SG (2001) Nav1.3 sodium channels: rapid repriming and slow closed-state inactivation display quantitative differences after expression in a mammalian cell line and in spinal sensory neurons. The Journal of neuroscience : the official journal of the Society for Neuroscience 21:5952-5961.

de Kloet AD, Pati D, Wang L, Hiller H, Sumners C, Frazier CJ, Seeley RJ, Herman JP, Woods SC, Krause EG (2013) Angiotensin type 1a receptors in the paraventricular nucleus of the hypothalamus protect against diet-induced obesity. The Journal of neuroscience : the official journal of the Society for Neuroscience 33:4825-4833.

Derakhshan F, Toth C (2013) Insulin and the brain. Current diabetes reviews 9:102-116.

Dong HW (2008) The Allen reference atlas: A digital color brain atlas of the C57Bl/6J male mouse: John Wiley & Sons Inc.

Duan PG, Kawano H, Masuko S (2008) Collateral projections from the subfornical organ to the median preoptic nucleus and paraventricular hypothalamic nucleus in the rat. Brain Res 1198:68-72.

Eberwine J, Yeh H, Miyashiro K, Cao Y, Nair S, Finnell R, Zettel M, Coleman P (1992) Analysis of gene expression in single live neurons. Proceedings of the National Academy of Sciences of the United States of America 89:3010-3014.

Edmonds B, Reyes R, Schwaller B, Roberts WM (2000) Calretinin modifies presynaptic calcium signaling in frog saccular hair cells. Nature neuroscience 3:786-790.

Ednie AR, Horton KK, Wu J, Bennett ES (2013) Expression of the sialyltransferase, ST3Gal4, impacts cardiac voltage-gated sodium channel activity, refractory period and ventricular conduction. Journal of molecular and cellular cardiology 59:117-127.

Elmquist JK, Elias CF, Saper CB (1999) From lesions to leptin: hypothalamic control of food intake and body weight. Neuron 22:221-232.

Fan W, Boston BA, Kesterson RA, Hruby VJ, Cone RD (1997) Role of melanocortinergic neurons in feeding and the agouti obesity syndrome. Nature 385:165-168.

Ferguson AV, Bains JS (1996) Electrophysiology of the circumventricular organs. Frontiers in neuroendocrinology 17:440-475.

Ferguson AV, Bains JS (1997) Actions of angiotensin in the subfornical organ and area postrema: implications for long term control of autonomic output. Clinical and experimental pharmacology & physiology 24:96-101.

Ferguson AV, Bicknell RJ, Carew MA, Mason WT (1997) Dissociated adult rat subfornical organ neurons maintain membrane properties and angiotensin responsiveness for up to 6 days. Neuroendocrinology 66:409-415.

Ferguson AV, Kasting NW (1986) Electrical stimulation in subfornical organ increases plasma vasopressin concentrations in the conscious rat. The American journal of physiology 251:R425-428.

Ferguson AV, Li Z (1996) Whole cell patch recordings from forebrain slices demonstrate angiotensin II inhibits potassium currents in subfornical organ neurons. Regulatory peptides 66:55-58.

Fink L, Kinfe T, Seeger W, Ermert L, Kummer W, Bohle RM (2000) Immunostaining for cell picking and real-time mRNA quantitation. The American journal of pathology 157:1459-1466.

Finkelstein EA, Trogdon JG, Cohen JW, Dietz W (2009) Annual medical spending attributable to obesity: payer-and service-specific estimates. Health Aff (Millwood) 28:w822-831.

Fiumelli H, Kiraly M, Ambrus A, Magistretti PJ, Martin JL (2000) Opposite regulation of calbindin and calretinin expression by brain-derived neurotrophic factor in cortical neurons. Journal of neurochemistry 74:1870-1877.

Friedman JM, Halaas JL (1998) Leptin and the regulation of body weight in mammals. Nature 395:763-770.

Fry M (2006) Developmental expression of Na+ currents in mouse Purkinje neurons. The European journal of neuroscience 24:2557-2566.

Fry M, Ferguson AV (2007a) The sensory circumventricular organs: brain targets for circulating signals controlling ingestive behavior. Physiology & behavior 91:413-423.

Fry M, Ferguson AV (2007b) Subthreshold oscillations of membrane potential of rat subfornical organ neurons. Neuroreport 18:1389-1393.

Fry M, Ferguson AV (2010) Ghrelin: central nervous system sites of action in regulation of energy balance. International journal of peptides 2010.

Fry M, Hoyda TD, Ferguson AV (2007) Making sense of it: roles of the sensory circumventricular organs in feeding and regulation of energy homeostasis. Exp Biol Med (Maywood) 232:14-26.

Fuxe K, Tinner B, Caberlotto L, Bunnemann B, Agnati LF (1997) NPY Y1 receptor like immunoreactivity exists in a subpopulation of beta-endorphin immunoreactive nerve cells in the arcuate nucleus: a double immunolabelling analysis in the rat. Neuroscience letters 225:49-52.

Ghamari-Langroudi M, Bourque CW (1998) Caesium blocks depolarizing after-potentials and phasic firing in rat supraoptic neurones. The Journal of physiology 510 (Pt 1):165-175.

Giles ME, Fernley RT, Nakamura Y, Moeller I, Aldred GP, Ferraro T, Penschow JD, McKinley MJ, Oldfield BJ (1999) Characterization of a specific antibody to the rat angiotensin II AT1 receptor. The journal of histochemistry and cytochemistry : official journal of the Histochemistry Society 47:507-516.

Gracia-Llanes F, Blasco-Ibáñez J, Nácher J, Varea E, Liberia T, Martínez P, Martínez-Guijarro F, Crespo C (2010) Synaptic connectivity of serotonergic axons in the olfactory glomeruli of the rat olfactory bulb. Neuroscience 169:770-780.

Gregoire N (1989) The blood-brain barrier. Journal of neuroradiology Journal de neuroradiologie 16:238-250.

Gross PM (1991) Morphology and physiology of capillary systems in subregions of the subfornical organ and area postrema. Canadian journal of physiology and pharmacology 69:1010-1025.

Gross PM (1992) Circumventricular organ capillaries. Progress in brain research 91:219-233.

Grouselle D, Chaillou E, Caraty A, Bluet-Pajot MT, Zizzari P, Tillet Y, Epelbaum J (2008) Pulsatile cerebrospinal fluid and plasma ghrelin in relation to growth hormone secretion and food intake in the sheep. Journal of neuroendocrinology 20:1138-1146.

Gruber K, McRae-Degueurce A, Wilkin LD, Mitchell LD, Johnson AK (1987) Forebrain and brainstem afferents to the arcuate nucleus in the rat: potential pathways for the modulation of hypophyseal secretions. Neuroscience letters 75:1-5.

Guan XM, Yu H, Palyha OC, McKee KK, Feighner SD, Sirinathsinghji DJ, Smith RG, Van der Ploeg LH, Howard AD (1997) Distribution of mRNA encoding the growth hormone secretagogue receptor in brain and peripheral tissues. Brain research Molecular brain research 48:23-29.

Guo F, Yu N, Cai JQ, Quinn T, Zong ZH, Zeng YJ, Hao LY (2008) Voltage-gated sodium channel Nav1.1, Nav1.3 and beta1 subunit were up-regulated in the hippocampus of spontaneously epileptic rat. Brain research bulletin 75:179-187.

Hains BC, Klein JP, Saab CY, Craner MJ, Black JA, Waxman SG (2003) Upregulation of sodium channel Nav1.3 and functional involvement in neuronal hyperexcitability associated with central neuropathic pain after spinal cord injury. The Journal of neuroscience : the official journal of the Society for Neuroscience 23:8881-8892.

Hains BC, Saab CY, Waxman SG (2005) Changes in electrophysiological properties and sodium channel Nav1.3 expression in thalamic neurons after spinal cord injury. Brain : a journal of neurology 128:2359-2371.

Hillebrand JJ, de Wied D, Adan RA (2002) Neuropeptides, food intake and body weight regulation: a hypothalamic focus. Peptides 23:2283-2306.

Hindmarch C, Fry M, Yao ST, Smith PM, Murphy D, Ferguson AV (2008) Microarray analysis of the transcriptome of the subfornical organ in the rat: regulation by fluid and food deprivation. American journal of physiology Regulatory, integrative and comparative physiology 295:R1914-1920.

Hopfield JJ (1982) Neural networks and physical systems with emergent collective computational abilities. Proceedings of the National Academy of Sciences of the United States of America 79:2554-2558.

Horvath TL, Diano S, van den Pol AN (1999) Synaptic interaction between hypocretin (orexin) and neuropeptide Y cells in the rodent and primate hypothalamus: a novel circuit implicated in metabolic and endocrine regulations. The Journal of neuroscience : the official journal of the Society for Neuroscience 19:1072-1087.

Horvath TL, Naftolin F, Kalra SP, Leranth C (1992) Neuropeptide-Y innervation of beta-endorphin-containing cells in the rat mediobasal hypothalamus: a light and electron microscopic double immunostaining analysis. Endocrinology 131:2461-2467.

Hoyda TD, Fry M, Ahima RS, Ferguson AV (2007) Adiponectin selectively inhibits oxytocin neurons of the paraventricular nucleus of the hypothalamus. The Journal of physiology 585:805-816.

Hoyda TD, Smith PM, Ferguson AV (2009) Gastrointestinal hormone actions in the central regulation of energy metabolism: potential sensory roles for the circumventricular organs. Int J Obes (Lond) 33 Suppl 1:S16-21.

Janzer RC, Raff MC (1987) Astrocytes induce blood-brain barrier properties in endothelial cells. Nature 325:253-257.

Jegou S, Blasquez C, Delbende C, Bunel DT, Vaudry H (1993) Regulation of alpha-melanocyte-stimulating hormone release from hypothalamic neurons. Annals of the New York Academy of Sciences 680:260-278.

Johnson AK, Gross PM (1993) Sensory circumventricular organs and brain homeostatic pathways. FASEB journal : official publication of the Federation of American Societies for Experimental Biology 7:678-686.

Kalra SP, Dube MG, Sahu A, Phelps CP, Kalra PS (1991) Neuropeptide Y secretion increases in the paraventricular nucleus in association with increased appetite for food. Proceedings of the National Academy of Sciences of the United States of America 88:10931-10935.

Kawano H, Masuko S (2010) Region-specific projections from the subfornical organ to the paraventricular hypothalamic nucleus in the rat. Neuroscience 169:1227-1234.

Kim J, Nakajima K, Oomura Y, Wayner MJ, Sasaki K (2009) Electrophysiological effects of ghrelin on pedunculopontine tegmental neurons in rats: An in vitro study. Peptides 30:745-757.

Kishi T, Aschkenasi CJ, Choi BJ, Lopez ME, Lee CE, Liu H, Hollenberg AN, Friedman JM, Elmquist JK (2005) Neuropeptide Y Y1 receptor mRNA in rodent brain:

distribution and colocalization with melanocortin-4 receptor. The Journal of comparative neurology 482:217-243.

Kiss T (2008) Persistent Na-channels: origin and function. A review. Acta biologica Hungarica 59 Suppl:1-12.

Kjeldsen T, Andersen AS, Wiberg FC, Rasmussen JS, Schaffer L, Balschmidt P, Moller KB, Moller NP (1991) The ligand specificities of the insulin receptor and the insulin-like growth factor I receptor reside in different regions of a common binding site. Proceedings of the National Academy of Sciences of the United States of America 88:4404-4408.

Koizumi A, Jakobs TC, Masland RH (2004) Inward rectifying currents stabilize the membrane potential in dendrites of mouse amacrine cells: patch-clamp recordings and single-cell RT-PCR. Mol Vis 10:1.

Kojima M, Hosoda H, Date Y, Nakazato M, Matsuo H, Kangawa K (1999) Ghrelin is a growth-hormone-releasing acylated peptide from stomach. Nature 402:656-660.

Kotz CM, Glass MJ, Levine AS, Billington CJ (2000) Regional effect of naltrexone in the nucleus of the solitary tract in blockade of NPY-induced feeding. American journal of physiology Regulatory, integrative and comparative physiology 278:R499-503.

Krahe R, Gabbiani F (2004) Burst firing in sensory systems. Nature reviews Neuroscience 5:13-23.

Krisch B, Leonhardt H, Buchheim W (1978) The functional and structural border between the CSF- and blood-milieu in the circumventricular organs (organum

vasculosum laminae terminalis, subfornical organ, area postrema) of the rat. Cell and tissue research 195:485-497.

Kuchler-Bopp S, Delaunoy JP, Artault JC, Zaepfel M, Dietrich JB (1999) Astrocytes induce several blood-brain barrier properties in non-neural endothelial cells. Neuroreport 10:1347-1353.

Lakhi S, Snow W, Fry M (2013) Insulin modulates the electrical activity of subfornical organ neurons. Neuroreport 24:329-334.

Lalchandani RR, van der Goes MS, Partridge JG, Vicini S (2013) Dopamine D2 receptors regulate collateral inhibition between striatal medium spiny neurons. The Journal of neuroscience : the official journal of the Society for Neuroscience 33:14075-14086.

Lampert A, Hains BC, Waxman SG (2006) Upregulation of persistent and ramp sodium current in dorsal horn neurons after spinal cord injury. Experimental brain research 174:660-666.

Lee EB, Mattson MP (2013) The neuropathology of obesity: insights from human disease. Acta neuropathologica.

Lehnert T, Sonntag D, Konnopka A, Riedel-Heller S, Konig HH (2013) Economic costs of overweight and obesity. Best practice & research Clinical endocrinology & metabolism 27:105-115.

Lenkei Z, Corvol P, Llorens-Cortes C (1995) The angiotensin receptor subtype AT1A predominates in rat forebrain areas involved in blood pressure, body fluid homeostasis and neuroendocrine control. Brain research Molecular brain research 30:53-60.

Levin BE (2007) Why some of us get fat and what we can do about it. The Journal of physiology 583:425-430.

Lind RW, Swanson LW, Ganten D (1985) Organization of angiotensin II immunoreactive cells and fibers in the rat central nervous system. An immunohistochemical study. Neuroendocrinology 40:2-24.

Lindia JA, Abbadie C (2003) Distribution of the voltage gated sodium channel Na(v)1.3-like immunoreactivity in the adult rat central nervous system. Brain Res 960:132-141.

Lindia JA, Köhler MG, Martin WJ, Abbadie C (2005) Relationship between sodium channel NaV1. 3 expression and neuropathic pain behavior in rats. Pain 117:145.

Liu YD, Harding M, Pittman A, Dore J, Striessnig J, Rajadhyaksha A, Chen X (2014) Cav1.2 and Cav1.3 L-type calcium channels regulate dopaminergic firing activity in the mouse ventral tegmental area. Journal of neurophysiology.

Lowenstein DH, Miles MF, Hatam F, McCabe T (1991) Up regulation of calbindin-D28K mRNA in the rat hippocampus following focal stimulation of the perforant path. Neuron 6:627-633.

Luiten PG, ter Horst GJ, Karst H, Steffens AB (1985) The course of paraventricular hypothalamic efferents to autonomic structures in medulla and spinal cord. Brain Res 329:374-378.

Maejima Y, Sedbazar U, Suyama S, Kohno D, Onaka T, Takano E, Yoshida N, Koike M, Uchiyama Y, Fujiwara K, Yashiro T, Horvath TL, Dietrich MO, Tanaka S, Dezaki K, Oh IS, Hashimoto K, Shimizu H, Nakata M, Mori M, Yada T (2009) Nesfatin-1-regulated oxytocinergic signaling in the paraventricular nucleus causes

anorexia through a leptin-independent melanocortin pathway. Cell Metab 10:355-365.

Mantegazza M, Franceschetti S, Avanzini G (1998) Anemone toxin (ATX II)-induced increase in persistent sodium current: effects on the firing properties of rat neocortical pyramidal neurones. The Journal of physiology 507 (Pt 1):105-116.

Matsuda M, Petersson M, Lenkei R, Taupin JL, Magnusson I, Mellstedt H, Anderson P, Kiessling R (1995) Alterations in the signal-transducing molecules of T cells and NK cells in colorectal tumor-infiltrating, gut mucosal and peripheral lymphocytes: correlation with the stage of the disease. International journal of cancer Journal international du cancer 61:765-772.

McCormick DA, Huguenard JR (1992) A model of the electrophysiological properties of thalamocortical relay neurons. Journal of neurophysiology 68:1384-1400.

McKinley M, Allen A, Burns P, Colvill L, Oldfield B (1998) Interaction of circulating hormones with the brain: the roles of the subfornical organ and the organum vasculosum of the lamina terminalis. Clinical and Experimental Pharmacology and Physiology 25:S61-S67.

McKinley MJ, R.M.McAllen, P.Davern, M.E.Giles, J.Penschow (2003) The sensory circumventricular organs of the mammalian brain : subfornical organ, OVLT and area postrema. Berlin ; New York: Springer-Verlag.

McNicol A, Richmond J (1998) Optimizing immunohistochemistry: antigen retrieval and signal amplification. HISTOPATHOLOGY-OXFORD- 32:97-103.

Medeiros N, Dai L, Ferguson AV (2012) Glucose-responsive neurons in the subfornical organ of the rat--a novel site for direct CNS monitoring of circulating glucose. Neuroscience 201:157-165.

Meier F, Giesert F, Delic S, Faus-Kessler T, Matheus F, Simeone A, Holter SM, Kuhn R, Weisenhorn DM, Wurst W, Prakash N (2014) FGF/FGFR2 Signaling Regulates the Generation and Correct Positioning of Bergmann Glia Cells in the Developing Mouse Cerebellum. PloS one 9:e101124.

Mimee A, Smith PM, Ferguson AV (2013) Circumventricular organs: targets for integration of circulating fluid and energy balance signals? Physiology & behavior 121:96-102.

Miselis RR, Shapiro RE, Hand PJ (1979) Subfornical organ efferents to neural systems for control of body water. Science 205:1022-1025.

Moore DS, McCabe GP Introduction to the Practice of Statistics, 1993. From this book I learned a lot of statistics, especially quadratic regressions and outliers.

Morrison SF, Madden CJ, Tupone D (2012) Central control of brown adipose tissue thermogenesis. Frontiers in endocrinology 3.

Morrison SF, Madden CJ, Tupone D (2014) Central Neural Regulation of Brown Adipose Tissue Thermogenesis and Energy Expenditure. Cell metabolism.

Must A, Spadano J, Coakley EH, Field AE, Colditz G, Dietz WH (1999) The disease burden associated with overweight and obesity. JAMA : the journal of the American Medical Association 282:1523-1529.

Nehme B, Henry M, Mouginot D, Drolet G (2012) The Expression Pattern of the Na(+) Sensor, Na(X) in the Hydromineral Homeostatic Network: A Comparative Study between the Rat and Mouse. Frontiers in neuroanatomy 6:26.

Okuya S, Inenaga K, Kaneko T, Yamashita H (1987) Angiotensin II sensitive neurons in the supraoptic nucleus, subfornical organ and anteroventral third ventricle of rats in vitro. Brain research 402:58-67.

Ono K, Xu S, Hitomi S, Inenaga K (2012) Comparison of the electrophysiological and immunohistochemical properties of acutely dissociated and 1-day cultured rat trigeminal ganglion neurons. Neuroscience letters 523:162-166.

Paxinos G, Watson C (2006) The rat brain in stereotaxic coordinates: hard cover edition: Academic press.

Peruzzo B, Pastor FE, Blazquez JL, Schobitz K, Pelaez B, Amat P, Rodriguez EM (2000) A second look at the barriers of the medial basal hypothalamus. Experimental brain research 132:10-26.

Petrov T, Howarth AG, Krukoff TL, Stevenson BR (1994) Distribution of the tight junction-associated protein ZO-1 in circumventricular organs of the CNS. Brain research Molecular brain research 21:235-246.

Pickel VM, Chan J, Ganten D (1986) Dual peroxidase and colloidal gold-labeling study of angiotensin converting enzyme and angiotensin-like immunoreactivity in the rat subfornical organ. The Journal of neuroscience : the official journal of the Society for Neuroscience 6:2457-2469.

Pulman KJ, Fry WM, Cottrell GT, Ferguson AV (2006) The subfornical organ: a central target for circulating feeding signals. The Journal of neuroscience : the official journal of the Society for Neuroscience 26:2022-2030.

Qu D, Ludwig DS, Gammeltoft S, Piper M, Pelleymounter MA, Cullen MJ, Mathes WF, Przypek R, Kanarek R, Maratos-Flier E (1996) A role for melanin-concentrating hormone in the central regulation of feeding behaviour. Nature 380:243-247.

Rinaman L (1998) Oxytocinergic inputs to the nucleus of the solitary tract and dorsal motor nucleus of the vagus in neonatal rats. The Journal of comparative neurology 399:101-109.

Sahu A, Kalra PS, Kalra SP (1988) Food deprivation and ingestion induce reciprocal changes in neuropeptide Y concentrations in the paraventricular nucleus. Peptides 9:83-86.

Saper CB, Levisohn D (1983) Afferent connections of the median preoptic nucleus in the rat: anatomical evidence for a cardiovascular integrative mechanism in the anteroventral third ventricular (AV3V) region. Brain research 288:21-31.

Schwaller B, Meyer M, Schiffmann S (2002) 'New'functions for 'old'proteins: the role of the calcium-binding proteins calbindin D-28k, calretinin and parvalbumin, in cerebellar physiology. Studies with knockout mice. The cerebellum 1:241-258.

Schwartz MW, Baskin DG, Kaiyala KJ, Woods SC (1999) Model for the regulation of energy balance and adiposity by the central nervous system. The American journal of clinical nutrition 69:584-596.

Schwartz MW, Porte D, Jr. (2005) Diabetes, obesity, and the brain. Science 307:375-379.

Schwartz MW, Woods SC, Porte D, Jr., Seeley RJ, Baskin DG (2000) Central nervous system control of food intake. Nature 404:661-671.

Seftor EA, Seftor RE, Weldon DS, Kirsammer GT, Margaryan NV, Gilgur A, Hendrix MJ (2014) Melanoma tumor cell heterogeneity: a molecular approach to study subpopulations expressing the embryonic morphogen nodal. Seminars in oncology 41:259-266.

Sgro S, Ferguson AV, Renaud LP (1984) Subfornical organ--supraoptic nucleus connections: an electrophysiologic study in the rat. Brain research 303:7-13.

Shao XM, Feldman JL (2007) Micro-agar salt bridge in patch-clamp electrode holder stabilizes electrode potentials. Journal of neuroscience methods 159:108-115.

Shields M (2006) Overweight and obesity among children and youth. Health reports 17:27-42.

Shields M, Tremblay MS, Laviolette M, Craig CL, Janssen I, Connor Gorber S (2010) Fitness of Canadian adults: results from the 2007-2009 Canadian Health Measures Survey. Health reports 21:21-35.

Simpson JB, Routtenberg A (1973) Subfornical organ: site of drinking elicitation by angiotensin II. Science 181:1172-1175.

Smith DW, Day TA (1995) Hypovolaemic and osmotic stimuli induce distinct patterns of c-Fos expression in the rat subfornical organ. Brain Res 698:232-236.

Smith PM, Chambers AP, Price CJ, Ho W, Hopf C, Sharkey KA, Ferguson AV (2009) The subfornical organ: a central nervous system site for actions of circulating leptin. American journal of physiology Regulatory, integrative and comparative physiology 296:R512-520.

Smith PM, Ferguson AV (2010) Circulating signals as critical regulators of autonomic state—central roles for the subfornical organ. American Journal of Physiology-Regulatory, Integrative and Comparative Physiology 299:R405-R415.

Smith PM, Rozanski G, Ferguson AV (2010) Acute electrical stimulation of the subfornical organ induces feeding in satiated rats. Physiology & behavior 99:534-537.

Snow WM, Fry M, Anderson JE (2013) Increased density of dystrophin protein in the lateral versus the vermal mouse cerebellum. Cellular and molecular neurobiology 33:513-520.

Stahlberg A, Aman P, Strombom L, Zoric N, Diez A, Nilsson O, Kubista M, Ridell B (2014) Comparison of reverse transcription quantitative real-time PCR, flow cytometry, and immunohistochemistry for detection of monoclonality in lymphomas. ISRN oncology 2014:796210.

Stanley BG, Kyrkouli SE, Lampert S, Leibowitz SF (1986) Neuropeptide Y chronically injected into the hypothalamus: a powerful neurochemical inducer of hyperphagia and obesity. Peptides 7:1189-1192.

Sucher NJ, Deitcher DL, Baro DJ, Warrick RMH, Guenther E (2000) Genes and channels: patch/voltage-clamp analysis and single-cell RT-PCR. Cell and tissue research 302:295-307.

Swanson LW, Lind RW (1986) Neural projections subserving the initiation of a specific motivated behavior in the rat: new projections from the subfornical organ. Brain research 379:399-403.

Tanaka J, Kaba H, Saito H, Seto K (1985) Electrophysiological evidence that circulating angiotensin II sensitive neurons in the subfornical organ alter the activity of hypothalamic paraventricular neurohypophyseal neurons in the rat. Brain Res 342:361-365.

Teruyama R, Armstrong WE (2007) Calcium-dependent fast depolarizing afterpotentials in vasopressin neurons in the rat supraoptic nucleus. Journal of neurophysiology 98:2612-2621.

Tschop M, Smiley DL, Heiman ML (2000) Ghrelin induces adiposity in rodents. Nature 407:908-913.

Unger J, McNeill TH, Moxley RT, 3rd, White M, Moss A, Livingston JN (1989) Distribution of insulin receptor-like immunoreactivity in the rat forebrain. Neuroscience 31:143-157.

Vaidyanathan S, Weldon D, Koong V, Smith-McCollum B (2014) Detecting Circulating Tumor Cells.

Valassi E, Scacchi M, Cavagnini F (2008) Neuroendocrine control of food intake. Nutrition, metabolism, and cardiovascular diseases : NMCD 18:158-168.

van Leeuwen F, Caffe R (1983) Vasopressin-immunoreactive cell bodies in the bed nucleus of the stria terminalis of the rat. Cell and tissue research 228:525-534.

Volgin DV, Swan J, Kubin L (2004) Single-cell RT-PCR gene expression profiling of acutely dissociated and immunocytochemically identified central neurons. Journal of neuroscience methods 136:229-236.

Walker DL, Toufexis DJ, Davis M (2003) Role of the bed nucleus of the stria terminalis versus the amygdala in fear, stress, and anxiety. European journal of pharmacology 463:199-216.

Wang Y, Lobstein T (2006) Worldwide trends in childhood overweight and obesity. International journal of pediatric obesity : IJPO : an official journal of the International Association for the Study of Obesity 1:11-25.

Wang YC, McPherson K, Marsh T, Gortmaker SL, Brown M (2011) Health and economic burden of the projected obesity trends in the USA and the UK. Lancet 378:815-825.

Washburn DL, Anderson JW, Ferguson AV (2000) A subthreshold persistent sodium current mediates bursting in rat subfornical organ neurones. The Journal of physiology 529 Pt 2:359-371.

Washburn DL, Beedle AM, Ferguson AV (1999) Inhibition of subfornical organ neuronal potassium channels by vasopressin. Neuroscience 93:349-359.

Weiss J, Pyrski M, Jacobi E, Bufe B, Willnecker V, Schick B, Zizzari P, Gossage SJ, Greer CA, Leinders-Zufall T, Woods CG, Wood JN, Zufall F (2011) Loss-of-function mutations in sodium channel Nav1.7 cause anosmia. Nature 472:186-190.

White JD, Kershaw M (1990) Increased hypothalamic neuropeptide Y expression following food deprivation. Molecular and cellular neurosciences 1:41-48.

Willesen MG, Kristensen P, Romer J (1999) Co-localization of growth hormone secretagogue receptor and NPY mRNA in the arcuate nucleus of the rat. Neuroendocrinology 70:306-316.

Williams G, Bing C, Cai XJ, Harrold JA, King PJ, Liu XH (2001) The hypothalamus and the control of energy homeostasis: different circuits, different purposes. Physiology & behavior 74:683-701.

Williams KW, Elmquist JK (2012) From neuroanatomy to behavior: central integration of peripheral signals regulating feeding behavior. Nature neuroscience 15:1350-1355.

Wren AM, Small CJ, Abbott CR, Dhillo WS, Seal LJ, Cohen MA, Batterham RL, Taheri S, Stanley SA, Ghatei MA, Bloom SR (2001) Ghrelin causes hyperphagia and obesity in rats. Diabetes 50:2540-2547.

Yokosuka M, Dube MG, Kalra PS, Kalra SP (2001) The mPVN mediates blockade of NPY-induced feeding by a Y5 receptor antagonist: a c-FOS analysis. Peptides 22:507-514.

Yu FH, Catterall WA (2003) Overview of the voltage-gated sodium channel family. Genome biology 4:207.

Zigman JM, Elmquist JK (2003) Minireview: From anorexia to obesity--the yin and yang of body weight control. Endocrinology 144:3749-3756.